Cape Peninsula
University of Technology

SORPTION MECHANISMS OF SELECTED HEAVY METALS ON SPENT COFFEE GROUNDS

by

LEROY LESLIE FORD

Thesis submitted in fulfilment of the requirements for the degree

Master of Applied Sciences in Analytical Chemistry

in the Faculty of Applied Science (Bellville)

at the Cape Peninsula University of Technology

Supervisor: Dr Andre Ronald Lee Spies

December 2021

DECLARATION

I, Leroy Leslie Ford (213189860), declare that the contents of this dissertation/thesis represent my own unaided work and that the dissertation/thesis has not previously been submitted for academic examination towards any qualification. Furthermore, it represents my own opinions and not necessarily those of the Cape Peninsula University of Technology.

Signed **Date**

ABSTRACT

This study investigated the use of spent coffee grounds (SCG) for the sorption of cadmium and nickel ions from synthetic aqueous solutions. Batch kinetic and equilibrium experiments were conducted to study the effects of pH, contact time, sorbent dosage, initial concentration and temperature on the sorption of Cd and Ni. The spent coffee was stripped of its remaining oils using supercritical fluid extraction (SFE) before sorption. Maximum sorption occurred at pH 6 for both metals.

Equilibrium data for Ni sorption were best modelled by the Langmuir isotherm, with linear regression coefficient R^2 = 0.9916, whereas Cd sorption was best modelled by the Freundlich isotherm (R^2 = 0.9888). The theoretical sorption capacities of Cd and Ni were 2.5500 $mg \cdot g^{-1}$ and 2.0590 $mg \cdot g^{-1}$, respectively.

Thermodynamic studies suggested sorption of both metals was exothermic ($\Delta H°_{Cd}$ = -31.54 $kJ \cdot mol^{-1}$; $\Delta H°_{Ni}$ = -23.84 $kJ.mol^{-1}$), and spontaneous ($\Delta G° < 0$) over the temperature range 10 °C to 40 °C. The $\Delta G°$ decreased with increasing temperature, suggesting sorption was more spontaneous at higher temperatures. Disorder of magnitudes $\Delta S°$= 107.51 $J/mol^{-1} \cdot K^{-1}$ (Cd) and 76.44 $J/mol^{-1} \cdot K^{-1}$ (Ni), suggested sorption was random.

Equilibrium was reached in less than 60 minutes for both Cd and Ni. Kinetic data for both metals best fitted a pseudo-second order model, indicating that chemisorption was the predominant mechanism.

ACKNOWLEDGEMENTS

I wish to thank:

- The Source of life, through whom all things are possible.
- My parents, for their love and support.
- Dr Andre R. L. Spies, my supervisor, for all the care and support throughout my entire student career, both undergrad and postgrad. It is an honour to know you, to learn from you and join in this work with you.
- Professor Merrill Wicht, for her assistance with the XRD analyses.
- Mr Tafi Madzimbamuto and his team, for their assistance with the supercritical CO_2 extraction of the sorbent.
- Professor Lynn D. McMaster, for proofreading and editing of the thesis.
- Dr Madelaine Frazenburg from the Electron Microbeam Unit of Stellenbosch University's Central Analytical Facility, for assistance with the SEM-EDS analysis.
- Special thanks to Cape Peninsula University of Technology staff – Mrs Dawn Petersen (admin), Mrs Zandile Mthembu, Gillian Fennessy-Yon (Technical), and Mrs Shaheeda Adonis (lecturing staff), for their continual support, encouragement, and advice throughout the postgraduate journey.

The financial assistance of the National Research Foundation towards this research is acknowledged. Opinions expressed in this thesis and the conclusions arrived at, are those of the author, and are not necessarily to be attributed to the National Research Foundation.

DEDICATION

I dedicate this work to my late Godfather Leslie Alfred Davis, and my parents Lindsay and Carolina Ford.

GLOSSARY

TERM	DEFINITION
Absorption	Absorption is a physical or chemical phenomenon or a process in which atoms, molecules or ions enter some bulk phase – liquid or solid material. This is a different process from adsorption since molecules undergoing absorption are taken up by the volume, not by the surface. (Imessaoudene et al., 2016)
Adsorption	Adsorption is the adhesion of atoms, ions or molecules from a gas, liquid or dissolved solid to a surface. (Imessaoudene et al., 2016)
Bioaccumulation	Bioaccumulation is the gradual accumulation of substances (generally via metabolic processes), such as pesticides or other chemicals, in an organism – as described by Volesky (2007)
Biosorption	Biosorption is a physiochemical process that occurs naturally in certain biomass which allows it to passively concentrate and bind contaminants onto its cellular structure. (Gadd, 2009)

TABLE OF CONTENTS

LIST OF FIGURES

LIST OF TABLES

ACRONYMS & ABBREVIATIONS	Definition
ANOVA	Analysis Variance
Cd	Elemental symbol for cadmium
EDS	Energy dispersive x-ray spectroscopy
FEG-SEM	Field emission gun scanning electron microscope
FTIR	Fourier-transform infrared
ICDD	International Centre for Diffraction Data
ICP-OES	Inductively coupled plasma optical emission spectroscopy
Ni	Elemental symbol for nickel
RPM	Revolutions per minute
SCG	Spent coffee grounds
SEM	Scanning electron microscopy
SPE	Solid-phase extraction
SFE	Supercritical fluid extraction
SSE	Sum of squares error
UCG	Unwashed coffee grounds
WCG	Washed coffee grounds
WHO	World health organisation
XRD	X-ray Diffraction

APPENDICES

CHAPTER 1
INTRODUCTION

1.1 Background

Heavy metals and dyes are reported to be among the most concerning environmental pollutants to date. Since heavy metal ion pollutants, in general, cannot be degraded and destroyed, these pose severe health threats to fauna, flora and human beings alike (Naga Babu et al., 2018). Cadmium (Cd) and nickel (Ni) are known to be major pollutants of surface and groundwater emanating from mining-rich regions within South Africa (Rahimzadeh et al., 2017). The need to rid these waters of these highly toxic pollutants is imperative as the water is used by surrounding communities.

Nickel is a lustrous white, hard, ferromagnetic metal with a specific density of 8.90 $g \cdot cm^{-3}$ at 25 °C and has a melting point of 1 555 °C. Nickel generally has an oxidation state of 2+, but oxidation states of 1+, 3+ and 4+ can also exist in nature. The metal occurs predominantly in the hydrated form as $Ni(H_2O)_6^{2+}$. Acetate, chloride, nitrate, and sulphate salts of Ni are soluble in water whereas carbonates and hydroxides are not as soluble. Nickel can enter the body not only through inhalation and ingestion, but traces of the element can enter by means of simple skin contact. Upon entering the body, there is a risk of the metal accumulating in major organs that can cause cardiovascular and kidney disease. One of the principal sources of Ni pollution in drinking water is from water which originates via leaching from a metal source in contact with a water source. Acid rain may also influence the mobility of Ni and can lead to an increase in soluble Ni content in underground water sources.

Similarly, Cd can enter the human body by the ingestion of Cd polluted water or food, the inhalation of tobacco smoke, or from Cd - contaminated air. Cadmium is absorbed through the gastrointestinal tract and its solubility is influenced by intestinal pH (Rahimzadeh et al., 2017). The metal accumulates predominantly in the liver and kidneys. Exposure to the element raises health concerns which include acute toxicity, cancer, pregnancy complications, kidney problems or even death. Recent studies also reported that Cd can adversely affect the reproductive and cardiovascular systems (Rahimzadeh et al., 2017).

Over the last decade, biosorption has been gaining popularity as an alternative to man-made heavy metal adsorbents for the treatment of heavy metal and dye contaminated wastewaters.

Bio-sorbents such as bacteria, fungi and algae (Gadd, 2009), cellulose driven materials (Park et al., 2010), eggshells (Rao et al., 2010), cow dung (Imessaoudene et al., 2013), industrial wastes (Mussatto et al., 2012), rice husks (Dávila-Guzmán et al., 2013) and agricultural wastes (Hardgrove & Livesley, 2016) have been investigated for their ability to remove heavy metals from polluted sources Primarily, adsorbents such as activated carbons and ion exchange resins have been dominating this industry but these processes are costly. Biosorption using non-living biomass represents only one application of the bioaccumulation process. Biosorption is considered to be easier and more practical for industrial application than is the more complex phenomenon of bioaccumulation itself. Bioaccumulation is based on *"active metabolic transport"* using complex bioreactor systems that contain viable microorganisms. In a scientific review paper by Volesky (2007), biosorption was defined as *"the property of certain biomolecules or biomass to bind and concentrate selected ions or other molecules from aqueous solutions"*. Biosorption by nonviable biomass is reported to occur mainly due to the affinity between the biomass and adsorbate molecules as well as active functional groups. In agreement with numerous review papers, Park et al. (2010) reported that the oldest- studies on heavy metal biosorption were done by L. Hecke in 1902, who made use of fungal spores to investigate copper uptake by viable microorganisms.

The use of waste biomass as an eco-friendly sorbent for the removal of heavy metals and other pollutants from the environment is becoming popular worldwide. In the last decade, an exponential increase in publications that refer to the alternate uses for spent coffee grounds (SCG) has been noted. Reported alternative uses for SCG include; as a bio-sorbent for heavy metal adsorption (Tokimoto et al., 2005; Utomo & Hunter, 2006; Davila-Guzman et al., 2016), for ethanol production by fermentation (Mussatto et al., 2012) and as a source of lipids and polysaccharides (Massaya et al., 2019). It has also been reported that when mixed directly with soil, SCG retard plant growth (Hardgrove and Livesey, 2016). To date, there are no industrial processes in which SCG are re-utilised. This is appalling, considering that coffee, after petroleum, is reported to be the world's second-largest traded commodity (Mussatto, Machado, et al., 2011).

Most of the proposed work relating to SCG has only been verified and conducted on a laboratory scale. Published work indicates that SCG show great promise as a bio-sorbent for the adsorption of heavy metals and could very well rival traditional adsorbents such as activated carbon and ion-exchange resins. Understanding the underlying mechanisms of the biosorption process using this inexpensive waste material is therefore crucial.

1.2 Problem statement

Heavy metals such as Cd and Ni are major contributors to environmental pollution. Emissions and effluents from the electroplating, ammunition, paint & pigment, and mining industries are all possible sites of contamination from which these two metals enter the environment (Rahimzadeh et al., 2017). In addition, activities such as the use of pesticides, wastewater irrigation and the spillage of petrochemicals are known sources of heavy metal pollution.

Finding efficient methods of separating and isolating heavy metals using an environmentally friendly approach may not only be beneficial but deemed necessary as there are mandatory legislative requirements in place pertinent to dealing with environmental pollution. Section 24 of the South African constitution states; "*everyone has the right to an environment that is not harmful to their health or well-being*". Ion exchange resins have been extensively used as sorbents for heavy metal ion removal, but these are expensive when compared with biowastes. Furthermore, the detailed chemistry of the heavy metal biosorption process and adsorption mechanism when using SCG are not yet well understood and are generally poorly discussed and need to be elucidated (Anastopoulos et al., 2017).

This investigation, therefore, aims to explore the separation of the heavy metals Cd and Ni from synthetic mixtures with the goal of separating these from binary mixtures using SCG as a bio-sorbent.

1.3 Objectives

This study intends to report on the sorption mechanisms of the heavy metals Cd and Ni onto SCG before and after the grounds have been stripped of remaining oils and compounds by using Supercritical Fluid Extraction (SFE). Results obtained will then be compared with published research done elsewhere on the sorption capacity of untreated SCG.

The effects of the following parameters on the sorption capacity of the sorbent will be investigated:

- pH of the analyte solution,
- initial concentration of the metal ions in solution,
- contact time of the metal ion with the sorbent,
- temperature of the sorption solution, and
- sorbent dosage.

Sorption equilibrium data will be collected and applied to two isotherm models, namely the Langmuir and Freundlich isotherms. Sorption kinetics data will be applied to two kinetic models, namely the Lagergren pseudo-first order and Ho & McKay pseudo-second order. Linear as well as non-linear regression methods, combined with statistical analysis (sum of squares error) will be used to determine which mathematical model best fits the experimental data. From these results, conclusions will be drawn as to the mechanism by which the metal ions are sorbed, i.e., whether via physical or chemical processes, monolayer, or multilayer coverage of the sorbent surface.

The surface morphology of the sorbent before and after sorption will be characterised using the following analytical techniques:

- Fourier-Transform Infrared (FTIR)
- Scanning Electron Microscopy (SEM)
- X-Ray Diffraction (XRD)

1.4 Delimitations

Further analysis of the extract obtained from the supercritical fluid extraction process will not be considered in this study. The desorption/stripping of the metal from the sorbent will not be investigated.

1.5 Research questions

- Can SCG stripped of all remaining oils by means of SFE be used for the sorption of heavy metals cadmium and nickel?
- How does the sorption capacity of the SFE-SCG compare with that of SCG?
- What sorption mechanisms are followed for the sorption of the individual metals?

CHAPTER 2
LITERATURE REVIEW

This chapter highlights recent scientific research on the use of coffee as a bio-sorbent for the removal of heavy metal ions from aqueous solutions.

2.1 A brief history of coffee

Coffee is known universally as the hot caffeine-containing beverage of choice. The coffee tree/shrub belongs to the Rubiaceae[1] family and subfamily Ixoriadeae[2]. According to the ISO 3509:2005[3] vocabulary, coffee is defined as: “Fruits and seeds of plants of the genus *Coffea*, usually of the cultivated species, and the products of these fruits and seeds, in different stages of processing and use intended for human consumption”. The coffee peel, husks and pulp (figure 2.1) amount to approximately 45 % of the cherry mass (Campos-Vega et al., 2015).

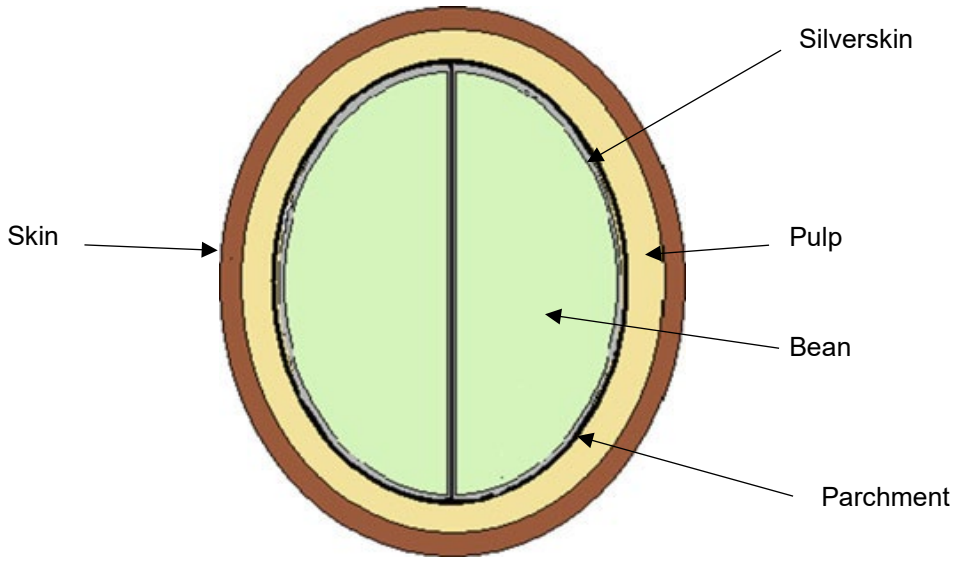

Figure 2.1: Longitudinal cross-section representation of the coffee cherry adapted from (Mussatto, et al., 2011)

The SCG are the organic residue that remain after the raw coffee bean has been brewed. Spent grounds are also obtained in large quantities during the industrial manufacturing of instant “soluble” coffee. After water, coffee is the world’s second most consumed beverage (Atabani et al., 2019), and instant coffee comprises 50 % of global coffee consumption.

[1] The Reubiaceae are a family of flowering plants, tropical herbs, shrubs, and trees.
[2] Ixoriadeae are a large genus of tropical shrubs or small trees.
[3] ISO 3509:2005 defines the most used terms relating to coffee and its products.

It is known that 2 kg of SCG are generated for each kg of instant coffee produced (Somnuk et al., 2017).

A review paper by Anastopoulos et al. (2017) on statistical findings published by the United States Department of Agriculture (USDA) regarding coffee production between 2012-2013, states that approximately 150 million 60 kg bags (or 9 billion tons) of coffee were produced during this period. The authors corroborated findings by Mussatto, Machado, et al. (2011), that 1 kg of green coffee beans generates between 60 % to 65 % SCG as waste. Anastopoulos et al. (2017) concluded that there are three main by-products generated by the coffee industry, namely spent coffee grounds (SCG), coffee silverskin (CS) and coffee husks. The CS is obtained as a by-product of the roasting process whereas SCG are obtained from the treatment of raw coffee with steam or hot water for the preparation of instant coffee.

2.2 Chemical composition of coffee

Exhausted coffee, along with many other organic materials such as bark, zeolites and clays are tannin-containing materials. Tannins are defined as "*a class of astringent, polyhydroxy, polyphenolic biomolecules that bind and precipitate proteins*" (Savolainen, 1992). According to Campos-Vega et al. (2015), materials that contain these acidic functional groups are very effective in binding cations. Tannins are also reported to bind to numerous other organic compounds including amino acids and alkaloids (see figure 2.2).

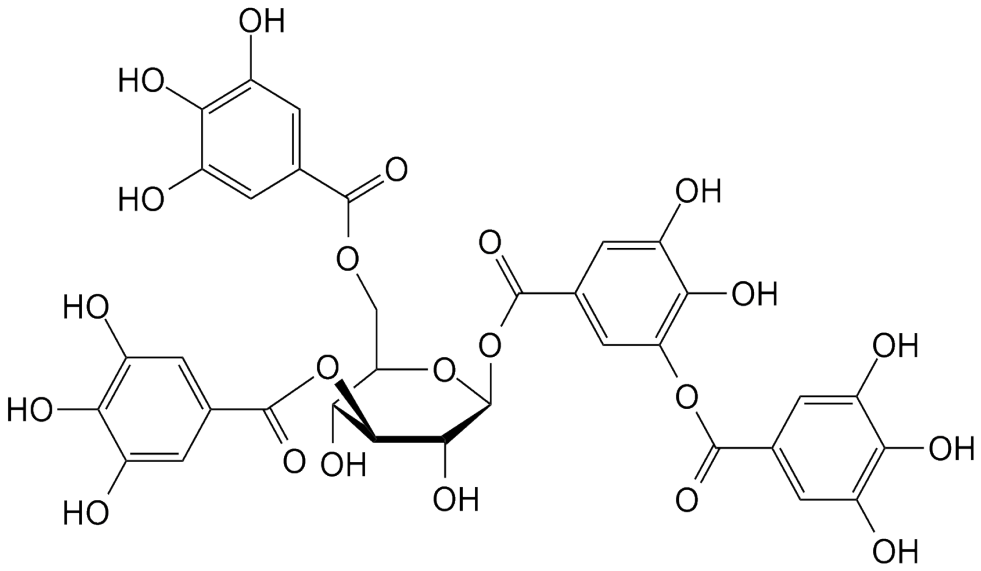

Figure 2.2: Chemical structure of tannic acid
(Savolainen, 1992)

Similarly, weak basic functional groups such as amides and amines are also effective in adsorbing metal ions. Although coffee beans are reported to contain several other components such as sugars (*sucrose, glucose, fructose, galactose, arabinose & mannose*), lipids, minerals (*K, Mg, Ca, Na, Fe, Ti, Cd, Co, Ni, Cu)* and polyphenols (Belitz et al., 2004), coffee is known particularly for its caffeine content. Figure 2.3 shows the structural formula of caffeine.

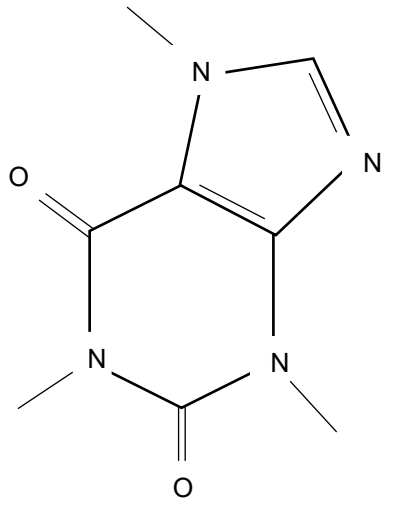

Figure 2.3*:* The Structural formula of caffeine

.

Polysaccharides are the most abundant chemical compound found in coffee, comprising approximately 50 % of the unbrewed green beans' dry mass. Lipids are the second most common. A review paper by Campos-Vega et al. (2015), cited work by Mussatto, Carneiro, et al. (2011) who stated that SCG contain a high concentration of sugars. Approximately 45 % w/w of the dry weight of SCG is polymerized (cellulose and hemicellulose) sugar content, of which 46.8 % mannose, 30.4 % galactose, 19 % glucose and 3.8 % arabinose. Elsewhere, Mussatto et al., (2012) published slightly different results, claiming SCG is comprised of 21.2 % mannose, 13.8 % galactose, 8.6 % glucose, and 1.7 % arabinose. In another study, Simões et al. (2009), reported the sugar content of SCG was 57 %, 26 %, 11 % & 6 % for mannose, galactose, glucose, and arabinose, respectively. These anomalies may be attributed to the different types of beans investigated. The differences in the beans can be attributed to many factors, such as the harvest and environmental growing conditions of the plants (temperature, humidity, altitude) (Oestreich-Janzen, 2010).

2.3 Heavy metal extraction methods

Traditional methods for trace metal recovery include fractional crystallization, solvent extraction, co-precipitation, and more recently solid-phase extraction (SPE) (Spies & Wewers, 2020). The SPE has a few advantages over traditional methods. These are that SPE is highly selective, has a short analysis time and is simple to apply. Solid-phase extraction uses the affinity of the solutes in the matrix (mobile phase) for solid support to separate the desired and undesired components from the matrix. The analyte can be introduced to the solid either by batch or column methods.

In the case of the column method, a column is used to separate the analyte from the solution (mobile phase) where the affinity of the sorbate to the sorbent is known. The analyte either passes through the column or is retained on the stationary phase/solid support. If the analyte is retained on the stationary phase, it can be removed by rinsing/washing with an appropriate eluent which is generally a dilute acid. Figure 2.4 illustrates the SPE process using the column method.

For batch method reactions the analyte and solid phase are shaken for a predetermined time in the same container.

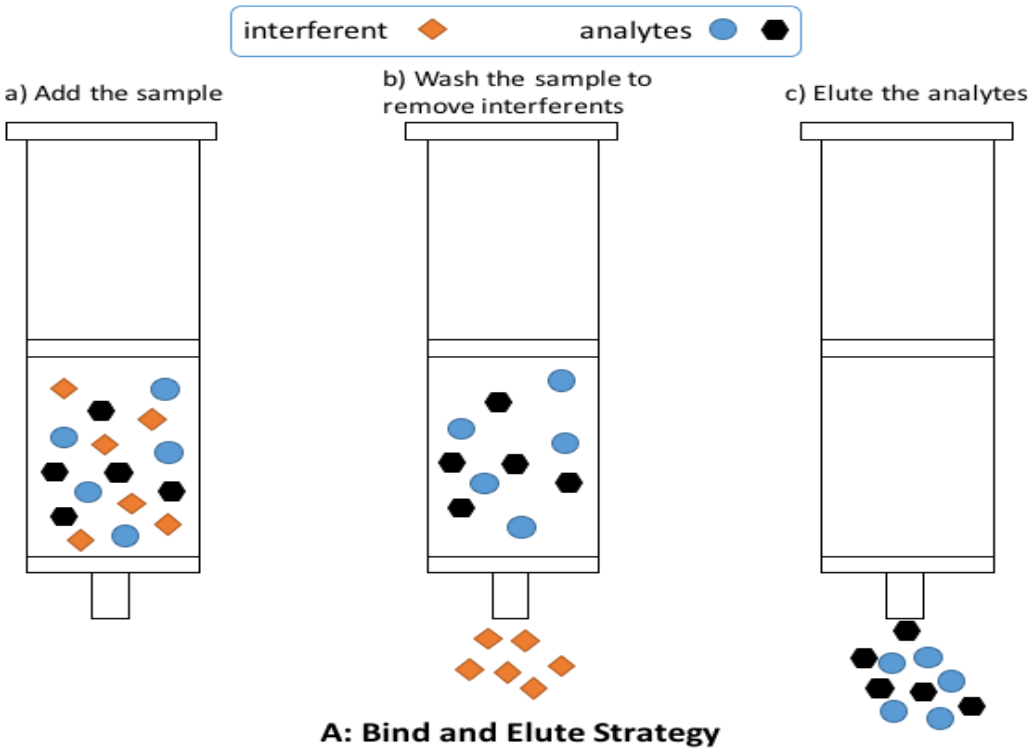

Figure 2.4: SPE via column method (adapted from Google Scholar, date accessed: 05/08/2020)

Although traditional extraction methods are known to work effectively, recent trends seem to pursue “greener” alternatives. This is evident from the increasing number of publications reporting on biosorption, a relatively new and environmentally friendly method for heavy metal contaminant removal.

The advantages of bio-sorbents are:

- simple operation,
- low operational cost,
- ability to remove metals from very dilute solutions and
- high efficiency

A disadvantage of bio-sorbents is that they are difficult to regenerate (Sameera et al., 2011)

Despite its potential for use in industrial applications, biosorption has to date only been investigated at laboratory scale levels (Park et al., 2010).

2.4 Review of SCG based adsorption studies

A search for the keywords "spent coffee grounds" on Scopus generated 604 articles. The first article was published in 1977. Of these articles, 96 % were published in the last decade (2010 – 2020), 284 of which were published in 2019/2020.

A survey of the most recent relevant literature revealed a bias towards environmental studies; SCG are predominantly used for the extraction of metals from wastewater. Multiple studies using different forms of coffee (*spent coffee grounds, coffee husks, coffee silverskin*) focus on the same metals namely Pb, Cu, Zn, Cd and Hg (Mussatto, Machado, et al., 2011). Ayala and Fernández (2019) investigated the removal of Ca, Na, K, Mg, Cu, Cd, Ni and Zn from waste leachate by means of batch experiments using SCG as the solid support. These authors investigated parameters such as pH dependence, metal and adsorbate contact time, initial metal ion concentration, adsorbate concertation, particle size and the effect of co-ions. They reported that adsorption was significantly affected by pH, where a pH range of 5 – 7 showed the highest affinity for metal uptake. The particle size of the adsorbent did not seem to influence the sorption capacity. Furthermore, they found the adsorption of the heavy metals to fit Langmuir and Freundlich isotherms. Equilibrium was reached within three hours, with 75 % of the total sorption achieved within the first minutes. A comparison of washed coffee grounds (WCG) and unwashed coffee grounds (UCG) proved UCG to have a greater sorption capacity for Zn (10.22 $mg \cdot g^{-1}$ *cf* 5.36 $mg \cdot g^{-1}$), Cd (5.96 $mg \cdot g^{-1}$ *cf* 4.28 $mg \cdot g^{-1}$) and Ni (7.51 $mg \cdot g^{-1}$ *cf* 4.37 $mg \cdot g^{-1}$).

The authors reported that as the pH increased, sorption improved, and this was attributed to the "simultaneous and competitive" sorption of H^+ ions.

Utomo and Hunter (2006) examined heavy metal adsorption onto chemically modified coffee grounds and proved it to be efficient over a wide pH range (4 – 8). They claimed the adsorbed metals were easily eluted with dilute acid (0.1 M HCl). Furthermore, the exhausted coffee grounds were reported to maintain their adsorptive properties without significant loss of their adsorptive capacity. They confirmed previous studies that highlighted the potential of exhausted coffee, Turkish coffee, and walnut shells for heavy metal removal. A study by Alpat et al. (2010) demonstrated that the washing of coffee wastes such as SCG and CS with deionised water as pre-treatment was sufficient and that no modification was necessary. In their investigation, the authors employed SCG for Cu^{2+} and Cd^{2+} removal from aqueous solutions using batch methods.

Qaiser et al. (2007), who investigated the effects of temperature on the sorption capacity of bio-sorbents for Ni in the range 20 °C – 40 °C reported that sorption capacity increased with increasing temperature. However, sorption decreased between 40 °C and 60 °C. This was believed to occur due to an increase in the number of potential binding sites and an upsurge in porosity that ultimately led to an overall pore volume increase of the adsorbent. Similar findings were reported by both Alpat et al. (2010) who used *Circinella* sp[4] as a bio-sorbent and Anastopoulos et al. (2017) who investigated the use of dyes as sorbents. This decrease in sorption was claimed to occur due to a decrease in the thickness of the boundary layer as temperature increased.

Azouaou et al. (2010) investigated the effect of pH on the adsorption of Cd^{2+} onto SCG within the pH range 2.5 – 7.5. An optimum sorbate dosage of 9 g at pH 7 was reported, with a sharp adsorption rate occurring between pH 2.5 – 3.5. They ascribed the rapid initial adsorption to the interaction of the sorbate with the cell wall functional groups of the SCG. They further concluded that the percentage of metal ion removal increased with increasing adsorbent dosage until a plateau was reached after 120 minutes when using 9 g sorbent and an initial metal ion concentration of 100 $mg \cdot L^{-1}$. Under these conditions, Cd^{2+} sorption onto SCG was exothermic and followed second-order kinetics. The maximum sorption capacity derived from the Langmuir isotherm was 15.65 $mg \cdot g^{-1}$. Patterer et al. (2017) also investigated the sorption of Cd^{2+} onto untreated coffee grounds and reported a sorption capacity (q_{max} = 4.48 $mg \cdot g^{-1}$), three times less than that of Azouaou et al. (2010).

[4] *Circinella* species comprise a small portion of the fungal biota.

The high theoretical sorption capacity obtained by Azouaou and co-workers may be attributed to the high initial concentration values used for their investigation. Concentration ranges of 10 mg·L^{-1} to 700 mg·L^{-1} were used.

Dávila-Guzmán et al. (2013) investigated the uptake of copper ions by SCG by means of batch experiments using varying metal ion concentrations (0.1 – 1 mmol) and stirring speeds (100 – 400 rpm). They found that the Cu^{2+} uptake best fitted the Freundlich isotherm and claimed that the maximum adsorption capacity of SCG was considerably greater (2 – 3-fold) than other adsorbents such as activated carbon. A later study by the same group reported maximum sorption of 0.12, 0.21 and 0.32 mmol·g^{-1} for Cd^{2+}, Cu^{2+} and Pb^{2+} onto SCG, respectively. Dilute HNO_3, $CaCl_2$ and $C_6H_8O_7$ were used to desorb the metal, and nitric acid proved to be most effective, and $C_6H_8O_7$ the least effective eluents. In a later study, Gomez-Gonzalez et al. (2016) conducted batch experiments using 0.2 g – 1.2 g SCG with a predetermined amount of stock metal (Pb) solution at pH 5. The solution was agitated over a period of five days. A maximum sorption capacity of 22.9 mg of Pb per gram of SCG at optimum pH 5 was achieved.

Elsewhere, Prabhakaran et al. (2009), reported that sorption of Cr^{4+} ions onto activated carbon followed pseudo-second-order kinetics and was believed to occur mainly by means of film diffusion and intra-particle diffusion mechanisms. The Cr^{4+} adsorption was found to reach maximum at pH 4. The Cr^{4+} uptake by untreated SCG was also investigated by Bhuvaneshwari and Sivasubramanian (2014) using the column method. They reported the reaction followed pseudo-second-order kinetics with optimum adsorption occurring at pH 4.

Imessaoudene et al. (2013) investigated the biosorption of strontium (Sr^{2+}) onto SCG. Their method involved rinsing the SCG with deionised water followed by air drying for 24 hours. The SCG were then dried at 80 °C for another 24 hours. They reported an optimum pH of 4 using a sorbent dosage of 10 g·L^{-1} and postulated that particle size had no significant influence on the adsorption capacity. The same authors later examined the effect of contact time on the removal of Co^{2+} ions in the range of 0 to 120 minutes (Imessaoudene et al., 2016). They concluded that the metal adsorption had to be physical in nature due to a high initial adsorption rate that was reached relatively early in the reaction. An extension of the reaction time to 120 minutes did not seem to improve the percentage uptake either – all indications of an equilibrium state. The thermodynamic parameters of the adsorption of Co^{2+} on the SCG were reported as $\Delta G° < 0$ (the reaction is spontaneous), $\Delta S° > 0$, $\Delta H° < 0$ (exothermic), with low activation energy (E_a = 10.992 kJ.mol^{-1}), suggesting physisorption.

2.5 Temperature-dependence of sorption

By investigating the sorption process over a given temperature range, additional information about the sorption mechanisms can be obtained and used to distinguish whether sorption is controlled by reactions or diffusion processes. Sorption energy values between 25 – 30 $kJ \cdot mol^{-1}$ imply that sorption onto the solid support is controlled by diffusion mechanisms, whereas energy values above 25 – 30 $kJ \cdot mol^{-1}$ indicate that the sorption is reaction controlled (Azouaou et al., 2010). In addition, the sorption process can be described quantitatively by thermodynamic parameters such as $\Delta H°$ (enthalpy change) $\Delta S°$ (entropy change) and $\Delta G°$ (Gibbs free energy). At constant temperature and pressure, the Gibbs free energy provides crucial information regarding the spontaneity of the sorption. If the Gibbs free energy is negative at a given temperature and pressure, it can be concluded that the reaction is spontaneous under those conditions (Park et al., 2010). A detailed description of the thermodynamic equations and calculations are outlined in chapter 3 below.

2.6 Time-dependence of sorption

Sorption kinetics deal with the time it takes for a reaction to reach equilibrium (completion of the reaction). It involves investigations as to how experimental conditions influence the speed of a reaction and provides insight into the reaction mechanisms from which rate laws and rate constants can be derived. Various mathematical models (sorption diffusion models) have been designed to describe the kinetic process of the sorption of metal onto a solid surface. The kinetic process of sorption can be classified by reaction models or diffusion models (Spies & Wewers, 2020). Diffusion can occur in three ways depending on the conditions of the reaction: (i) pore diffusion, (ii) bulk diffusion or (iii) film diffusion. According to Spies and Wewers (2020), bulk diffusion is easily controlled and considered negligible. Film diffusion can be influenced by rigorous stirring to the extent that it can also be considered negligible; hence bulk diffusion (intra-particle diffusion) is considered the rate-controlling mechanism. Figure 2.5 is a schematic illustration of the diffusion processes:

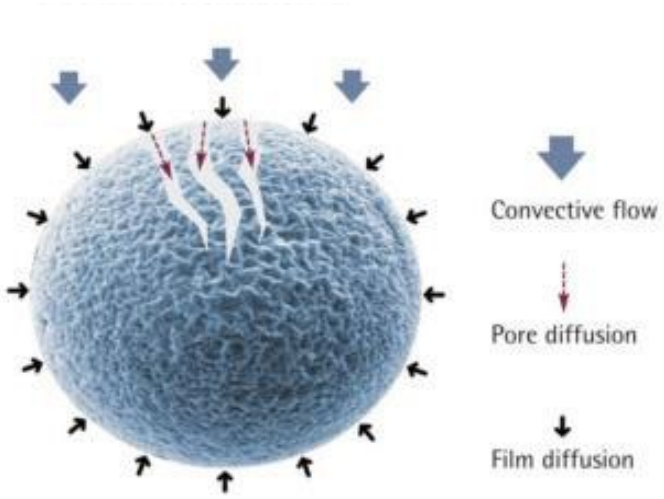

Figure 2.5: A schematic illustration of three types of diffusion processes -adapted from (Spies & Wewers, 2020)

In figure 2.5, corrective flow represents bulk diffusion. Sorption reaction models that describe the chemical reaction kinetics are centred on the entire process of sorption and do not take into account the diffusion reaction models mentioned above.

If equilibrium is reached in less than three hours, it can be deduced that the reaction is kinetically controlled. If reaction equilibrium is reached after 24 hours the reaction is considered diffusion-controlled (Spies & Wewers, 2020). Between 3 and 24 hours, either of the two mechanisms can be the rate-controlling step. Equations used to model sorption reaction kinetics include pseudo-first and pseudo-second-order reactions. The prefix “pseudo” means to “mimic”, hence, a pseudo-first-order reaction is therefore not a true first-order reaction by nature. A detailed description of the pseudo-first and pseudo-second-order reaction equations is outlined in chapter 3 (methodology).

2.7 Sorption equilibrium

The relationship between the amount of solute sorbed and that remaining in the sorbate medium at equilibrium (q_e) is described by sorption isotherms. Isotherms give valuable information regarding the nature of the sorption mechanism. i.e., whether it occurred by a chemical reaction (chemisorption) or as a result of long-range, weak van der Waals forces between the sorbate and the sorbent (physisorption). In addition, chemisorption is believed to occur in a monolayer fashion while physisorption is believed to occur in a multilayer fashion. Most known isotherms are Langmuir and Freundlich.

The Langmuir isotherm can be associated with chemisorption while the Freundlich isotherm is associated with multilayer sorption (physisorption). To date, there are more than 20 different isotherm models that have been developed (Albadarin and Mangwandi, 2015). For this study, the Langmuir and Freundlich isotherms were applied and used to describe the sorption processes. A detailed description of the Langmuir and Freundlich isotherm formulae is presented below.

2.7.1 Langmuir isotherm

The Langmuir adsorption model was the brainchild of Irvin Langmuir in 1916, for which he received the Nobel Prize in 1932 for his work concerning surface chemistry. Langmuir hypothesised that any given surface has a specific number of sites that a given species can "adhere" or "stick" to by either chemisorption or physisorption. The Langmuir isotherm quantitatively describes the formation of a monolayer sorbate on the surface of the solid.

The linear form of the Langmuir isotherm can be written as:

$$\frac{C_e}{q_e} = \left(\frac{1}{K_L Q_o}\right) + \left(\frac{1}{Q_o}\right) C_e \qquad (2.1)$$

[Where: C_e = equilibrium concentration of the sorbate ($mg \cdot L^{-1}$), Q_o = maximum monolayer sorption capacity ($mg \cdot g^{-1}$), q_e = experimental equilibrium sorption capacity ($mg \cdot g^{-1}$) and K_L = binding strength ($L \cdot mg^{-1}$).]

The Langmuir isotherm model implies monolayer sorption over a theoretically homogenous sorbent surface. From the Langmuir equation the theoretical maximum monolayer sorption (Qo), the binding strength (K_L) and the separation factor (R_L) can be calculated using the formulae 2.2, 2.3 and 2.4 respectively:

$$\frac{1}{Q_o} = gradient \qquad (2.2)$$

The theoretical sorption capacity can be compared with the experimental value to establish whether any errors occurred during the analysis.

The binding strength, K_L, can be calculated using:

$$\frac{1}{Q_O \times \mathrm{K_L}} = \text{ intercept}$$

$$\downarrow$$

$$K_L = \frac{1}{intercept \times Q_O} \qquad (2.3)$$

From the binding strength $K_{L,}$ the separation factor R_L can be calculated using:

$$R_L = \frac{1}{1+K_L C_o} \tag{2.4}$$

If $R_L > 1$ the reaction is unfavourable, $R_L = 1$ is linear; $R_L = 0$ is irreversible and $0 < R_L < 1$ is favourable.

2.7.2 Freundlich isotherm

Various research articles report that Freundlich and Kuster published the first mathematical isotherm in 1906 (Spies & Wewers, 2020). It is a purely empirical formula for gaseous adsorbates. In contrast to the Langmuir isotherm, the Freundlich isotherm suggests that sorption occurs in a multilayer fashion on a heterogeneous surface. The Freundlich isotherm is suitable for a particularly heterogeneous surface and a sorption isotherm lacking a sorption plateau. The general expression of the Freundlich isotherm provides a mathematical description of the surface heterogeneity.

$$q_e = K_F {C_e}^{1/n} \tag{2.5}$$

Where:

- K_F is a constant
- *n* is a constant ($n > 1$)

The logarithmic form of the Freundlich isotherm is more useful, as data fitted to the logarithmic form generate a straight line with intercept K_F (at $C_e = 0$) and slope 1/n

$$\log q_e = \frac{1}{n} \log C_e + \log K_F \tag{2.6}$$

The Langmuir and Freundlich isotherms are useful principally for simulating data collected at a fixed pH and are less easily applied to pH-dependent adsorption studies (Jeppu and Clement, 2012).

CHAPTER 3
METHODOLOGY

An exhaustive review of the relevant literature revealed that to date, there is no research which reports on the use of supercritical fluid extraction (SFE) to extract oils from spent coffee grounds (SCG) prior to the latter being used as a sorbent. Subsequently in the current study, the sorption mechanisms of heavy metals onto SCG after SFE were investigated.

Multiple publications list pH as the most important parameter when investigating heavy metal adsorption onto a solid surface; hence, it was decided to conduct the pH dependence studies first. After obtaining the optimum pH for the respective metals, the remaining parameters (sorbent dosage, initial metal concentration, time dependence and temperature dependence) were then investigated at the optimum pH as determined. This chapter provides a broad overview of the instrumentation used for characterisation and analysis. It describes in detail how the sorbent was prepared, how sorption parameters were investigated and how calibration standards, stock solutions and working solutions were prepared for experimental procedures and analysis.

3.1 Instrumentation

3.1.1 Supercritical fluid extraction (SFE) vessel

The spent coffee grounds were stripped of their remaining oils in a 5.5 L pressure vessel (SEPAREX) using supercritical CO_2 extraction, with a service temperature of 20 - 250 °C, design temperature of 20 - 300 °C, service pressure of 0 – 800 bar and design pressure of 0 – 1150 bar.

The actual experimental parameters used during this investigation were 40 °C, 2 bar pressure with an extraction time of 1 hour per extraction. Initial extraction of oils was conducted on the SCG as supplied. The sorbent was then rinsed with de-ionised H_2O post CO_2 extraction until the runoff was clear. The sorbent in this form was then used for batch sorption experiments.

3.1.2 Inductively coupled plasma optical emission spectroscopy (ICP-OES)

The metal ion content of all solutions was determined using a Spectro^{TM} ACROS ICP-OES spectrometer with Smart Analyzer Vision software.

The ICP was selected for metal analysis because of its satisfactory detection limits and because the method is suitable for multi-element analysis.

Analyses were conducted over multiple recommended wavelengths and the optimum wavelength was selected based on the lowest detection limit (DL), background equivalent concentration (BEC) and relative standard deviation (RSD). All measurements were done in triplicate and the average value was recorded. The operating parameters of the instrument are listed in Table 3.1.

Table 3.1: ICP operating parameters

RF Power	1400 W
Argon Flow	12 $L \cdot min^{-1}$
Auxiliary flow	1.0 $L \cdot min^{-1}$
Nebuliser	0.8 $L \cdot min^{-1}$
Peristaltic Pump	63 rpm

3.1.3 pH meters and orbital shaker

The pH measurements were performed using a Crison GLP 21+, Lasec (South Africa) pH meter that was calibrated daily before use with pH buffers 4, 7 and 9, respectively. Batch experiments were conducted on an automatic orbital platform shaker (Labotec model 262). Temperature-dependent studies were conducted using an incubating orbital shaker from Labcon.

3.1.4 Attenuated total reflection – Fourier transform infrared (ATR-FTIR)

The PerkinElmer UATR Spectrum Two fitted with a diamond crystal was used to characterise the sorbent before and after sorption experiments.

3.1.5 Scanning electron microscopy (SEM)

Surface morphological studies were performed using a Zeiss MERLIN Field Emission Scanning Electron Microscope; Zeiss Smart SEM software was used to generate backscattered electron images.

3.1.6 Energy dispersive spectroscopy (EDS)

The samples were chemically quantified by using semi-quantitative Energy Dispersive X-Ray Spectrometry (EDS) using an Oxford Instrument® X-Max 20 mm^2 detector and Oxford Aztec software at the Electron Microbeam Unit of Stellenbosch University's central analytical facility.

3.1.7 Power x-ray diffraction (PXRD)

Confirmation of sorption was done by XRD analyses using a Bruker PXRD with Lynexe detector, Cu tube @ 1.54 A°, 30kV and 10 Amp current. The SCG before and after sorption with Cd and Ni were analyzed and the results were interpreted using OriginPro® software for comparison of peaks with those of the International Center for Diffraction Data (ICDD) reference spectra.

The SCG sample (1 g) was analysed by PXRD to confirm the sorption of the metal by the sorbent. The results were analysed using Excel for the comparison of peaks.

3.2 Reagents and solutions

3.2.1 Sorbent sampling and preparation

The SCG were collected at a coffee kiosk situated on the Cape Peninsula University of Technology Campus (Bellville). A single batch of approximately 3 kg of wet SCG was obtained. The SCG were stripped of remaining oils in two successive extractions using supercritical CO_2 extraction at 40 °C and 2 bar. Approximately 1 kg of oven dried SCG were put into the pressure vessel and the extract was collected in a glass autoclavable sample jar. The SCG were then rinsed with de-ionised H_2O and dried overnight at approximately 60 °C in an oven to remove excess moisture. The dried SCG were sifted through a 180-micron screen and collected on a 150-micron screen. The sifted SCG were stored in a cleaned beaker and sealed with parafilm. SCG not subjected to SFE was also stored in a clean beaker and sealed with parafilm for later characterisation.

3.2.2 Stock solutions

All reagents used were of analytical grade. Metal ions of Cd and Ni were obtained from their respective salts; CdO and $NiCl_2$ and were supplied by BDH Chemicals Ltd and Merck (SA) Pty (Ltd) for Cd and Ni, respectively. Deionised water was obtained from the Millipore-MilliQ apparatus and was used in the preparation of all solutions. Stock solutions (1000 $mg \cdot L^{-1}$) were initially prepared and appropriately diluted to obtain concentrations of the working solutions.

Stock solutions of Cd(II) were prepared by dissolving 0.2856 g CdO in dilute HNO_3 and filled to the 250 mL mark with deionised H_2O. Similarly, Ni(II) stock solutions were prepared by dissolving 1.0125 g $NiCl{\cdot}6H_2O$ in 250 mL deionised H_2O.

3.2.3 Calibration standards

Cadmium and nickel ICP standard solutions (1000 $mg{\cdot}L^{-1}$) were obtained from $Cd(SO_4)$ and $Ni(NO_3)_2$ in 0.5 $mol{\cdot}L^{-1}$ HNO_3. These solutions were diluted sequentially to obtain calibration standards of 2, 4, 6, 8, 10 and 12 $mg{\cdot}L^{-1}$. The dilution formula was applied to determine the volume necessary to prepare each calibration standard. The required volume of 1000 $mg{\cdot}L^{-1}$ standard solution was measured and transferred to a 50 mL volumetric flask and filled to the mark using 5% analytical grade nitric acid. The calibration control was 5% nitric acid.
Dilution formula:

$$C_1V_1 = C_2V_2 \quad (3.1)$$

Where:

- C_1 & C_2 = initial and final concentrations respectively
- V_1 & V_2 = Initial and final volumes respectively

3.2.4 Working solutions

Each working solution was prepared from the stock solution by accurately measuring the calculated volume of the stock solution and transferring it quantitatively to a 50 mL volumetric flask. To the same volumetric flask, 25 mL of the desired buffer solution were added and filled to the mark with deionised water. The contents of this volumetric flask were then transferred to a plastic sample holder containing the weighed sorbent for batch experiments. An image of the working solutions used during this study is shown in Appendix J.

3.2.5 Preparation of buffers

Buffers of pH 1 and pH 2 were prepared using hydrochloric acid and potassium chloride. Buffers pH 3 to 6 were also prepared using different ratios of acetic acid and sodium acetate. Table 3.2 shows the quantities of acid and conjugate base that were used to prepare each buffer.

Table 3.2: Acid ratios used to prepare buffers 1 to 6

pH	**Volume HCl** (mL)	**Mass KCl** (g)
1	0.659	0.3725
2	0.064	0.3725
	Volume CH_3COOH (mL)	**Mass CH_3COONa** (g)
3	0.562	0.0145
4	0.485	0.1255
5	0.204	0.5275
6	0.029	0.6955

The pH of each buffer was verified before adding to the metal-ion solution.

3.3 Procedures

3.3.1 Characterization of sorbent

The SCG were characterised by using five analytical methods: ATR-FTIR, PXRD, SEM, EDS, and ash content determination. A description of each characterisation technique is detailed below.

3.3.1.1 Attenuated total reflectance – Fourier transform infrared spectroscopy (ATR-FTIR)

The ATR-FTIR was used to study the surface properties and available functional groups involved in the adsorption mechanism. Surface functional groups of the sorbent are directly related to the affinity for the sorbate and provide information about the primary binding mechanism.

The SCG before and after adsorption were subjected to ATR-FTIR. To obtain a blank value for the instrument, the diamond crystal was cleaned using 90 % isopropyl alcohol solution. Once cleaned and dried, the control value was obtained by scanning the atmosphere to ensure that the diamond crystal was free of any solid or liquid contaminants. After the control value was obtained, sufficient spent coffee grounds were placed on the diamond crystal such that the entire surface was covered. The pressure arm was lowered onto the sample until a pressure limit of 50 % was reached. This allowed for satisfactory contact between the sample and diamond crystal.

3.3.1.2 Scanning electron microscopy (SEM) and Energy dispersive x-ray spectroscopy (EDS)

Sample preparation was done using ACE200 gold sputter. The sample was coated with a 10 nm layer of gold to ensure that the sample surface was electrically conductive. The operating conditions during the EDS quantitative analysis and backscattered electron imaging on the Zeiss MERLIN were 20 kV, 16 nA probe current, a working distance of 9.5 mm and a beam current of 11 nA. Due to the gold coating, gold was automatically excluded from the analysis.

3.3.1.3 Ash content determination

The ash content was determined by accurately weighing 5 g of the SFE-SCG into a ceramic crucible. Initially, the crucible was heated for approximately 30 minutes at 105 °C and then allowed to cool to room temperature in a desiccator containing silica gel. The mass of the crucible was recorded before and after the addition of the SCG and the mass of the SCG added was calculated by subtracting the actual mass of the crucible containing the SCG from the original crucible mass without SCG. The SCG were thoroughly dried to remove excess moisture content, prior to the ash content investigation. As the coffee had been subjected to high temperatures during the brewing process it was decided to dry the SCG overnight in an oven at approximately 90 °C.

The furnace was set to a maximum temperature of 500 °C with a heating rate of 10 °C per min. The SCG sample was placed in the furnace at exactly 12:00 PM CET and taken out of the furnace the next morning at exactly 8:00 AM CET. The crucible was allowed to cool to room temperature in a desiccator and the mass was recorded after 5 minutes of cooling.

The percentage inorganic content was calculated using the formula:

$$\%\ inorganic\ content = \frac{m_1 - m_2}{m_1} \times 100\ \% \qquad (3.2)$$

Where:

- m_1 = mass of SCG before being placed in the furnace
- m_2 = mass of SCG after 20 hours in the furnace

3.3.2 Sorption experiments

All adsorption experiments were conducted using the batch method. Reference samples were prepared for all concentrations and the concentration of the solutions were determined by ICP-

OES. All experiments were carried out in duplicate. The extent of sorption was expressed as sorption capacity (q_e) and as percentage sorption.

The sorption capacity at equilibrium was calculated using the formula:

$$q_e = (C_o - C_e) \times \frac{V}{m} \quad (3.3)$$

[Where: q_e = sorption capacity (mg·g^{-1}), C_o = initial metal concentration (mg·L^{-1}), C_e = metal concentration at equilibrium (mg·L^{-1}), V = volume in litres, m = mass of sorbent (g)].

Similarly, the percentage sorption was calculated using the formula:

$$\%\, sorption = \frac{(C_o - C_e)}{C_o} \times 100\% \quad (3.4)$$

3.3.2.1 pH-dependent studies

The pH studies for both cadmium and nickel were conducted over the pH range 1 – 7. It is known that certain metals tend to precipitate in a basic medium. A precipitation test for Ni was conducted by using a concentrated (1000 mg·L^{-1}) standard solution of the metal with buffer pH 7. Immediate precipitation was observed. Similarly, cadmium is also known to form hydroxy complexes as pH increases. All pH studies were therefore restricted to pH 1 – 6.

The SCG (1 g) were accurately weighed into each of 6 × 50 mL polyurethane sample bottles. In a separate 50 mL volumetric flask, a calculated volume of stock solution was transferred to prepare a metal ion solution of known concentration. To this solution, 25 mL of the respective buffer (1 to 6) was added and filled to the mark using de-ionised water. The buffered solution was added to the polyurethane bottle containing the 1 g SCG and shaken on an open-top orbital shaker at 150 rpm for 24 hours. After 24 hours the contents of each bottle were filtered, and the metal ion content of the filtrate was determined by ICP-OES.

3.3.2.2 Sorbent dosage

Sorbent dosage varied from 0.1 g to 1.0 g per 50 mL solution. The metal ion concentration and pH were both maintained at constant values of 10 mg·L^{-1} and 6 respectively.

3.3.2.3 Initial metal-ion concentration

Initial metal concentration studies were carried out by maintaining constant sorbent mass and pH. However, the metal concentration was varied. The experiments were conducted over two

concentration ranges. Stock solution concentrations were increased in increments of 1 mg·L^{-1} from 1 mg·L^{-1} to 10 mg·L^{-1} in 50 mL volumetric flasks for experiment 1, and from 10 mg·L^{-1} to 40 mg·L^{-1} for experiment 2, in increments of 10 mg·L^{-1}. Reference solutions that matched the matrix of the working solutions and corresponded to each initial metal ion concentration were prepared. The concentration of each reference solution was determined by ICP-OES, and the values obtained were used as C_0 in equation 3.3 to determine the amount of sorbed metal ion (q_e).

3.3.3 Thermodynamics (Temperature dependence studies)

With the aid of an incubating shaker, temperature-dependent studies were done on multiple batch experiments at temperatures of 15, 20, 25, 30, and 40 °C. For each batch experiment, a single Erlenmeyer flask was used. This flask contained 0.1 g SCG in a 50 mL metal ion solution of known concentration and pH. All working solutions were allowed to reach thermal equilibrium (approximately 20 minutes) before the sorbent was added. The mixtures were then shaken for 3 hours.

The Van't Hoff equation was used to construct graphs of ln K_d vs 1/T and these graphs were used to calculate the thermodynamic parameters ($\Delta H°$, $\Delta S°$ & $\Delta G°$).

$$\ln K_d = -\frac{\Delta H^\circ}{R}\left(\frac{1}{T}\right) + \frac{\Delta S^\circ}{R} \quad (3.5)$$

[Where: ΔH° = Change in standard enthalpy; (kJ·mol^{-1}), R = Ideal gas constant (8.314 J·K^{-1}·mol^{-1}), T = Absolute temperature (K), K_d = Distribution coefficient (q_e/C_e)]

Since the above equation is in the form y = mx + c, the equation enthalpy was calculated using:

$$-\frac{\Delta H^\circ}{R} = \text{slope} \quad (3.6)$$

The constant "C" is related to change in entropy and was calculated using the formula below:

$$\frac{\Delta S^\circ}{R} = \text{intercept} \quad (3.7)$$

And the Gibbs free energy using:

$$\Delta G^\circ = \Delta H^\circ - T\Delta S^\circ \quad (3.8)$$

Distribution coefficient/partition coefficient:

$$K_d = \frac{[solute]\ in\ organic\ phase}{[solute]\ in\ aqueous\ phase} \quad (3.9)$$

if $K_d > 1$: solute prefers organic phase. $K_d < 1$: solute favours the aqueous phase

The relationship between the sorption rate constant (k) and the activation energy (E_a) is represented by the Arrhenius equation (Spies & Wewers, 2020)

$$\ln k_1 = \left(-\frac{E_a}{R}\right)\frac{1}{T} + lnA \quad (3.10)$$

The activation energy (E_a) of ion-exchange relates to the rate-determining step.

- E_a < 16.7 kJ·mol^{-1}: film-diffusion controlled
- E_a < 42 kJ·mol^{-1}: particle-diffusion controlled
- E_a = 50.2 kJ·mol^{-1}: reaction controlled

Research done elsewhere showed that E_a values exceeding 40 kJ·mol^{-1} suggest that the sorption occurred by chemisorption mechanisms whereas activation energies below 40 kJ·mol^{-1} are generally associated with physisorption (Cantu et al., 2014).

3.3.4 Kinetics (contact time)

The sorption kinetics of Cd^{2+} and Ni^{2+} were studied using batch experiments. Individual batch solutions were prepared for each given time interval investigated. The pH of the solution was adjusted to pH 6 using the respective buffers. A mass of 0.1 g SCG was shaken with 50 mL of a buffered [Cd/Ni] = 10 mg·L^{-1} solution. The mixture was shaken at 150 rpm and aliquots of the supernatant solution were drawn at predetermined time intervals. One Erlenmeyer flask per batch experiment was used per working solution. The flasks were removed from the orbital shaker at predetermined intervals, filtered, and the supernatant solution was analysed for its metal content using ICP-OES.

During initial kinetic batch experiments supernatant aliquots were drawn in 5-minute intervals to establish an estimate of the equilibrium point. Subsequent experiments focused on optimizing the conditions to attain the maximum experimental sorption capacity.

Batch reaction data were analyzed using Lagergren pseudo-first-order and Ho and McKay (Ho & McKay, 1998) pseudo-second-order models, respectively.

3.3.4.1 Pseudo-first order

The Lagergren pseudo-first-order expression can be written as follows:

$$\frac{dq_t}{d_t} = k(q_{e-}\, q_t) \tag{3.11}$$

Applying boundary conditions t = 0 to t = t and q_t = 0 to q_t = q_t, the integrated form of the equation becomes:

$$\log(q_e - \, q_t) = \log q_e - \frac{K}{2.303}\, t \tag{3.12}$$

[Where: q_e = equilibrium concentration (mg·g^{-1}), q_t = concentration sorbed at time t(s), k = pseudo-first-order rate constant.]

If a reaction best fits Pseudo-first order, it can be concluded that the reaction occurs mainly by means of physisorption.

3.3.4.2 Pseudo-second order

The Ho and McKay pseudo-second-order expression was used as:

$$\frac{dq_t}{dt} = k(q_e - q_t)^2 \tag{3.13}$$

With the integrated form for boundary condition t = 0 being:

$$\frac{1}{q_t} = \frac{1}{h} + \frac{1}{q_e} t \tag{3.14}$$

[Where: h = $k_2 q_e^2$ initial sorption rate (mg/g·min^{-1}), and rate constant k_2 is (g/mg·min^{-1})]

If a reaction best fits pseudo-second-order kinetics, it can be deduced that the reaction occurs mainly via chemisorption.

CHAPTER 4

RESULTS AND DISCUSSION

4.1 Introduction

This chapter focuses on the analyses of the data of the sorption of heavy metals Cd and Ni onto spent coffee grounds. The ANOVA (analysis of variance) principles were used to investigate variable patterns and grouping trends of the sorption process. Data were applied to Langmuir and Freundlich mathematical isotherms as described in Chapter 3. The time dependence of the sorption was analysed with Lagergren pseudo-first-order models and Ho and McKay pseudo-second-order models. Characterisation of the sorbent before and after metal sorption, as well as before and after supercritical CO_2 extraction of the oils, were investigated by XRD, SEM, EDS and ATR-FTIR analysis.

4.2 Characterisation of the sorbent

4.2.1 Scanning electron microscopy (SEM)

Electron images of the surface of the sorbent before and after supercritical CO_2 extraction are shown in figures 4.1 and 4.2 respectively.

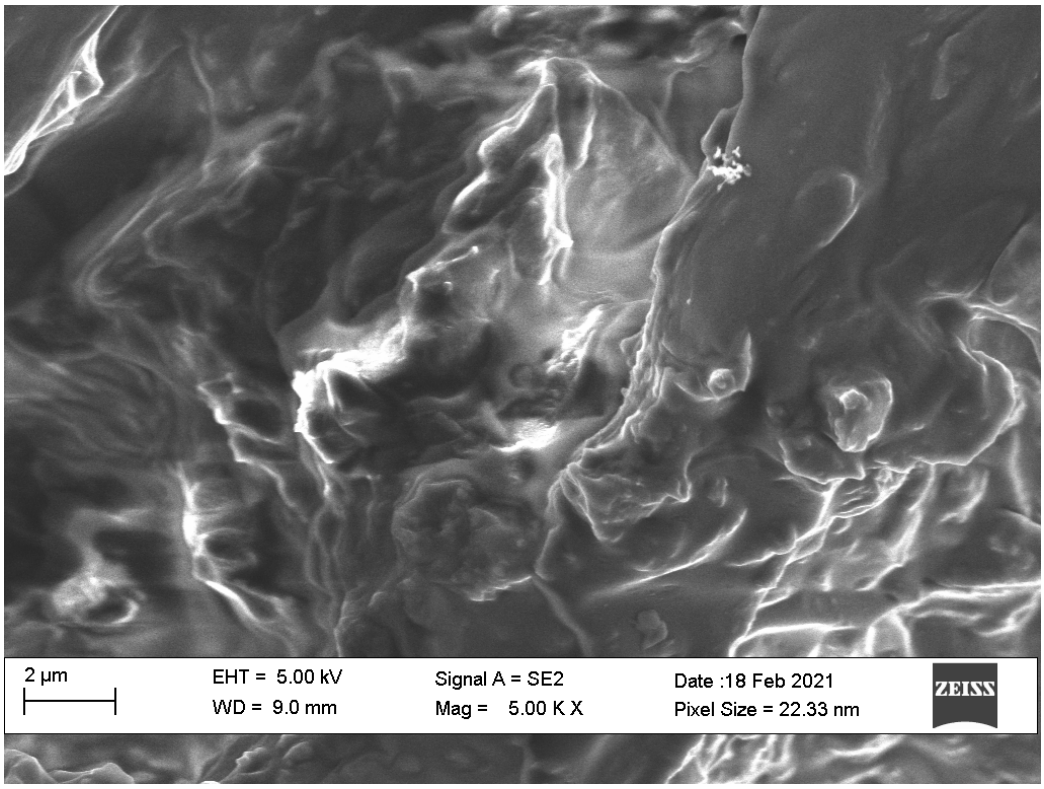

Figure 4.1: SEM image of SCG before SFE

Figure 4.2 shows a more porous surface for the sorbent after SFE. The increase in pore size should, theoretically, improve the sorption capacity of the sorbent. Given that biosorption is primarily a surface process and that pore size is directly related to the surface area, the more porous a sorbent the better the interaction of the sorbate species to the sorbent (Ofomaja & Naidoo, 2011). In addition, supercritical fluid extraction should strip the coffee of most of its remaining functional groups resulting in fewer available coordination sites, thus decreasing the possibility of chemisorption.

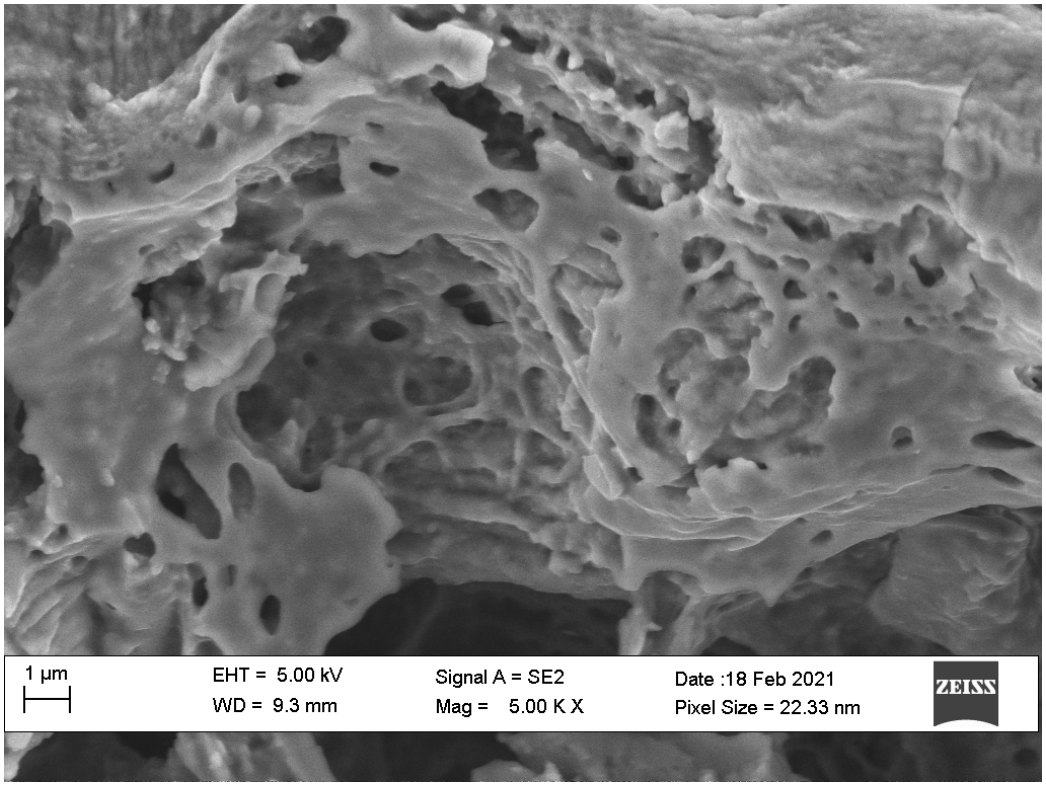

Figure 4.2: SEM image of SCG after supercritical CO_2 extraction of the sorbent

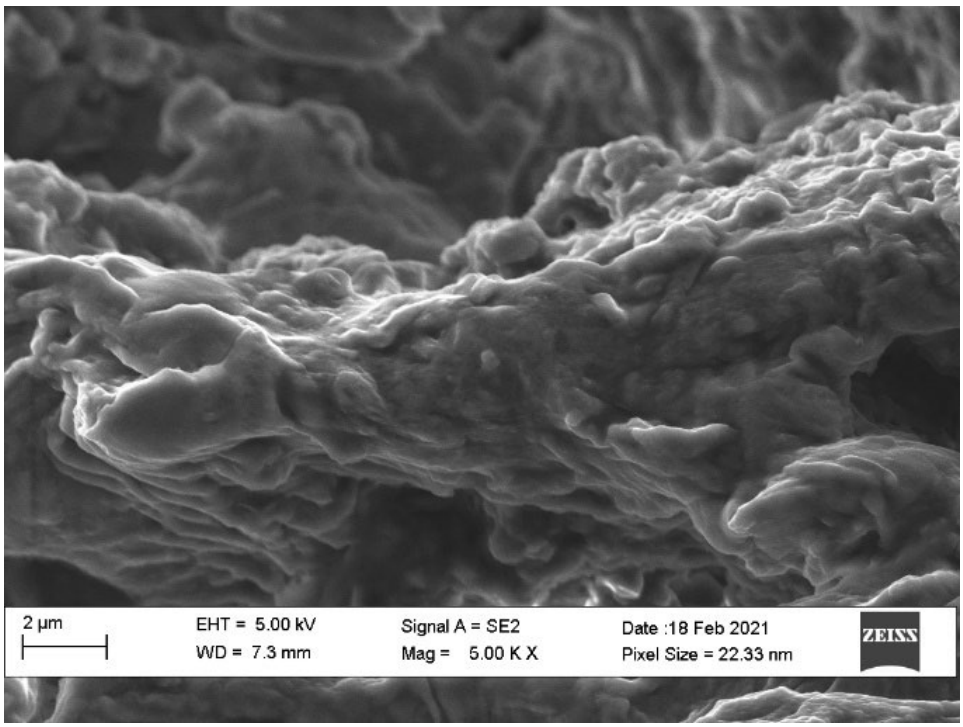

Figure 4.3: SEM image of SCG + Cd after sorption experiments

Figure 4.3 shows the morphology of the sorbent after Cd sorption. The evident decrease in pore size when compared with figure 4.2 suggests a pore-filling mechanism. A similar picture emerged after Ni sorption (see Figure 4.4).

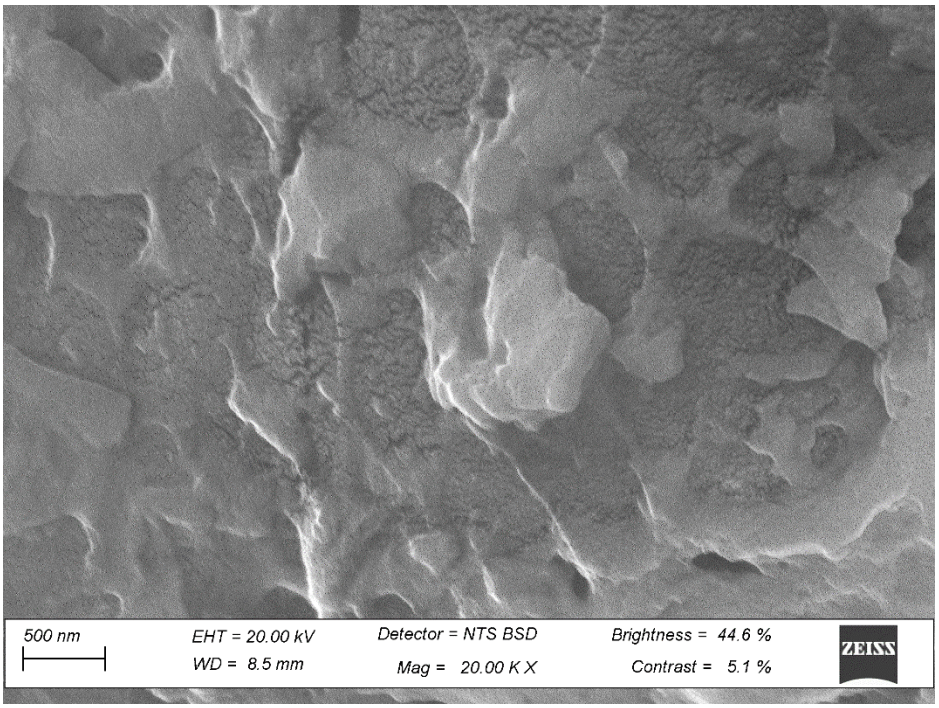

Figure 4.4: SEM image of SCG + Ni

Additional SEM images are shown in Appendices A – C.

4.2.2 EDS analysis

Figure 4.5 shows the EDS spectrum of the SCG before the extraction of oils.

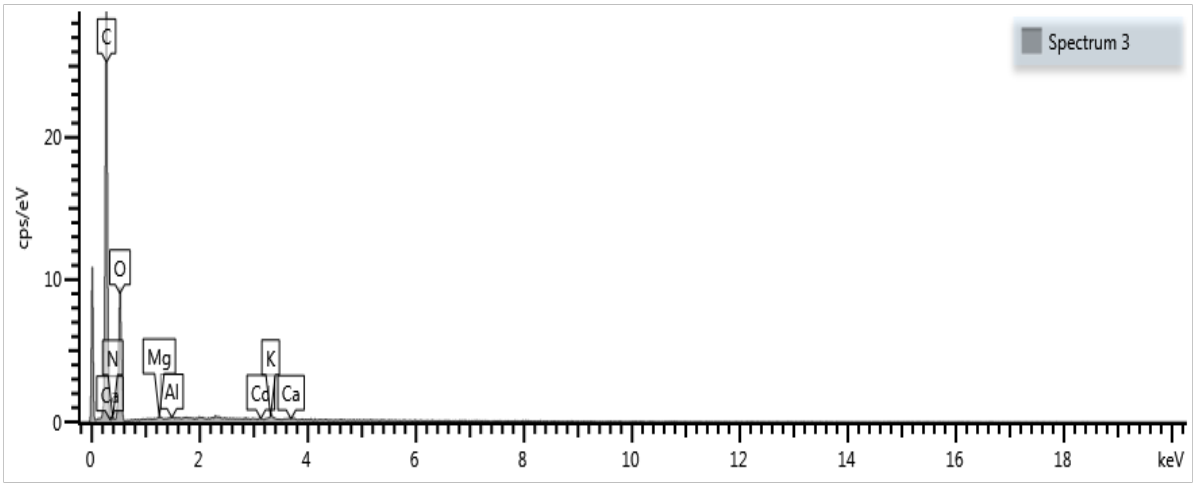

Figure 4.5: EDS spectrum of SCG before SFE

The sorbent contained trace amounts of magnesium, potassium, calcium, aluminium, and cadmium before removal of the oils. This result corroborates findings by Azouaou et al. (2010) who studied Cd sorption onto untreated coffee grounds (Table 4.1).

Table 4.1: EDS analysis summary of SCG before pre-treatment (SFE)

	C	N	O	Mg	Al	K	Ca	Cd	Si	Na	Reference
Atomic %	65.73	3.63	30.37	0.08	0.03	0.11	0.06	0.01	---	---	This study
	33.75	----	58.59	1.19	0.68	0.80	0.42	----	0.48	2.72	(Azouaou et al., 2010)

The slight variation in elemental composition for the EDS data obtained for this study and also reported by Azouaou et al. 2010, can be caused by several factors. The latter include; growing conditions of the bean (humidity, temperature, soil metal content, water quality), the brewing method of the coffee, and the brand and type of coffee investigated (McNutt & He, 2019).

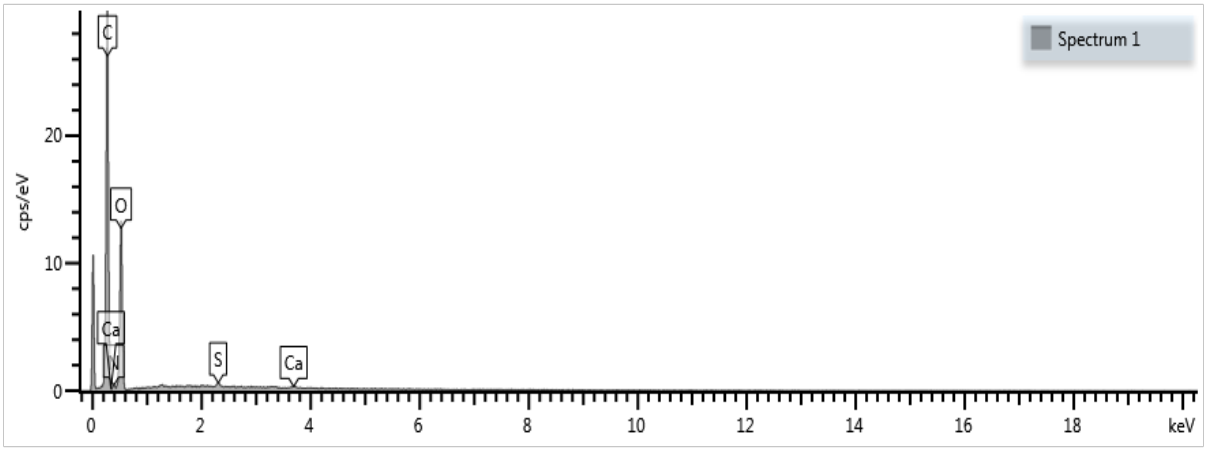

Figure 4.6: EDS spectrum of SCG after SFE

The EDS spectrum (Figure 4.6) after SFE shows a decrease in Mg, K, Al and Cd content of the sorbent. Table 4.2 compares the elemental content of the sorbent before and after SFE, respectively.

Table 4.2: EDS data of the atomic percentage of SCG before and after SFE

Element	Element Atomic%										
	C	N	O	Na	S	Mg	Al	K	Ca	Cd	Ni
SCG before SFE	65.73	3.63	30.37	----	----	0.08	0.03	0.11	0.06	0.01	----
SCG after SFE	60.08	5.07	34.71	----	0.01	----	----	----	0.05	----	----

As observed in table 4.2, the sorbent after SFE contained no detectable amounts of Cd and Ni; hence any Cd or Ni detected by means of EDS analyses post sorption batch experiments can be directly attributed to a positive confirmation of sorption.

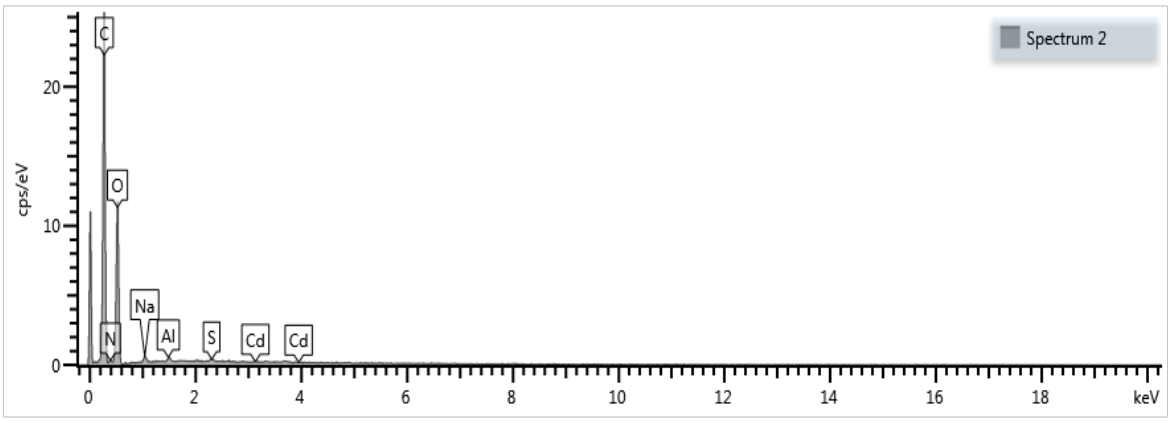

Figure 4.7: EDS spectra of SCG adsorbed with Cd

Figure 4.7 depicts the EDS spectrum of the sorbent after Cd sorption, showing an increase in Cd content from 0.01 % to 0.22 %, whereas the EDS spectrum after Ni sorption showed an increase in Ni content from 0 % to 0.14 % (see figure 4.8).

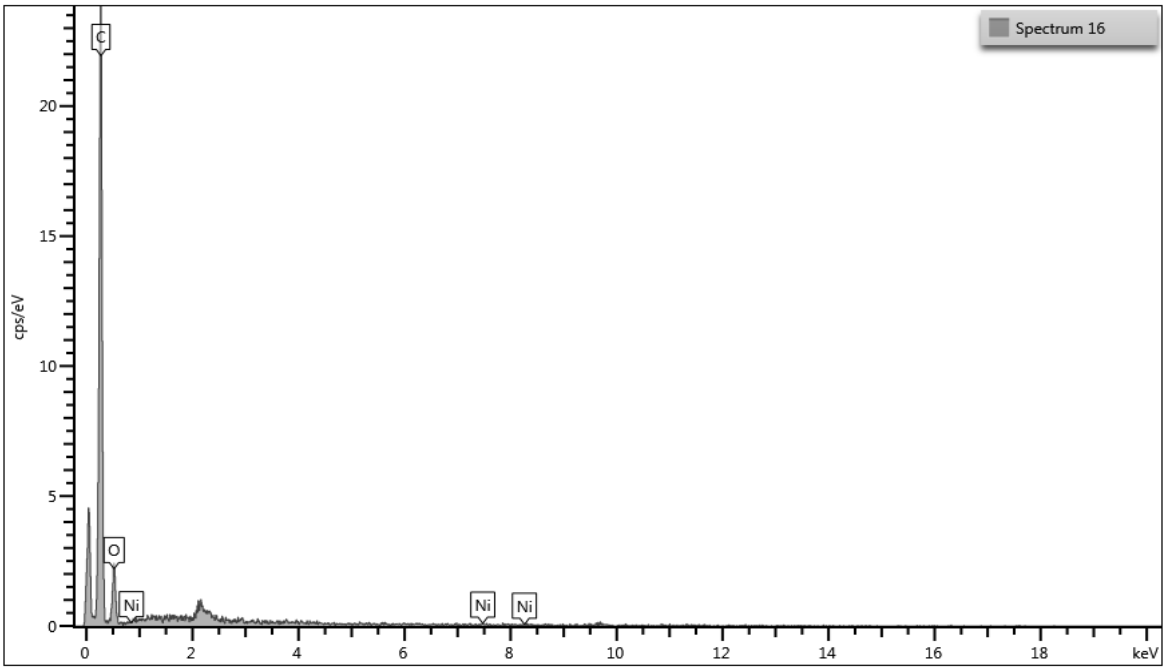

Figure 4.8: EDS spectra of SCG adsorbed with Ni

Table 4.3 summarises the elemental content of the sorbent after Cd and Ni sorption, respectively.

Table 4.3: Summary of EDS data of the sorbent before and after metal sorption.

Sample	Element Atomic%										
	C	N	O	Na	S	Mg	Al	K	Ca	Cd	Ni
SCG after SFE	60.08	5.07	34.71	----	0.01	----	----	----	0.05	----	----
SCG after Cd sorption	54.29	2.79	41.81	0.05	0.15	----	----	----	----	0.22	----
SCG after Ni sorption	74.63	----	25.21	----	----	----	----	0.02	----	----	0.14

As seen in TTable 4.3 above, there is a clear increase in the Cd and Ni content of the sorbent after sorption experiments. The modified SCG used for the sorption studies contained no evidence of Cd and Ni.

Both independent experiments yielded clear Cd and Ni content after adsorption studies implying successful biosorption of these metals by the stripped spent coffee grounds. In the Ni analyses elements S, Mg and Al were also detected but these trace amounts were too small to be quantified by the equipment used. It should also be noted that the sorbent did not contain any Na prior to sorption experiments. The Na in the sample after sorption may have been introduced during the batch reaction process as buffer pH 6 was contained acetic acid and sodium acetate.

4.2.3 ATR-FTIR

Figure 4.9 depicts the ATR-FTIR spectra of the sorbent before and after SFE pre-treatment

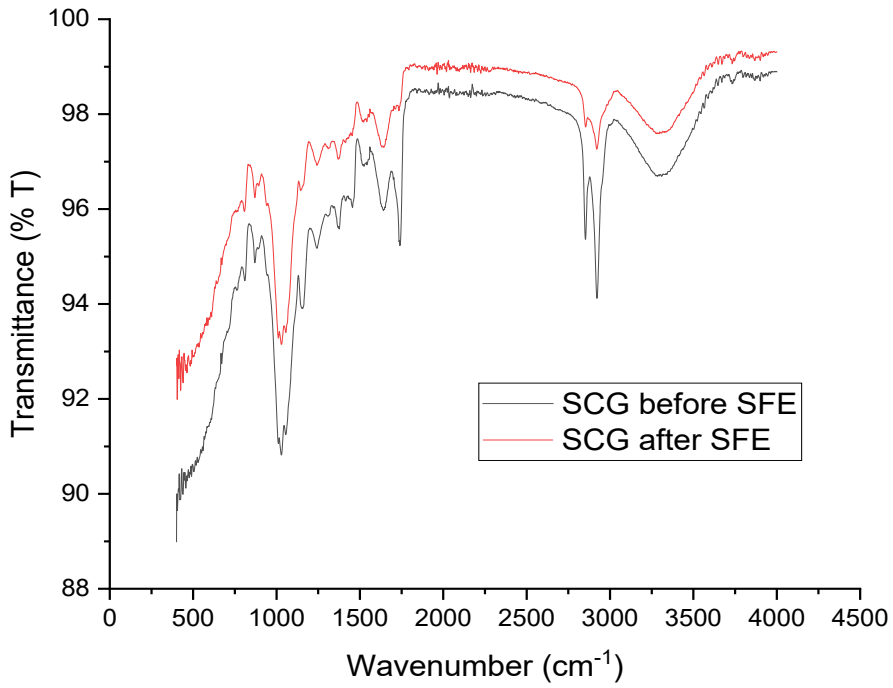

Figure 4.9: Sorbent before and after supercritical fluid extraction

The comparison of the sorbent before and after SFE permits the observation of the modifications introduced by the stripping of some of the functional groups of the sorbent. The most noticeable difference between the two forms of sorbents is the decrease in the intensity of the peaks after SFE. The intensity of a peak is directly related to its dipole of the bond; therefore, the absence of the peak around 1750 cm^{-1} after SFE could be indicative of the removal of carbonyl functional groups. The strong bands noted at 1050 cm^{-1} – 1250 cm^{-1} are most characteristic of C-O single bonds. This validates the argument that the sorbent contains carboxylic acid functional groups. The broad adsorption peak near 3250 cm^{-1} originating from the presence of carboxylic acids was supported by the presence of peaks at 1031.47 cm^{-1} and 1634.38 cm^{-1} allocated to O-H and C=O, respectively.

In addition, the fingerprint region is complex but still shows similar patterns for the sorbent before and after SFE, indicating that the overall chemical composition of the sorbent did not change markedly after SFE.

Moreover, the disappearance of peaks at approximately 1600 cm^{-1}, 1500 cm^{-1} and 1200 cm^{-1} after SFE symbolises a decrease in functionality of the sorbent. Medium to sharp intensity peaks at 1600 cm^{-1} can be attributed to carbonyl (C=O) functional groups, while peaks at 1500 cm^{-1} and 1200 cm^{-1} can be related to amine (N-H) functional groups and single bonded carbons (C-H) respectively.

Figure 4.10 shows the FTIR spectrum of the modified sorbent after Cd uptake

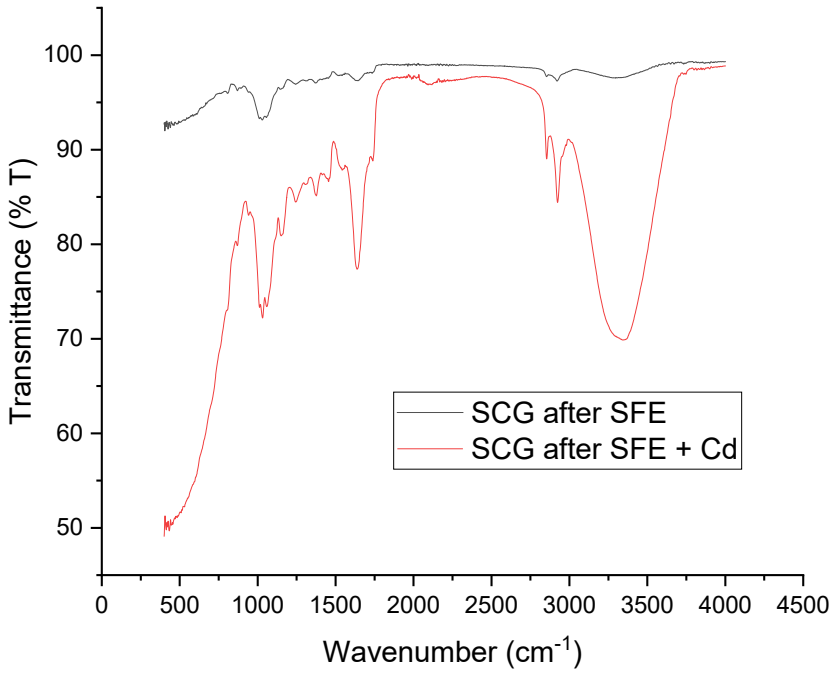

Figure 4.10: FTIR spectra of SCG after sorption with Cd.

The broad absorption peak near 3250 cm^{-1} originating from the presence of carboxylic acids was supported by the presence of peaks at 1031.47 cm^{-1} and 1634.38 cm^{-1} allocated to O-H and C=O groups, respectively. The stretching of the O–H group is generally due to inter-and intra-molecular hydrogen bonding of polymeric acids. The peak at approximately 2924.21 cm^{-1} signifies the symmetric or asymmetric C-H stretching vibrations of aliphatic acids, making it likely that carboxylic acid groups contributed to the sorption. Bands in the range of 1367.95 cm^{-1} are attributed to COO– symmetric stretching vibrations. Similar findings were published by Imessaoudene et al. (2016) who suggested similar peaks may be attributed to variations in counter-ions linked to carboxylate and hydroxylate anions.

It could thus be inferred that carboxyl and hydroxyl functional groups possibly played a role in the metal ion uptake.

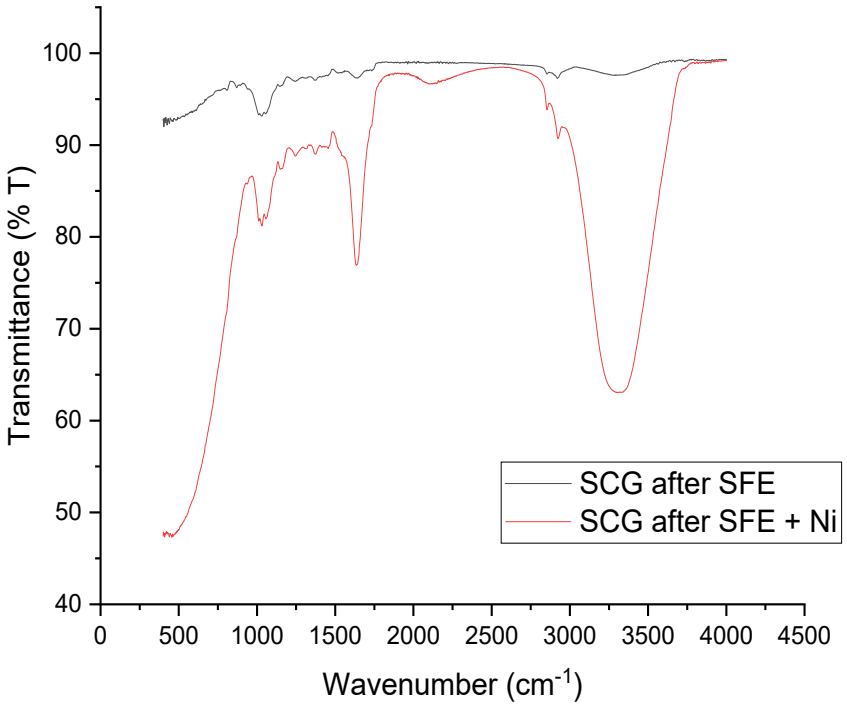

Figure 4.11: SCG before and after Ni sorption

Error! Reference source not found. above compares the SCG before and after sorption experiments with Ni. The first noticeable change was the increase in peak intensities after Ni sorption experiments. The broadband around 3250 cm^{-1} indicated that the stretching of the O–H group contributed to the Ni sorption. Another notable change after sorption was the sharp medium intensity peak at 1650 cm^{-1} which suggests that carbon-carbon double bonds or down field carbonyl groups played a role in the Ni sorption. The O-H groups together with the possibility of carbonyl (C=O) groups in turn indicated the presence of carboxylic (COOH) groups. These observations indicate that the functional groups O-H and C=O played a role in the overall Ni sorption. Similar results have previously been reported by Imessaoudene et al. (2013) who investigated the biosorption of strontium onto spent coffee grounds.

4.2.4 Ash content determination

Mass of crucible: 41.3323 g

Mass of crucible + SCG: 46.3329 g

Mass of SCG added = 5.0006 g

Mass of crucible + SCG after furnace: 41.3868 g

Mass of ash content: 41.3868 – 41.3323 = 0.0545 g

% Ash content = $\frac{0.0545}{5.0006} \times 100$ = 1.09 % inorganic content

Images of the SCG before and after furnace exposure during the ash content determination are shown in Appendices E and F respectively.

4.3 Sorption Equilibrium

Sorption equilibrium studies involved pH, adsorbent dosage, and initial metal concentration experiments.

4.3.1 pH dependence

4.3.1.1 Cadmium

Duplicate experiments to determine the pH dependence of Cd sorption produced similar results – Cd sorption increased rapidly with increasing pH (figure 4.13).

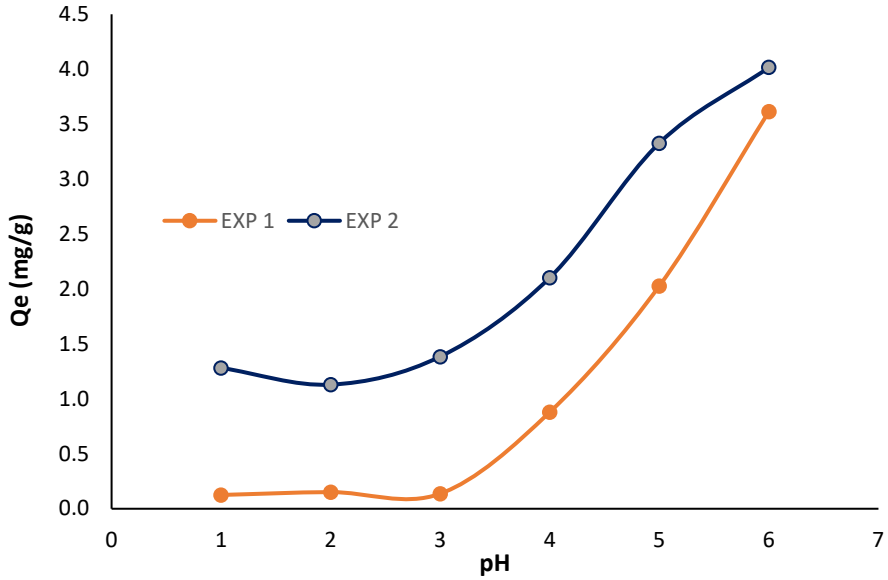

Figure 4.12: Cd uptake as a function of pH ([Cd^{2+}] = 10 mg·L^{-1} with 0.1 g SCG @ 289K).

The maximum sorption of Cd for both experiments occurred at pH = 6 (q_e = 4.02 mg·g^{-1} and q_e = 3.61 mg·g^{-1} for experiment 1 and 2 respectively. For all subsequent experiments involving Cd, pH = 6 was used as the optimum sorption pH. An additional graph of pH dependence, that shows the drop in Q_e after pH 6, is shown in Appendix L.

4.3.1.2 Nickel

The pH-dependent studies of Ni sorption produced similar results.

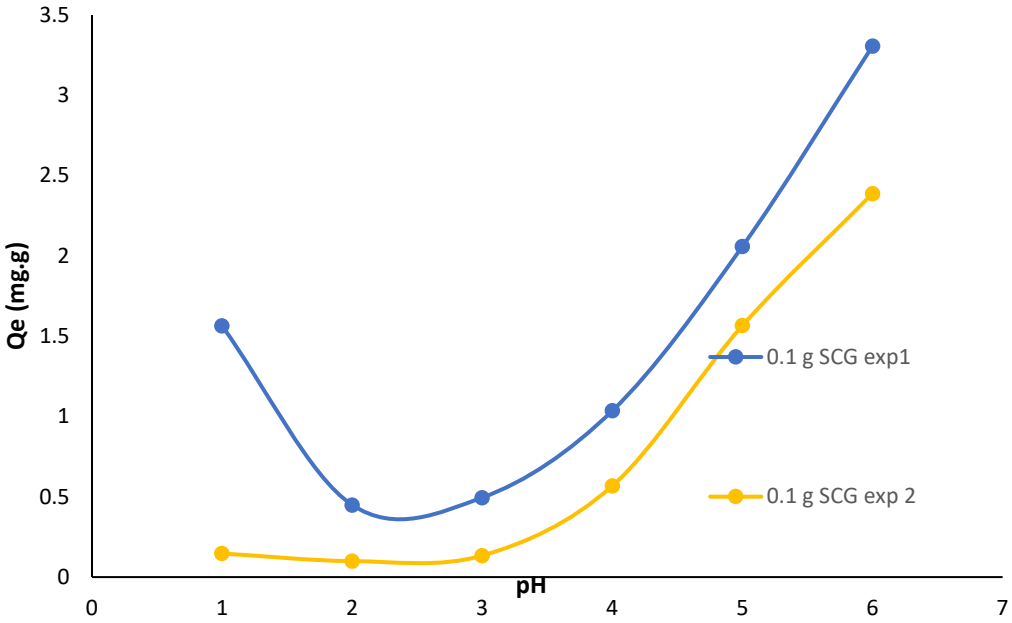

Figure 4.13: Ni pH studies, data overlay ([Ni] = 10 mg·L^{-1} & 0.1g SCG).

The low sorption at a more acidic pH may be due to the hydrogen ions competing for binding sites.

In summary, the optimal experimental pH for the sorption of both Cd and Ni was found to be pH = 6, using a sorbent mass of 0.1 g and shaken at 150 rpm. A maximum sorption capacity of q_e = 4.02 mg·g^{-1} and q_e = 3.31 mg·g^{-1} was achieved for the Cd and Ni sorption respectively.

4.3.2 Adsorbent dosage

For simplicity, the Cd and Ni adsorbent dosage data are discussed together. The results of sorbent dosage data for both Cd and Ni are shown in Table 4.4. The raw adsorbent dosage data for Cd are shown in Appendix D.

Table 4.4: Sorbent dosage data for both Cd and Ni sorption, ($[Cd]_o$ = 10.76 mg·L^{-1}, $[Ni]_o$ = 10.50 mg·L^{-1}. pH = 6 @ 150 rpm, V = 50 mL)

	Cd				Ni			
Mass (g)	C_e (mg·L^{-1})	$C_o - C_e$ (mg·L^{-1})	q_e (mg·g^{-1})	**% Sorption**	C_e (mg·L^{-1})	$C_o - C_e$ (mg·L^{-1})	q_e (mg·g^{-1})	**% Sorption**
0.1	4.65	6.12	3.06	56.83	6.02	4.47	2.24	42.63
0.2	2.51	8.25	2.06	76.67	4.22	6.28	1.57	59.82
0.3	1.82	8.95	1.49	83.14	3.19	7.30	1.22	69.59
0.4	1.49	9.27	1.16	86.13	2.53	7.96	1.00	75.06
0.5	1,31	9.46	0.95	87.87	2.20	8.30	0.83	79,06
0.6	1,17	9.59	0.80	89.13	1.95	8.54	0.71	81.38
0.7	1.05	9.72	0.69	90.26	1.76	8.74	0.62	83.28
0.8	0.98	9.79	0.61	90.94	1.64	8.86	0.55	84.38
0.9	0.88	9.88	0.55	91.82	1.54	8.96	0.50	85.38
1	0.80	9.97	0.50	92.60	1.44	9.06	0.45	86.28

The percentage metal ion removal increased with increasing sorbent dosage (figure 4.15).

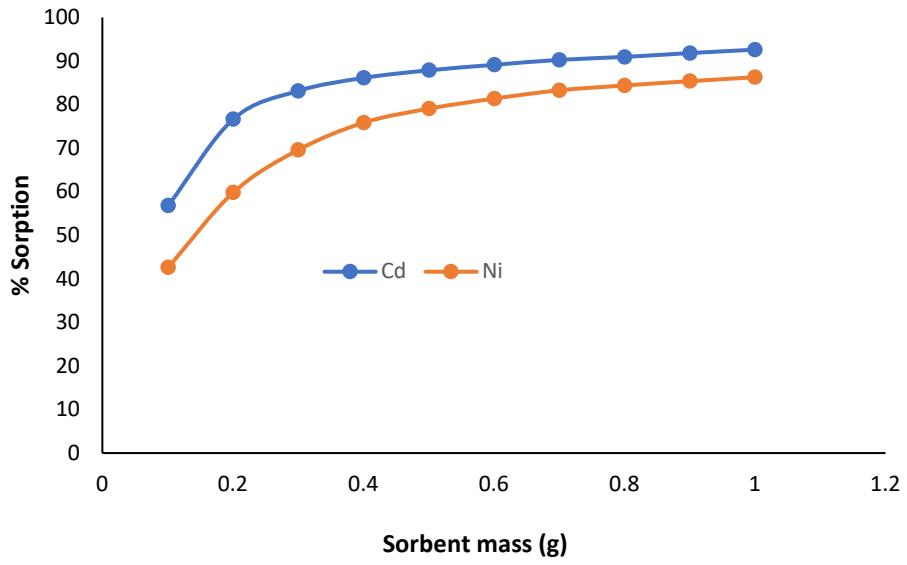

Figure 4.14: Sorbent dosage expressed as percentage sorption (Cd)

The maximum experimental sorption capacity for Cd was calculated as q_e = 3.03 mg·g^{-1} and q_e = 2.23 mg·g^{-1} for Ni. All subsequent experiments were carried out at sorbent dosages of 0.1 g SCG.

4.3.3 Initial metal ion concentration (isotherm studies)

The concentration dependence of the sorption was investigated at the optimal pH and sorbent dosage. Experimental data were applied to Langmuir and Freundlich isotherms.

4.3.3.1 Cadmium

4.3.3.1.1 Langmuir

The effect of initial Cd ion concentration was studied at pH = 6. The amount of Cd^{2+} sorbed increased with increasing initial ion concentration, as shown in Table 4.5.

Table 4.5: Variation of Cd^{2+} sorption with initial concentration; pH = 6; T = 294 K

C_o (mg·L^{-1})	C_e (mg·L^{-1})	$C_o - C_e$ (mg·L^{-1})	q_e (mg·g^{-1})	% Sorption
1.234	0.327	0.907	0.444	73.501
3.069	0.888	2.181	1.080	71.065
4.851	1.578	3.273	1.610	67.471
6.579	2.551	4.028	2.002	61.225
8.213	3.071	5.142	2.548	62.608

An almost linear relationship exists between q_e and C_o (figure 4.16), with no saturation plateau.

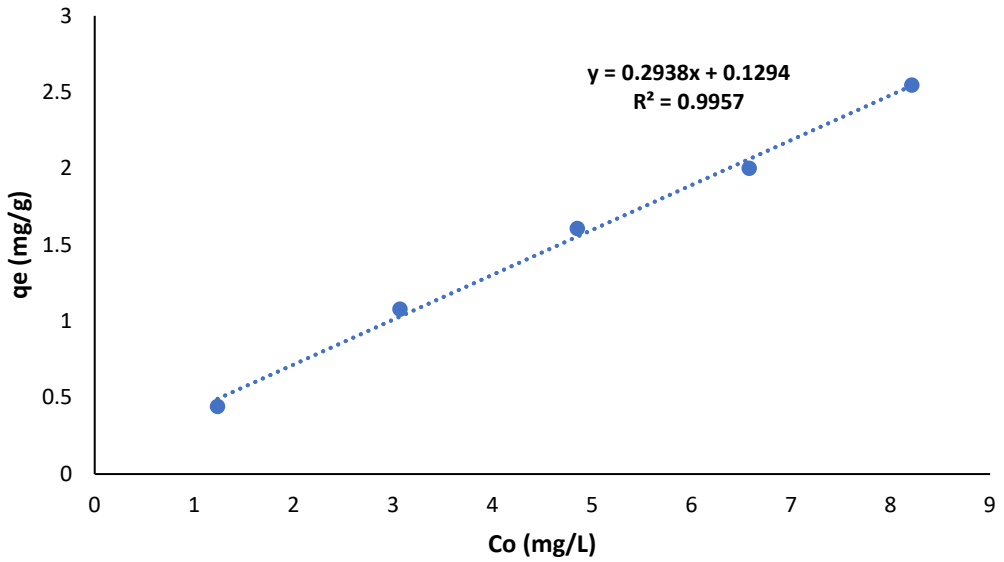

Figure 4.15: Graph showing the amount of Cd sorbed (q_e) versus initial concentration (C_o)

According to Spies and Wewers (2020), the linear relationship between q_e and C_o is in agreement with Henry's law which states "the sorption of a dilute solution is directly proportional to the number of sorbate species in solution". Figure 4.17 shows the graph obtained when the Langmuir model was applied to Cd sorption data.

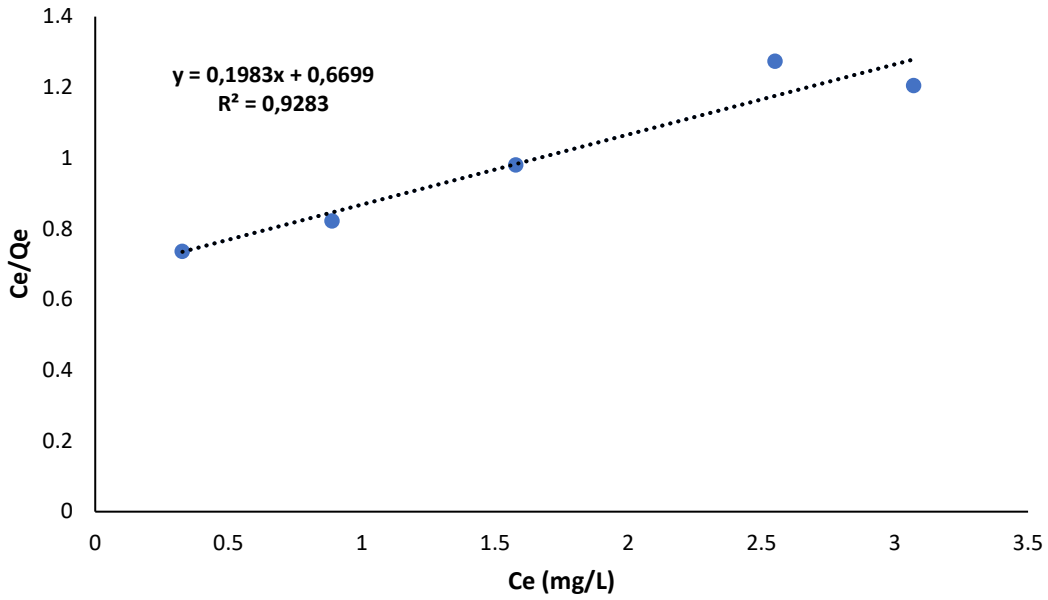

Figure 4.16: Langmuir isotherm of Cd sorption

The Langmuir isotherm for Cd sorption is represented by the linear equation:

$$\frac{C_e}{q_e} = 0.1983C_e + 0.6699 \quad (4.1)$$

From the slope and intercept of the graph, the theoretical maximum monolayer sorption capacity (q_o) and binding strength (K_L) were calculated, respectively:

$$\frac{1}{q_o} = 0.1983 \quad (4.2)$$

$$q_o = 5.04 \text{ mg·g}^{-1}$$

The theoretical sorption capacity for Cd obtained by the Langmuir isotherm (q_o = 5.04 mg·g^{-1}) differed remarkably from the experimental value obtained by the previous pH (q_e = 4.02 mg·g^{-1}) and sorbent dosage (q_e = 3.06 mg·g^{-1}) investigations. This may be due to insufficient data points used for the analyses or discrepancies in the volume to mass ratio. Later studies (kinetics) explored greater volume to mass ratios and an improved correlation between the theoretical and experimental sorption capacities was attained.

The binding strength (Langmuir constant, K_L) was calculated as follows:

$$\frac{1}{q_o K_L} = 0.6699 \quad (4.3)$$

$$K_L = 0.29 \text{ L·mg}^{-1}$$

The Langmuir constant, K_L, together with other Langmuir isotherm parameters for Cd are summarized in Table 4.6 below:

Table 4.6: Summarized Langmuir isotherm data for Cd

Langmuir data							
Metal	**Intercept**	**slope**	q_o (mg·g^{-1})	q_e (mg·g^{-1})	K_L	R^2	R^2 adjusted (origin)
Cd	0.669	0.198	5.043	2.560	0.296	0.928	0.904

The separation factor, R_L, was calculated using equation 2.4 as referred to in chapter 2 and the data are presented in Table 4.7 below:

Table 4.7: Summary of Cd separation factor data as calculated using the Langmuir expression

Metal	C_o (mg·L^{-1})	R_L
Cd	1.234	0.732
	3.069	0.524
	4.851	0.411
	6.579	0.339
	8.213	0.291

The separation factor, R_L, was in the range 0 – 1 for $[Cd^{2+}]_0$, indicating that the sorption of Cd onto SCG was favourable for all concentrations investigated. Tables 4.8 and 4.9 depict the statistical and ANOVA data for the Cd sorption as obtained from Langmuir data analysed using OriginPro® software.

Table 4.8: Summary of Cd Langmuir statistical data

	Intercept		**Slope**		**Statistics**
	Value	Standard Error	Value	Standard Error	Adj. R-Square
Ce/qe	0.66994	0.06256	0.19834	0.03182	0.90441

Table 4.9: Summary of Cd Langmuir ANOVA data

		DF	Sum of Squares	Mean Square	F Value	Prob>F
Ce/qe	Model	1	0.20306	0.20306	38.84566	0.00833
	Error	3	0.01568	0.00523		
	Total	4	0.21874			

4.3.3.1.2 Freundlich

Figure 4.18 below depicts the Freundlich isotherm obtained for Cd.

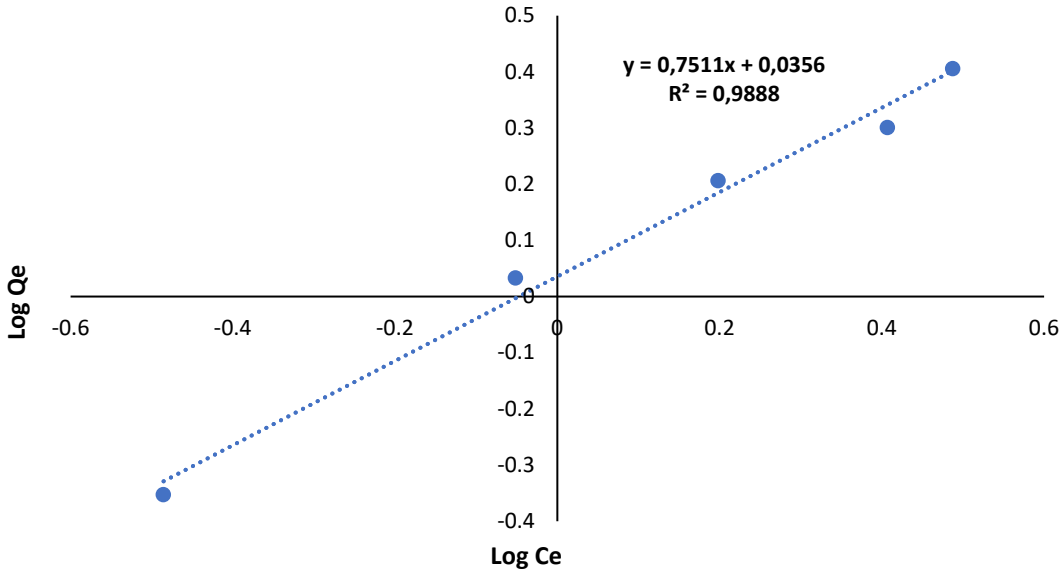

Figure 4.17: Freundlich isotherm of Cd (0.1 g @ pH 6)

The Freundlich isotherm provided a slightly better R^2 value (0.988), implying that the sorption of Cd is possibly due to physical processes. However, due to the favourable correlation coefficient reported for the Langmuir isotherm for Cd (R^2 = 0.9283), chemisorption cannot be ruled out. The Freundlich constant, K_f, was calculated using formula (4.4) illustrated below and summarized in Table 4.10.

$$\text{Log } q_e = \text{Log } K_f + 1/n \log C_e \qquad (4.4)$$

Table 4.10: Summary of Cd Freundlich isotherm data

Freundlich data						
Metal	**Intercept**	**slope**	**1/n**	**K_f**	**R^2**	**R^2 adjusted (OriginPro®)**
Cd	0.036	0.751	0.751	1.085	0.988	0.985

4.3.3.1.3 Non-linear regression error analysis of the Cd sorption onto SCG

By applying the data to non-linear regression, a better understanding can be obtained of the relationship between the experimental values and the theoretical values. The SSE relays information about the difference between the experimental value obtained and the theoretical/predicted value. The smaller the error, the better the estimation power of the regression. The general rule of thumb is that an SSE value between 0.2 and 0.5 implies the model predicts the data accurately. Moreover, an adjusted regression coefficient above 0.75 emphasises the accuracy of the model. The sum of squared errors for the Cd sorption were calculated according to equation 4.5 below and the data are graphically presented in figure 4.19.

$$SSE = \sum_{i}^{N} = 1(q_{e,1,calc} - q_{e,i,meas})^2 \quad (4.5)$$

[Where: $q_{e,calc}$ = theoretical equilibrium sorption capacity (mg·g^{-1}) obtained from the model, $q_{e,meas}$ = experimental sorption capacity (mg·g^{-1})].

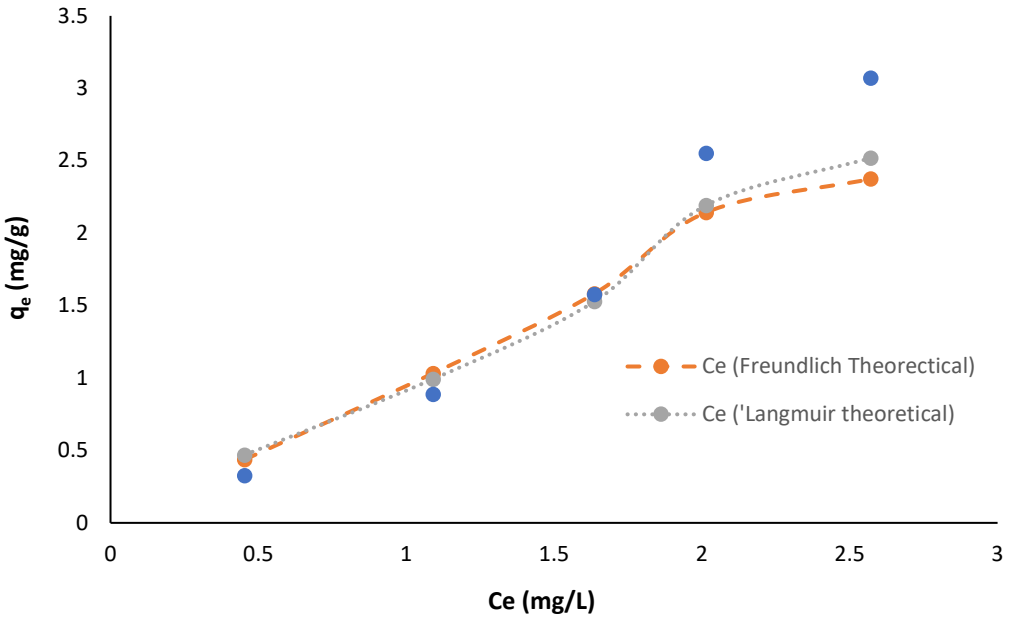

Figure 4.18: Non-linear regression plot of Langmuir and Freundlich data for the Cd sorption

Figure 4.19 above displays a good corelation between the theoretical and actual values. In addition, the R^2 value obtained for the non-linear regression (R^2 = 0.9803) was in good agreement with the results obtained for the linear regression (R^2 = 0.9888) data. In addition, the theoretical and actual sorption capacities still differed significantly. However, a better experimental sorption capacity was attained by increasing the volume to mass ratio during later contact time investigations.

Another important error function of the non-linear regression is the non-linear Chi-square test (X^2) expressed by equation 4.6, and summarized with the other non-linear regression data of the Cd sorption data in Table 4.11 below:

$$X^2 = \sum_{i}^{N} = 1 \frac{(q_{e,calc} - q_{e,meas})^2}{q_{e,meas}} \quad (4.6)$$

[Where: the closer the of $X^2 = 0$, the better the fit of the regression data.]

Table 4.11: Error functions of non-linear isotherms for Cd

Metal	Langmuir	Freundlich
Cd	$R^2 = 0.9756$	$R^2 = 0.9803$
	SSE = 0.0620	SSE = 0.0558
	$X^2 = 0.0289$	$X^2 = -0.0654$

In agreement with the linear regression data, the non-linear model suggested that the Freundlich model provided the best fit to the data.

4.3.3.2 Nickel

4.3.3.2.1 Langmuir

The effect of initial ion concentration on Ni^{2+} sorption was studied at pH = 6. The amount of Ni^{2+} sorbed increased as initial concentration increased until saturation was reached at C_0 > 8 mg/L (figure 4.20).

Table 4.12: Variation of Ni^{2+} sorption with initial concentration (pH = 6; *T* = 294 K)

Co (mg·L^{-1})	***Ce*** (mg·L^{-1})	***Co - Ce*** (mg·L^{-1})	q_e (mg·g^{-1})	**% Sorption**
0.979	0.111	0.868	0.433	88.661
2.216	0.602	1.614	0.802	72.834
3.458	1.135	2.323	1.155	67.178
4.552	1.503	3.049	1.514	66.982
5.82	2.506	3.314	1.656	56.942
6.969	3.239	3.730	1.861	53.522
7.694	4.019	3.675	1.836	47.764
8.763	4.753	4.010	2.001	45.761
10.112	5.928	4.184	2.084	41.377
11.237	7.11	4.127	2.059	36.727

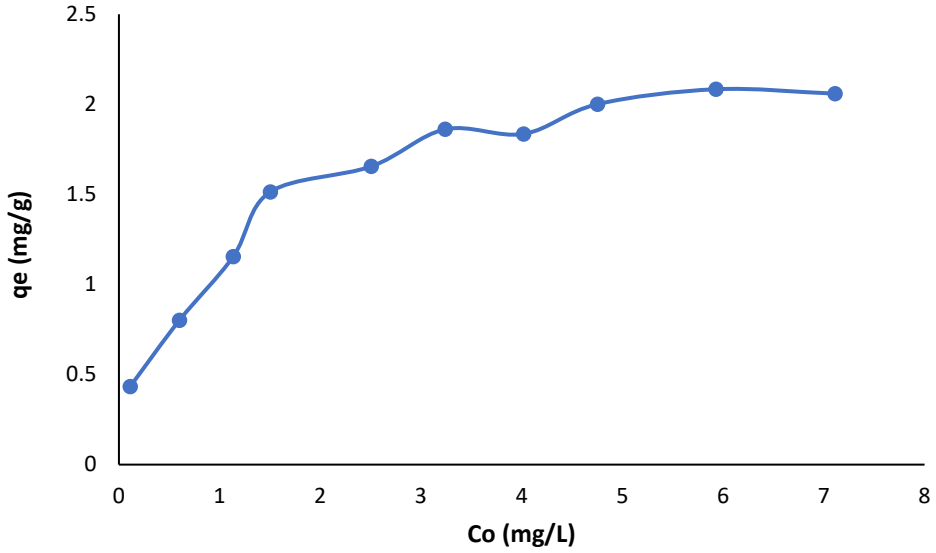

Figure 4.19: The amount of Ni sorbed (q_e) versus initial concentration (C_o) (pH= 6, mass = 0.1 g; T = 294 K)

For Ni sorption, the Langmuir isotherm provided the best fit to the experimental data with an R^2 = 0.9916 (figure 4.21).

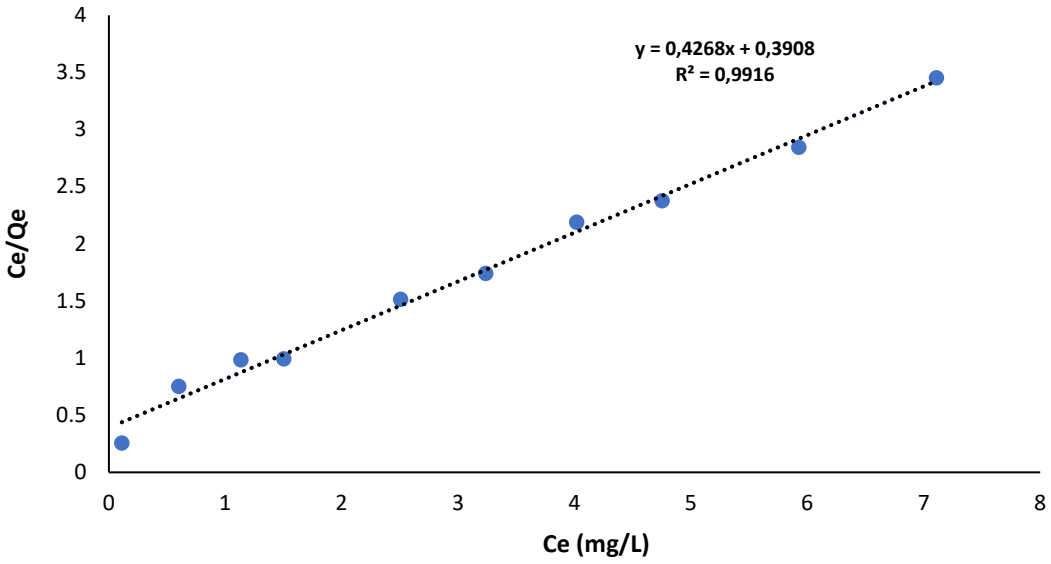

Figure 4.20: Langmuir isotherm of Ni (m = 0.1g, pH = 6 @ 150 rpm)

From figure 4.21, the Langmuir isotherm for Ni sorption is represented by the linear equation:

$$\frac{C_e}{q_e} = 0.4268C_e + 0.3908 \qquad (4.7)$$

Using the above equation, the theoretical maximum monolayer sorption capacity (q_o) and binding strength (K_L) were calculated.

$$\frac{1}{q_o} = 0.4268 \quad (4.8)$$

$$q_o = 2.34 \text{ mg·g}^{-1}$$

The calculated theoretical sorption capacity for the Ni sorption $q_o = 2.34$ mg·g^{-1} was in excellent agreement with the experimental sorption capacity obtained for the pH dependence investigation q_e = 2.23 mg·g^{-1}.

$$\frac{1}{q_o K_L} = 0.3908 \quad (4.9)$$

$$K_L = 1.094 \text{ L·mg}^{-1}$$

The separation factor, R_L, for the Ni sorption was calculated using equation 2.4 (see Chapter 2) and the data are presented in Table 4.13 below:

Table 4.13: Summary of Ni separation factor data as calculated using the Langmuir expression

Metal	C_o (mg·L^{-1})	R_L
Ni	0.979	0.483
	2.216	0.292
	3.458	0.209
	4.552	0.167
	5.82	0.136
	6.969	0.116
	7.694	0.106
	8.763	0.095
	10.112	0.083
	11.237	0.075

Since R_L was in the range 0 – 1 for $[Cd^{2+}]_0$ and $[Ni^{2+}]_0$ values, the sorption of both Cd and Ni onto SCG was favourable for all concentrations investigated. When the R_L value approaches 0 as concentration increases, it implies that the reaction of both metals was unfavourable at higher concentrations.

The SCG exhibited a greater sorption capacity for Cd when compared with Ni. The Langmuir constant, K_L, together with other Langmuir isotherm parameters for Ni are summarized in Table 4.16, while the Langmuir statistical and ANOVA data are represented in Tables 4.14 and 4.15 respectively.

Table 4.14: Summary of Ni Langmuir statistical data

	Intercept		Slope		Statistics
	Value	Standard Error	Value	Standard Error	Adj. R-Square
log q_e copy	0.03324	0.01494	0.396	0.02503	0.96516

Table 4.15: Summary of Ni ANOVA data

		DF	Sum of Squares	Mean Square	F Value	Prob>F
log q_e copy	Model	1	0.42895	0.42895	250.29829	2.54791×10^{-7}

Table 4.16: Summarized Langmuir isotherm data for Ni

Langmuir data							
Metal	**Intercept**	**slope**	**q_o** ($mg \cdot g^{-1}$)	**q_e** ($mg \cdot g^{-1}$)	**K_L**	**R^2**	**R^2** adjusted (OriginPro®)
Ni	0.391	0.427	2.343	2.059	1.092	0.992	0.991

The excellent agreement between the theoretical sorption capacity (q_o = 2.343 $mg \cdot g^{-1}$) and the experimental sorption capacity (q_e = 2.059 $mg \cdot g^{-1}$) corroborates the correctness of the sorption method.

4.3.3.2.2 Freundlich

Figure 4.22 below depicts the Freundlich isotherm obtained for Ni.

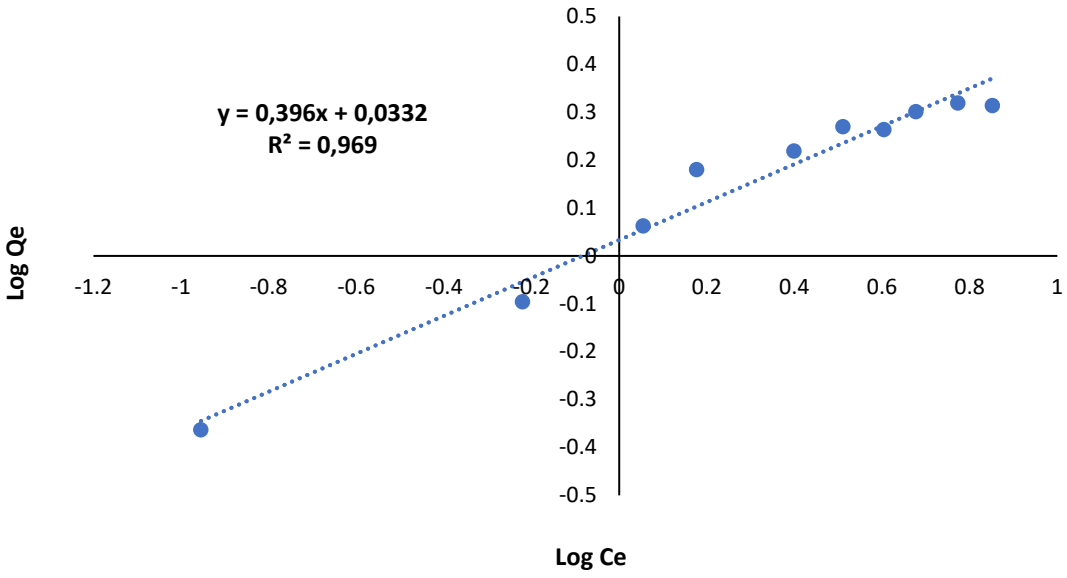

Figure 4.21: Freundlich isotherm of Ni (0.1g SCG @, pH 6)

Both Freundlich and Langmuir isotherms modeled the sorption data satisfactorily and provided acceptable correlation coefficients. The Langmuir isotherm provided a better R^2, hence it can be concluded that the sorption of Ni occurred by means of chemisorption in a monolayer fashion until all the active sites had been filled. This was followed by additional physical interactions between the sorbed metal ions and those in the sorbate medium. The Freundlich constant K_f was calculated using formula (4.7) and summarized in Table 4.17.

Table 4.17: Summary of Ni Freundlich isotherm data

Freundlich data						
metal	**Intercept**	**slope**	**1/n**	**K_f**	**R^2**	**R^2** adjusted (OriginPro®)
Ni	0.033	0.396	0.396	1.079	0.969	0.965

4.3.3.2.3 Non-linear regression error analysis of the Ni sorption onto SCG

In a similar manner to the Cd isotherm investigations, the SSE and X^2 were calculated according to equations 4.5 and 4.6 respectively and are graphically presented in figure 4.23 below. The non-linear error analyses data are summarized in Table 4.18.

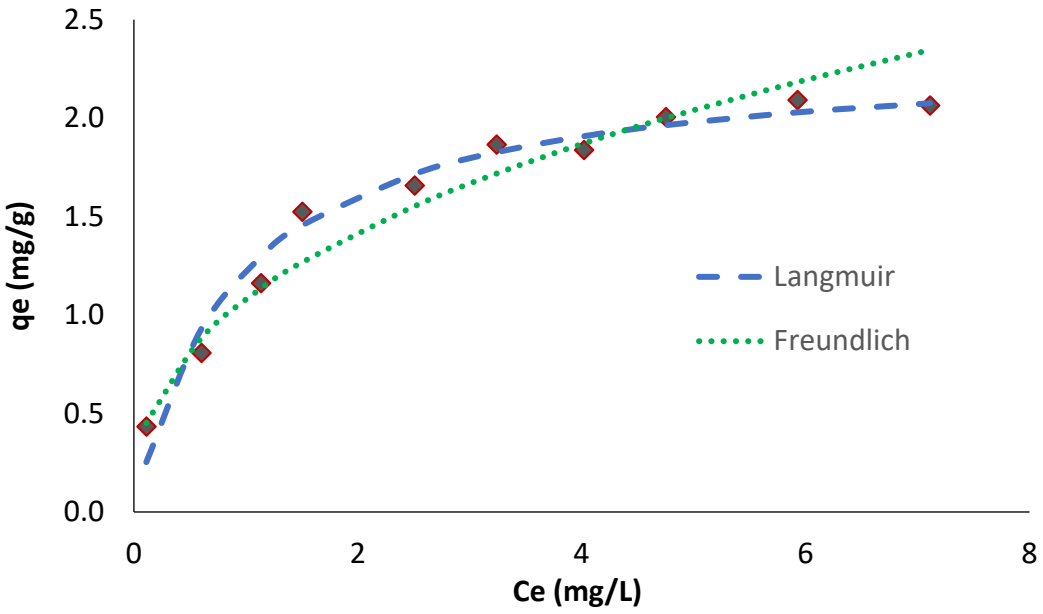

Figure 4.22: Non-linear regression plot of Langmuir and Freundlich data for the sorption of Ni

Table 4.18: Error functions of non-linear isotherms for Ni

Metal	Langmuir	Freundlich
Ni	R^2 = 0.97127	R^2 = 0.94058
	SSE = **0.0863**	*SSE* = 0.1944897
	X^2 = 0.11098	X^2 = 0.1131041

In agreement with the linear regression data, the non-linear regression data suggests that the Langmuir isotherm model provided the best fit of the data.

4.4 Effect of temperature (thermodynamics)

Experimental data were applied to the Van't Hoff equation and used to construct graphs of ln K_d versus 1/*T*. Data of duplicate experiments for the temperature-dependent analysis are represented in Tables 4.19 for Cd and 4.20 for Ni. The ln K_d versus 1/*T* graphs are presented in figures 4.24 and 4.25 for Cd and Ni respectively. The thermodynamic ICP data for Cd and Ni are shown in appendices H and I respectively.

Table 4.19: Thermodynamic data of Cd sorption (0.1 g SCG shaken @ 150 rpm for each investigated temperature)

	Experiment 1: $[Cd]_o$ =10.148 mg·L^{-1}				**Experiment 2**: **$[Cd]_o$** = 10.083 mg·L^{-1}			
Temp (K)	***Ce*** (mg·L^{-1})	$C_o - C_e$ (mg·L^{-1})	q_e (mg·g^{-1})	% Sorption	***Ce*** (mg·L^{-1})	$C_o - C_e$ (mg·L^{-1})	q_e (mg·g^{-1})	% Sorption
283	6.588	3.560	1.780	35.081	6.492	3.591	1.796	35.614
288	5.931	4.217	2.108	41.555	6.129	3.954	1.977	39.215
293	4.377	5.771	2.885	56.868	4.388	5.695	2.848	56.481
298	4.442	5.706	2.853	56.228	4.148	5.935	2.968	58.861
303	3.954	6.194	3.097	61.037	3.906	6.177	3.089	61.262
313	3.367	6.600	3.300	65.037	3.296	6.702	3.351	66.468

A maximum sorption capacity of q_e = 3.3 mg·g^{-1} was achieved at temperature 313 K indicating that the sorption may be endothermic in nature.

Table 4.20: Thermodynamic data of Ni sorption (0.1 g SCG. 150 rpm @ pH = 6)

	Experiment 1: $[Ni]_o$ = 11.693 mg·L^{-1}				**Experiment 2**: $[Ni]_o$ = 11.785 mg·L^{-1}			
Temp K	***Ce*** (mg·L^{-1})	$C_o - C_e$ (mg·L^{-1})	q_e (mg·g^{-1})	% Sorption	C_e (mg·L^{-1})	$C_o - C_e$ (mg·L^{-1})	q_e (mg·g^{-1})	% Sorption
283	8.413	3.280	1.640	28.050	8.490	3.295	1.648	27.959
288	8.018	3.675	1.838	31.429	8.052	3.733	1.867	31.676
293	7.247	4.446	2.223	38.023	7.011	4.774	2.387	40.509
298	7.077	4.616	2.308	39.477	6.927	4.858	2.429	41.222
303	7.071	4.622	2.311	39.528	6.938	4.847	2.423	41.129
313	4.92	5.472	2.736	52.656	4.875	5.517	2.756	53.089

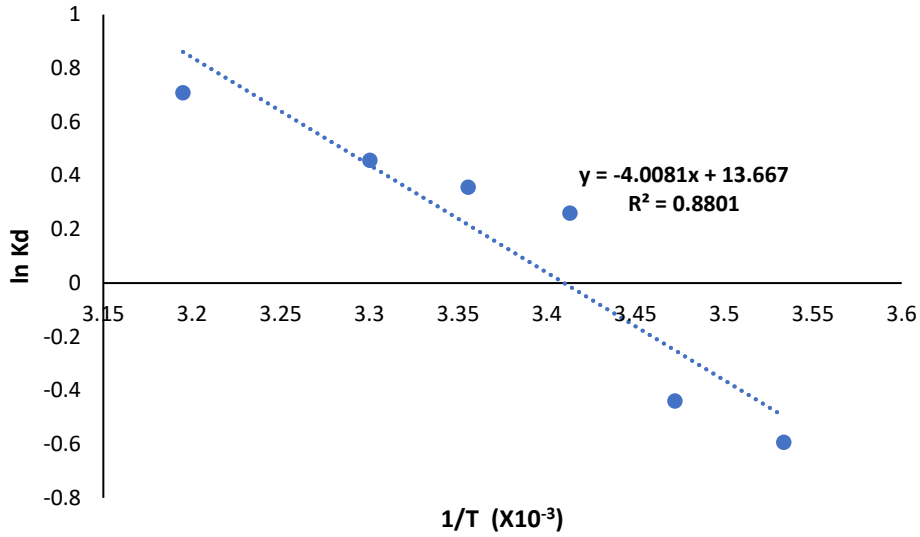

Figure 4.23: ln K_d versus 1/T for Cd

The enthalpy ($\Delta H°$) and entropy ($\Delta S°$) associated with the Cd sorption onto SCG was calculated from the graph of ln K_d versus $1/T$ as:

$$\ln(k_1) = \left(\frac{-\Delta H°}{\mathrm{R}}\right) \cdot \frac{1}{T} + \frac{\Delta S°}{\mathrm{R}}$$

$$\downarrow$$

$$y = mx + c$$

$$\downarrow$$

$$\text{Therefore, } m = \frac{-\Delta \mathrm{H}°}{R}$$

$$\downarrow$$

$$\Delta H° = -(-4008.1) \times 8.314 \text{ J·K}^{-1}\text{·mol}^{-1}$$

$$\downarrow$$

$$\Delta H° = 33323.34 \text{ or } 33.32 \text{ kJ·K}^{-1}\text{·mol}^{-1}$$

Similarly, the change in entropy was calculated from the intercept of the graph of ln K_d vs $1/T$ as:

$$c = \frac{\Delta S°}{\mathrm{R}}$$

$$\Delta S° = 13.667 \times 8.314 \text{ J·K}^{-1}\text{·mol}^{-1}$$

$$\downarrow$$

$$\Delta S° = 113.63 \text{ J/mol·K}^{-1}$$

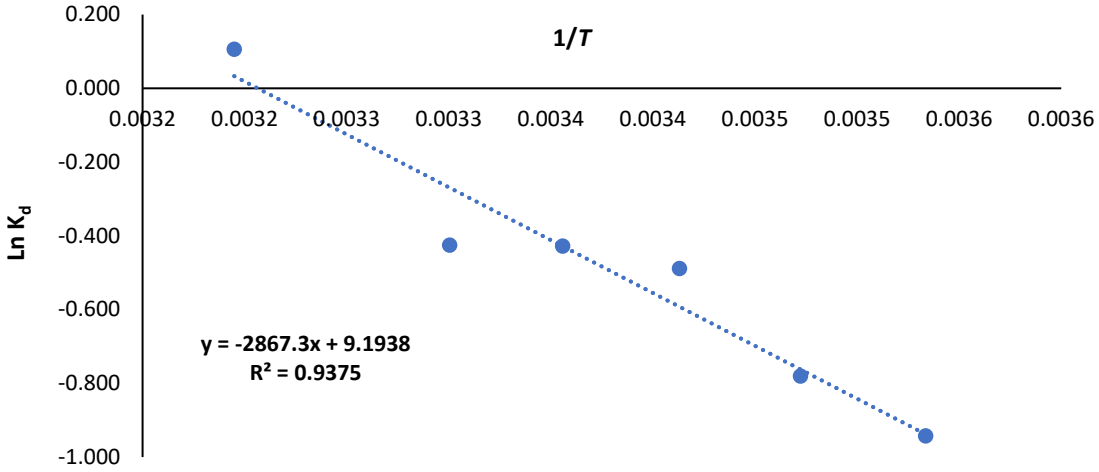

Figure 4.24: ln K_d versus 1/T for Ni

The enthalpy ($\Delta H°$) and entropy ($\Delta S°$) associated with the Ni sorption onto SCG was calculated from the graph of ln K_d versus 1/T as:

$$\ln(k_1) = \left(\frac{-\Delta H°}{\mathrm{R}}\right) \cdot \frac{1}{T} + \frac{\Delta S°}{\mathrm{R}}$$

$$\downarrow$$

$$y = mx + c$$

$$\downarrow$$

$$\text{Therefore, } m = \frac{-\Delta H°}{R}$$

$$\downarrow$$

$$\Delta H° = -(-2867.3) \times 8.314 \text{ J·K}^{-1}\text{·mol}^{-1}$$

$$\downarrow$$

$$\Delta H° = 23838.73 \text{ or } 23.84 \text{ KJ·Mol}^{-1}$$

Similarly, the change in entropy was calculated from the intercept of the graph of ln K_d vs 1/T as:

$$c = \frac{\Delta S°}{R}$$

$$\Delta S° = 9.1938 \times 8.314 \text{ J·K}^{-1}\text{·mol}^{-1}$$

$$\downarrow$$

$$\Delta S° = 76.48 \text{ J/mol·K}^{-1}$$

The relationship between percentage sorption and temperature is shown in figure 4.26 below:

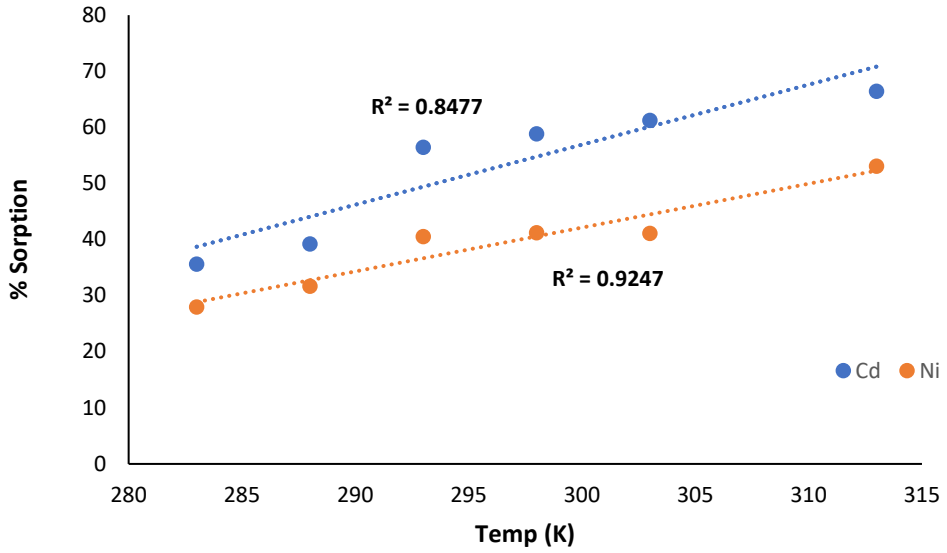

Figure 4.25: Plot % sorption versus Temperature dependence of Cd and Ni (0.1 g SCG with 10 mg·L^{-1} metal at pH = 6 for both metals)

The percentage sorption of both metals increased with increasing temperature. The experimental sorption capacities obtained for the temperature dependence investigation was in excellent agreement with the theoretical sorption capacity q_o as referred to in section 4.3.3 (initial concentration studies).

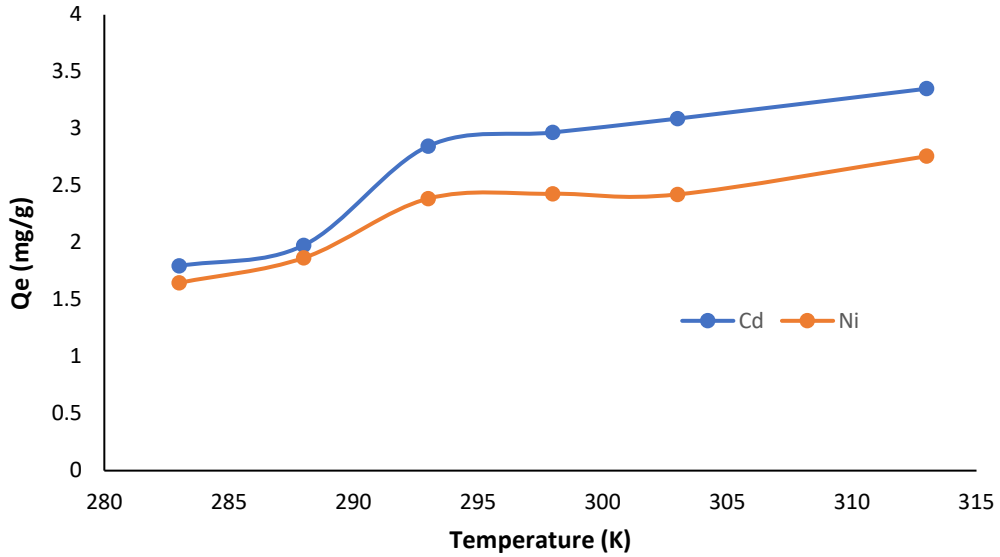

Figure 4.26: Temperature dependence of Cd & Ni data expressed as sorption capacity (q_e – mg·g^{-1})

The thermodynamic parameters were calculated according to equations 3.5 to 3.10 above and are summarized in Table 4.21 below:

Table 4.21: Summary of thermodynamic data

Metal	$\Delta H°$ (kJ/mol)	$\Delta S°$ (J/mol·K^{-1})	$\Delta G°$ (kJ·mol^{-1})					
			283K	**288K**	**293K**	**298K**	**303K**	**313K**
Cd	33.32	113.63	1.17	0.60	0.030	-0.54	-1.11	-2.25
Ni	23.84	76.44	2.33	1.95	1.57	1.19	0.81	0.05

The positive enthalpy ($\Delta H° > 0$) values for both metals suggest their sorption was endothermic. The endothermicity of the process was also confirmed by the negative slope obtained by the graphs of ln K_d vs $1/T$. The low enthalpy values suggest that physisorption contributed towards the overall sorption, as also demonstrated by the satisfactory correlation coefficient (R^2) value obtained for the Freundlich isotherm.

The spontaneity of the reaction was enhanced by increasing temperature as shown by the increase in negative value for the Gibbs free energy ($\Delta G°$) at elevated temperatures. The positive value of $\Delta S°$ suggested a greater chaotic distribution of the Cd^{2+} and Ni^{2+} ions in the solid phase when compared with the bulk phase.

4.5 Adsorption kinetics (contact time)

During initial kinetic experiments, three aliquots of the supernatant solutions were extracted for analyses of metal content at three different time intervals. After each interval, aliquots of the supernatant were withdrawn with a micropipette and analysed. This method proved ineffective as each time an aliquot was removed, the initial volume decreased and the sorbent to metal concentration ratio increased. To overcome this, separate batch solutions were prepared for each given time interval and only one aliquot was taken per batch reaction. This delivered more reliable results.

Cadmium

The experimental data of the time-dependent investigation are presented in Table 4.22 below:

Table 4.22: Initial Cd kinetic experimental data $[Cd]_o$ = 9.121 mg·L^{-1}, pH = 6 shaken at 150 revolutions per minute

Time (Min)	C_e (mg·L^{-1})	$C_o - C_e$ (mg·L^{-1})	q_t (mg·g^{-1})	% Sorption
15	5.987	3.134	0.784	8.590
20	4.131	4.990	1.248	13.677
25	3.266	5.855	1.464	16.048
30	2.735	6.386	1.597	17.504
35	3.489	5.632	1.408	15.437
40	3.629	5.492	1.373	15.053
45	3.464	5.657	1.414	15.505
50	3.439	5.682	1.421	15.574
60	2.821	6.300	1.575	17.268
90	2.909	6.212	1.553	17.027
120	4.007	5.114	1.279	14.017

Initial experimental data indicated equilibrium was attained within the first 60 minutes. Subsequent experiments investigated the contact time using 2.5-minute intervals. Experimental data used for the pseudo-first order and pseudo-second order calculations are represented in Table 4.23 below:

Table 4.23: Experimental data of time-dependent studies of Cd sorption (0.1 g SCG, pH = 6, 150 rpm and $[Cd]_o$ = 10 mg·L^{-1}

Time (Min)	C_e (mg·L^{-1})	C_o - C_e (mg·L^{-1})	q_e (mg·g^{-1})	% Sorption	Ce/qe	log (q_e-q_t)	log q_e	log C_e
2.5	7.96	1.31	0.65	14.12	3.22	0.36	-0.18	0.90
5.0	8.12	1.15	0.57	12.39	3.29	0.37	-0.24	0.91
7.5	6.47	2.81	1.40	30.26	2.62	0.19	0.15	0.81
10.0	6.73	2.54	1.27	27.40	2.73	0.22	0.10	0.83
12.5	6.92	2.36	1.18	25.41	2.80	0.25	0.07	0.84
15.0	6.51	2.77	1.38	29.83	2.63	0.19	0.14	0.81
20.0	6.36	2.91	1.46	31.40	2.58	0.17	0.16	0.80
25.0	6.34	2.93	1.47	31.64	2.57	0.17	0.17	0.80
30.0	6.03	3.24	1.62	34.94	2.44	0.12	0.21	0.78
35.0	5.94	3.33	1.67	35.96	2.40	0.11	0.22	0.77
40.0	5.39	3.89	1.94	41.92	2.18	0.00	0.29	0.73
45.0	5.56	3.71	1.86	40.04	2.25	0.04	0.27	0.74
50.0	5.43	3.85	1.92	41.47	2.20	0.01	0.28	0.73
55.0	5.69	3.58	1.79	38.66	2.30	0.06	0.25	0.75
60.0	5.33	3.94	1.97	42.50	2.16	-0.01	0.29	0.73
∞	4.33	4.94	2.47	53.26	1.75	-0.32	0.39	0.64
		Ave	1.992					
		SD	0.064					

It could be assumed with reasonable confidence that equilibrium was established after 40 minutes and the average experimental sorption capacity, q_e = 1.992 mg·g^{-1}, was obtained by calculating the average sorption capacity between 40 to 60 minutes.

As noted from figures 4.28 and 4.29, second-order kinetics provided the best fit for the Cd sorption indicating that chemisorption is the rate-limiting step. Under the conditions of the pseudo-second order kinetic model, the adsorption rate is dependent on the sorption capacity and not on the concentration of the adsorbate species.

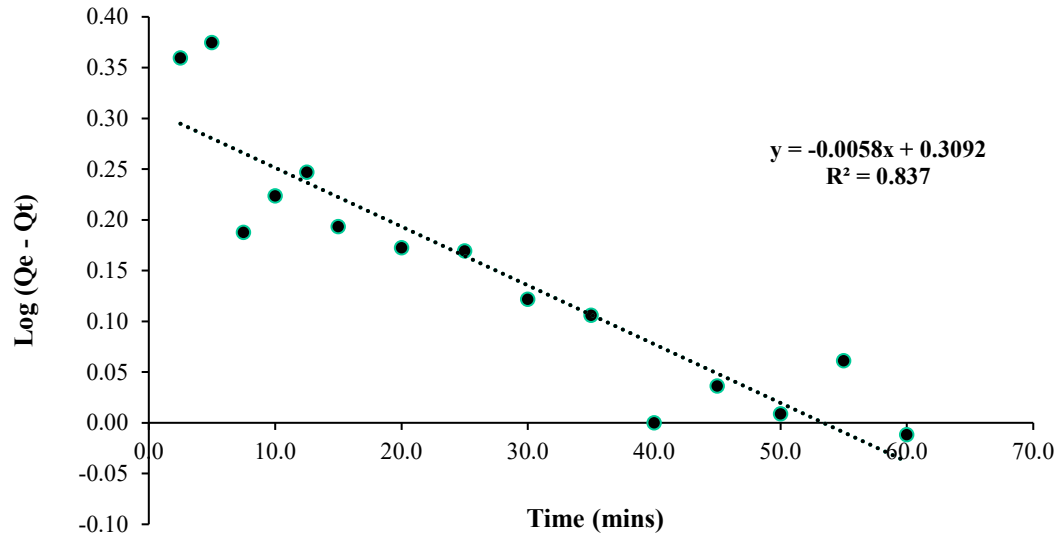

Figure 4.27: Lagergren pseudo-first order graph of Cd^{2+} sorption

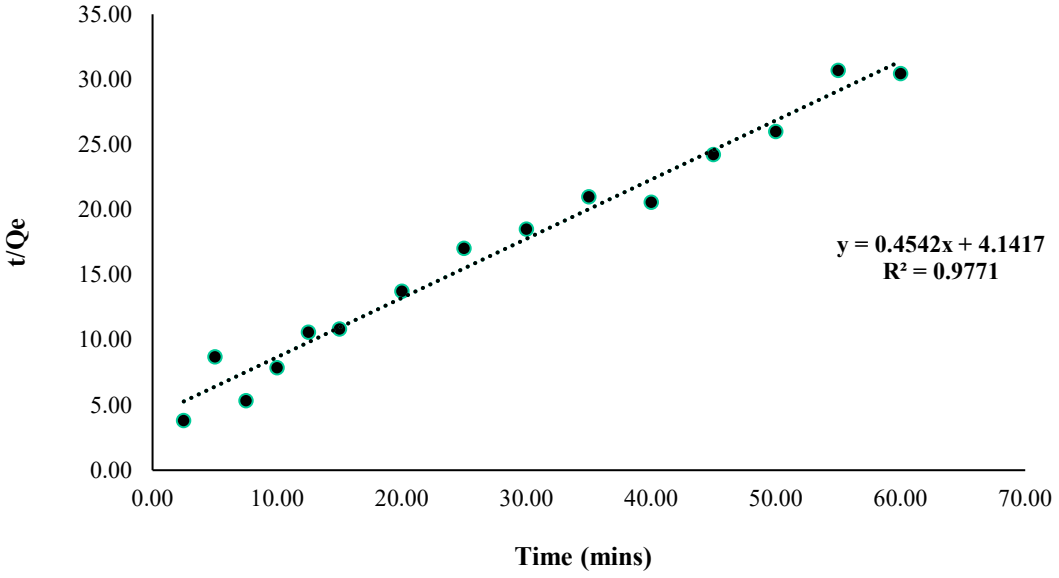

Figure 4.28: Pseudo-second order graph of reaction kinetics modelling Cd kinetics modelling of Cd^{2+} sorption

From pseudo-second order kinetics, the theoretical sorption capacity $q_{e,\,calc}$, was derived from the slope of the graph in figure 4.29 as:

$$\frac{1}{q_{e,calc}} = 0.4542$$

$q_{e,calc}$ = 2.202 mg·g^{-1}

The second-order rate constant, k_2, was derived from the intercept of the pseudo-second order graph (figure 4.29) and calculated according to equation 3.14:

$$\frac{1}{h} = \frac{1}{k_2 {q_e}^2} = 4.1417$$

k_2 = 0.0497 g/mg·min^{-1}

The value of the pseudo-first order rate constant, k_1, was derived from the corresponding graph:

$$\frac{k_1}{2.303} = 0.0058$$

k_1 = 0.0134 min^{-1}

There was a marked discrepancy between the theoretical sorption capacity (q_o = 5.04 mg·g^{-1}) obtained by the Langmuir isotherm and experimental sorption capacities ($q_{e,\,calc}$ = 2.202 mg·g^{-1}, q_e = 4.02 mg·g^{-1} and q_e = 3.3 mg·g^{-1} and q_e = 3.06 mg·g^{-1}) obtained for the kinetic, pH, thermodynamic and sorbent dosage investigations respectively. Hence, not satisfied with the obtained experimental sorption capacity, the initial concentration (C_o) values were increased 2.5 times ([Cd] = 25 mg·L^{-1}). Using the same mass of sorbent (0.1 g), succeeding initial Cd concentration studies used a concentration of [Cd] = 25.49 mg·L^{-1}, and all other parameters were kept constant (see Table 4.24).

Table 4.24: Repeat of Cd kinetics using 2.5x Cd concentration. ($[Cd]_o$ = 25.49 mg·L^{-1}, 0.1 g SCG @ pH = 6)

Time (Min)	C_o (mg·L^{-1})	C_e (mg·L^{-1})	$C_o - C_e$ (mg·L^{-1})	q_t (mg·g^{-1})	**% Sorption**
2.50	25.49	20.70	3.94	1.97	15.97
5.00	25.49	20.62	4.02	2.01	16.30
7.50	25.49	20.59	4.05	2.03	16.44
10.00	25.49	19.14	5.50	2.75	22.31
12.50	25.49	17.84	6.80	3.40	27.59
15.00	25.49	16.56	8.08	4.04	32.78
20.00	25.49	16.15	8.49	4.24	34.46
25.00	25.49	17.01	7.63	3.81	30.95
30.00	25.49	16.56	8.08	4.04	32.79
35.00	25.49	15.86	8.78	4.39	35.65
40.00	25.49	15.21	9.43	4.71	38.26
45.00	25.49	15.75	8.89	4.44	36.08
50.00	25.49	14.28	10.36	5.18	42.03
55.00	25.49	14.69	9.95	4.98	40.39
1440.00	25.49	13.50	11.99	6.00	48.67
			Ave	4.954	
			SD	0.636	

The notation q_t represents the sorption capacity at time t. Maximum sorption capacity was reached at 50 minutes (q_e = 5.18 mg·g^{-1}) and agreed with the theoretical sorption capacity (q_o = 5.04 mg·g^{-1}) derived from the Langmuir isotherm.

Nickel

Figures 4.30 and 4.31 below depict the data applied to the Lagergren pseudo-first order and Ho & McKay second-order kinetic model. The raw Ni contact time data are shown in Appendix G.

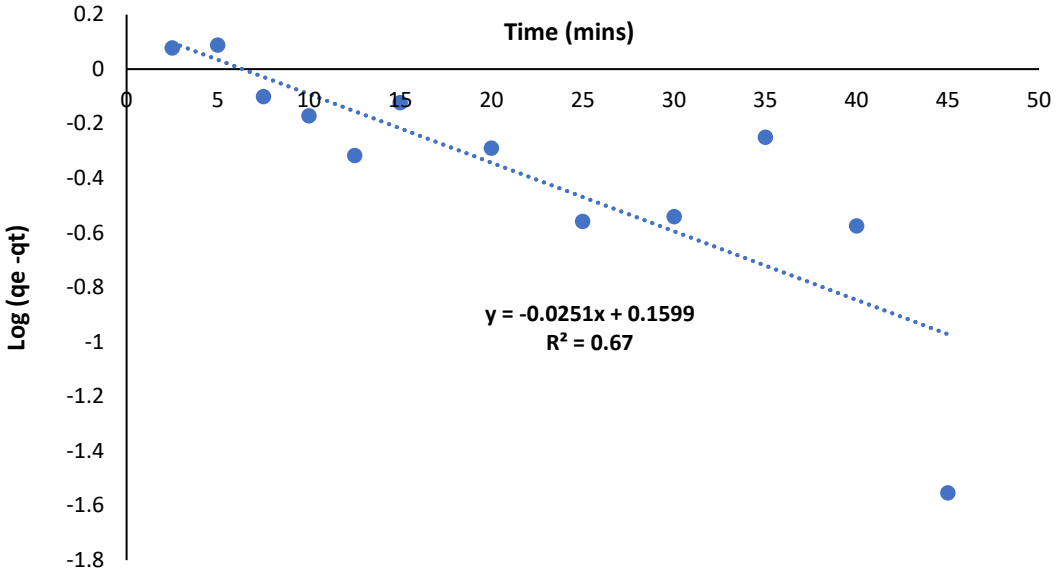

Figure 4.29: Lagergren pseudo-first order graph for Ni sorption

From the above graph (figure 4.30) of the Lagergren pseudo-first order graphs the correlation coeficcient (R^2) was found to be R^2 = 0.67. As the magnitude of the corelation coefficient directly realtes to the stregnth of the association between two variables, a R^2 value between 0.5 and 0.7 indicates a moderate corrletaion between the two variables.

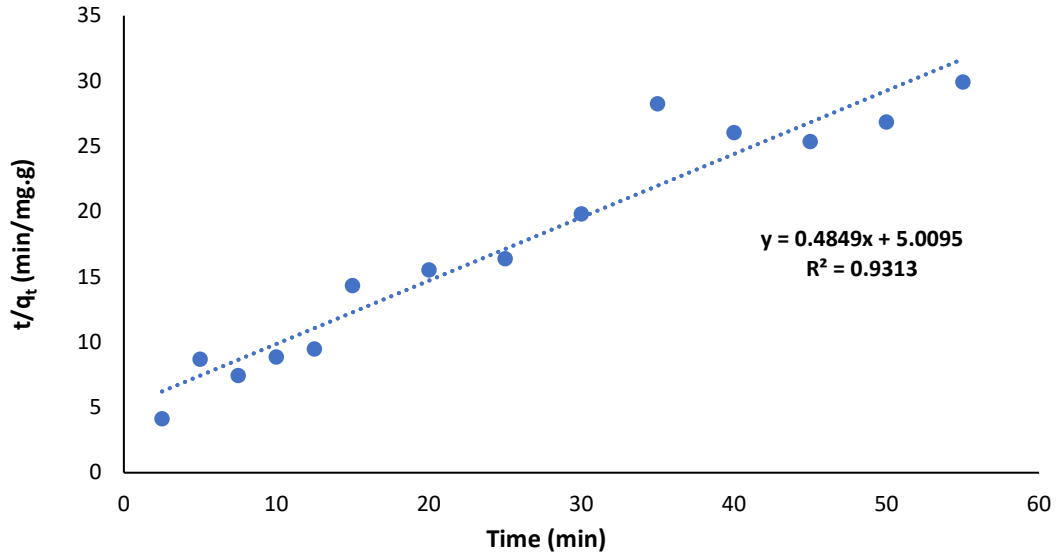

Figure 4.30: Ho and McKay pseudo-second order graph for Ni sorption

As illustrated in figures 4.28 to 4.31 above, the pseudo-second order reaction kinetics provided the best fit for both Cd and Ni sorption onto SCG. In the case of Cd, both pseudo-first and pseudo-second order yielded satisfactory correlation coefficients, indicating both chemisorption and physisorption strongly contributed to the overall sorption. In the case of Ni sorption, pseudo-second order provided a much better R^2, thus suggesting that the Ni sorption is more inclined to chemisorption.

4.6 Failed experiments and observations

As with any scientific investigation, initial trial and error experiments lead to a series of observations that in turn assist the smooth flow of the final experiments. Some of the most important observations made during trial-and-error experiments are discussed below.

4.6.1 Susceptibility to microbial attack

As pH is one of the most important influences on the sorption of heavy metals, initial experiments studied the pH dependence of the sorption. It was noted that when conducting batch experiments and storing the final filtered supernatant solution in the fridge, the solutions were susceptible to microbial attack. Even when stored in the fridge, mould growth was observed after approximately 5 to 7 days. It was noted that the solutions buffered at more acidic pH (1 and 2) were the first to show signs of mould growth. It was therefore concluded that supernatant solutions cannot be stored too long after batch reactions. Thus, all ICP analyses of samples were either carried out on the same day of filtration or within 24 hours after the collection of the supernatant solution.

4.6.2 Trial and error kinetic experiments

Another parameter that proved to be a tedious task was the time dependence of the sorption. Batch reactions were prepared in 50 mL sample bottles. For initial experiments, multiple aliquots of supernatant solution were measured into each bottle at different time intervals. A zigzag pattern was observed for the sorption when graphically plotting *Ce* (concentration at time *t*) vs. time in seconds. It was concluded that when removing more than 1 aliquot per sample bottle, the initial volume decreased with every aliquot removed. This, in turn, exponentially increased the sorption of the following aliquot. Hence for all other kinetic studies, only 1 aliquot per bottle was removed per time interval.

4.6.3 Investigation to determine whether filter paper sorbed the metals from solution

As a control measure and to ensure that no metal was lost due to filtration, the filter paper used throughout the analyses was tested for heavy metal sorption. A range of calibration standards was prepared for both Cd and Ni (2, 4, 6, 8 & 10 $mg \cdot L^{-1}$). The calibration standard concentrations were verified using the ICP-OES prior to the filtration. The calibration standards were then individually filtered through the filter paper and once again checked by ICP-OES to see if the instrument calibrated successfully. These data were further utilised to compare the correlation coefficients and concentrations obtained.

It was noted there was no change in concentration when filtering the calibration standards through the filter paper. Both calibration curves yielded correlation coefficients of $R^2 = 0.998$ and $R^2 = 0.0997$ for both filtered and non-filtered samples, respectively. These data clearly indicated that no metal sorption occurred on the filter paper. The ICP Cd data after filtration are shown in Appendix K.

CHAPTER 5
CONCLUDING REMARKS AND RECOMMENDATIONS

5.1 Summary of results

The pH studies indicated that maximum sorption of Cd and Ni onto SCG occurs at pH 6. Isotherm studies fitted both Langmuir and Freundlich isotherms well, indicating that both chemisorption and physisorption contribute towards the sorption mechanisms of the metals. In the case of cadmium sorption, the Freundlich isotherm exhibited a better correlation coefficient ($R^2 = 0.988$) for both linear and non-linear models - implying that the sorption of Cd onto SCG was inclined towards physisorption and that sorption occurred in a multilayer fashion.

For both Cd and Ni, smaller sorbent dosages provided the best sorption capacities. The maximum experimental sorption capacities for sorbent dosage experiments were calculated as q_e =3.06 mg·g^{-1} and q_e =2.24 mg·g^{-1} for Cd and Ni, respectively. These values were obtained when 0.1 g sorbent in 10 mg·L^{-1} buffered metal stock solution was used in batch experiments.

In the Ni isotherm studies, Langmuir provided the best correlation coefficient ($R^2 = 0.9916$) indicating that chemisorption may be the dominating sorption mechanism. Hence it can be deduced that the sorption of Ni occurred via chemisorption in a monolayer fashion until all the active sites had been occupied. This was followed by additional physical interactions between the functional groups on the active sites and surrounding metal ions.

Physisorption most likely occurred due to weak Van der Waal forces. Chemisorption was probably due to metal binding with the remaining functional groups present in the SCG. Additionally, the theoretical sorption capacity value for Cadmium $q_o = 5.04$ mg·g^{-1} was not in satisfactory agreement with that of the experimental $q_e = 2.56$ mg·g^{-1} obtained for Cd. The Ni values $q_o = 2.343$ mg·g^{-1} were in high accord with that of the experimental q_e = 2.059 mg·g^{-1} when using 10 mg·L^{-1} initial concentration.

The maximum theoretical sorption capacity for Cd (q_e = 5.043 mg·g^{-1}) reported for this study was approximately three times less than the maximum reported by Azouaou et al. (2010) ($q_o = 15.65$ mg ·g^{-1}) who used untreated coffee grounds. However, the sorption capacity for this study was in exceptional agreement with that reported by Patterer et al. (2017) ($q_o = 4.342$ mg·g^{-1}) and Yen and Lin (2016), who applied the Taguci experimental design and reported a q_o = 5.46 mg.g^{-1}. From the comparison of the sorption capacities with that of Patterer et al. (2017) and Yen and Lin (2016), it can be concluded that stripping the SCG of its oils by using SFE did not seem to have a major impact on the sorption capacity of the SCG.

The binding strength was calculated as K_L = 0.49 L·mg^{-1} for Cd and 1.09 L·mg^{-1} for Ni. Thus, Ni has a greater binding strength than Cd. By using the linearised equation (equation 4.7) the Freundlich constants were calculated as $K_F = 1.085\ mg \cdot g^{-1}$ and $K_F = 1.097\ mg \cdot g^{-1}$ for Cd and Ni, respectively.

The thermodynamic data for this study indicated the sorption to be non-spontaneous at room temperature. However, sorption became possible at elevated temperatures (spontaneity increased with increasing temperatures). In addition, in contrast to Azouaou et al. (2010) who reported Cd sorption to be exothermic, thermodynamic data for this study indicated the sorption onto SFE-SCG to be endothermic in nature ($\Delta H°$ = 33.32 kJ·mol^{-1} for Cd & 23.84 kJ·mol^{-1} for Ni). The positive entropy values suggest an increase in disorder; $\Delta S°$= 113.63 J/mol^{-1}· K^{-1} for Cd and 76.44 J/mol^{-1}·K^{-1} for Ni.

In the initial kinetic studies where metal concentrations of 10 mg·L^{-1} and 0.1 g SCG were used, equilibrium was reached in less than 60 minutes (at 50 minutes). The sorption kinetic data best fitted pseudo-second order kinetics with a correlation coefficient of (R^2= 0.9771) and (R^2 =0.9818) for Cd and Ni, respectively. The R_L values for both metals were between 0 and 1, and this implied that the sorption was favourable over the entire concentration range investigated. The R_L approached 0 as the metal concentration increased, indicating that the reaction was probably irreversible at higher concentrations. For the initial Cd kinetic experiments, the experimental sorption capacity was half of the theoretical sorption capacity. As the experimental sorption capacity was unsatisfactory, the kinetics were repeated at elevated metal concentrations. Subsequent Cd kinetic studies investigated increased (2.5×) initial Cd concentration (increased from 10 mg·L^{-1} to 25 mg·L^{-1}) and delivered a noticeably improved agreement of the theoretical sorption capacity (q_o = 5.04 mg·g^{-1}) with the experimental sorption capacity (q_e = 5.18 mg·g^{-1}).

It was established that despite being stripped of its remaining oils via SFE, SCG can be used as a low cost, non-toxic bio-sorbent to effectively remove heavy metals from water. However, a disadvantage was the susceptibility of SCG to microbial attack by acidophilic fungi. This susceptibility to microbial attack limits the analyses window. This contamination has not been reported for traditional SPE which uses activated carbons.

This study, therefore, has shown the dual function offered by the bio-sorbent SCG. It was demonstrated that SGC can be used to produce oils that could be used in the petrochemical industry (Le et al., 2017) and that the stripped SGC can also serve as an adsorbent for Cd and Ni present in aquatic solutions.

5.2 Recommendations

Based on the results obtained for this study, the recommendations for further research are:

- To explore the optimization of the supercritical fluid extraction process for the extraction of the oils from the SCG,
- Examine, quantify, and identify the functional groups of the extract obtained by using the SFE process,
- Investigate the bio-diesel production capability of the oil obtained from the SCG,
- Investigate more polluting metals for their sorption ability by SCG and
- Conduct column studies for the sorption of metals by SCG.

REFERENCES

Albadarin, A.B. & Mangwandi, C. 2015. Mechanisms of Alizarin Red S and Methylene blue biosorption onto olive stone by-product: Isotherm study in single and binary systems. *Journal of Environmental Management*, 164: 86–93. https://linkinghub.elsevier.com/retrieve/pii/S0301479715302449.

Alpat, Ş., Alpat, S.K., Çadirci, B.H., Özbayrak, Ö. & Yasa, I. 2010. Effects of biosorption parameter: Kinetics, isotherm and thermodynamics for Ni(II) biosorption from aqueous solution by Circinella sp. *Electronic Journal of Biotechnology*, 13(5).

Anastopoulos, I., Karamesouti, M., Mitropoulos, A.C. & Kyzas, G.Z. 2017. A review for coffee adsorbents. *Journal of Molecular Liquids*, 229: 555–565. https://linkinghub.elsevier.com/retrieve/pii/S0167732216335371.

Atabani, A.E., Al-Muhtaseb, A.H., Kumar, G., Saratale, G.D., Aslam, M., Khan, H.A., Said, Z. & Mahmoud, E. 2019. Valorization of spent coffee grounds into biofuels and value-added products: Pathway towards integrated bio-refinery. *Fuel*, 254: 115640. https://linkinghub.elsevier.com/retrieve/pii/S0016236119309925.

Ayala, J. & Fernández, B. 2019. Treatment of mining waste leachate by the adsorption process using spent coffee grounds. *Environmental Technology*, 40(15): 2037–2051. https://www.tandfonline.com/doi/full/10.1080/09593330.2018.1435739.

Azouaou, N., Sadaoui, Z., Djaafri, A. & Mokaddem, H. 2010. Adsorption of cadmium from aqueous solution onto untreated coffee grounds: Equilibrium, kinetics and thermodynamics. *Journal of Hazardous Materials*, 184(1–3): 126–134. http://dx.doi.org/10.1016/j.jhazmat.2010.08.014.

Belitz, H.-D., Grosch, W. & Schieberle, P. 2004. Coffee, Tea, Cocoa. In *Food Chemistry*. Berlin, Heidelberg: Springer Berlin Heidelberg: 939–969. http://link.springer.com/10.1007/978-3-662-07279-0_22.

Bhuvaneshwari, S. & Sivasubramanian, V. 2014. EQUILIBRIUM, KINETICS, AND BREAKTHROUGH STUDIES FOR ADSORPTION OF Cr(VI) ON CHITOSAN. *Chemical Engineering Communications*, 201(6): 834–854. http://www.tandfonline.com/doi/abs/10.1080/00986445.2013.793674.

Campos-Vega, R., Loarca-Piña, G., Vergara-Castañeda, H.A. & Dave Oomah, B. 2015. Spent coffee grounds: A review on current research and future prospects. *Trends in Food Science and Technology*, 45(1): 24–36.

Cantu, Y., Remes, A., Reyna, A., Martinez, D., Villarreal, J., Ramos, H., Trevino, S., Tamez, C., Martinez, A., Eubanks, T. & Parsons, J.G. 2014. Thermodynamics, Kinetics, and Activation energy Studies of the sorption of chromium(III) and chromium(VI) to a Mn 3 O 4 nanomaterial. *Chemical Engineering Journal*, 254: 374–383.

Davila-Guzman, N.E., Cerino-Córdova, F.J., Loredo-Cancino, M., Rangel-Mendez, J.R., Gómez-González, R. & Soto-Regalado, E. 2016. Studies of Adsorption of Heavy Metals onto Spent Coffee Ground: Equilibrium, Regeneration, and Dynamic Performance in a Fixed-Bed Column. *International Journal of Chemical Engineering*, 2016: 1–11. http://www.hindawi.com/journals/ijce/2016/9413879/.

Dávila-Guzmán, N.E., de Jesús Cerino-Córdova, F., Soto-Regalado, E., Rangel-Mendez, J.R., Díaz-Flores, P.E., Garza-Gonzalez, M.T. & Loredo-Medrano, J.A. 2013. Copper Biosorption by Spent Coffee Ground: Equilibrium, Kinetics, and Mechanism. *CLEAN - Soil, Air, Water*, 41(6): 557–564. http://doi.wiley.com/10.1002/clen.201200109.

Gadd, G.M. 2009. Biosorption: critical review of scientific rationale, environmental importance and significance for pollution treatment. *Journal of Chemical Technology & Biotechnology*, 84(1): 13–28. http://doi.wiley.com/10.1002/jctb.1999.

Gomez-Gonzalez, R., Cerino-Córdova, F.J., Garcia-León, A.M., Soto-Regalado, E., Davila-Guzman, N.E. & Salazar-Rabago, J.J. 2016. Lead biosorption onto coffee grounds: Comparative analysis of several optimization techniques using equilibrium adsorption models and ANN. *Journal of the Taiwan Institute of Chemical Engineers*, 68: 201–210. http://dx.doi.org/10.1016/j.jtice.2016.08.038.

Hardgrove, S.J. & Livesley, S.J. 2016. Applying spent coffee grounds directly to urban agriculture soils greatly reduces plant growth. *Urban Forestry & Urban Greening*, 18: 1–8. https://linkinghub.elsevier.com/retrieve/pii/S1618866716300103.

Ho, Y.S. & McKay, G. 1998. Sorption of dye from aqueous solution by peat. *Chemical Engineering Journal*, 70(2): 115–124.

Imessaoudene, D., Hanini, S. & Bouzidi, A. 2013. Biosorption of strontium from aqueous solutions onto spent coffee grounds. *Journal of Radioanalytical and Nuclear Chemistry*, 298(2): 893–902.

Imessaoudene, D., Hanini, S., Bouzidi, A. & Ararem, A. 2016. Kinetic and thermodynamic study of cobalt adsorption by spent coffee. *Desalination and Water Treatment*, 57(13): 6116–6123. http://www.tandfonline.com/doi/full/10.1080/19443994.2015.1041049.

Jeppu, G.P. & Clement, T.P. 2012. A modified Langmuir-Freundlich isotherm model for simulating pH-dependent adsorption effects. *Journal of Contaminant Hydrology*, 129–130: 46–53. https://linkinghub.elsevier.com/retrieve/pii/S0169772211001434.

Le, P.T.K., Vu, Q.T.H., Nguyen, Q.T.V., Tran, K.A. & Le, K.A. 2017. Spent coffee grounds as a valuable source of bioactive compounds and bioenergy. *Chemical Engineering Transactions*, 56: 37–42.

Massaya, J., Prates Pereira, A., Mills-Lamptey, B., Benjamin, J. & Chuck, C.J. 2019. Conceptualization of a spent coffee grounds biorefinery: A review of existing valorisation approaches. *Food and Bioproducts Processing*, 118.

McNutt, J. & He, Q. (Sophia). 2019. Spent coffee grounds: A review on current utilization. *Journal of Industrial and Engineering Chemistry*, 71: 78–88. https://linkinghub.elsevier.com/retrieve/pii/S1226086X18314825.

Mussatto, S.I., Carneiro, L.M., Silva, J.P.A., Roberto, I.C. & Teixeira, J.A. 2011. A study on chemical constituents and sugars extraction from spent coffee grounds. *Carbohydrate Polymers*, 83(2): 368–374. https://linkinghub.elsevier.com/retrieve/pii/S0144861710006119.

Mussatto, S.I., Machado, E.M.S., Carneiro, L.M. & Teixeira, J.A. 2012. Sugars metabolism and ethanol production by different yeast strains from coffee industry wastes hydrolysates. *Applied Energy*, 92: 763–768. http://dx.doi.org/10.1016/j.apenergy.2011.08.020.

Mussatto, S.I., Machado, E.M.S., Martins, S. & Teixeira, J.A. 2011. Production, Composition, and Application of Coffee and Its Industrial Residues. *Food and Bioprocess Technology*, 4(5): 661–672. http://link.springer.com/10.1007/s11947-011-0565-z.

Naga Babu, A., Reddy, D.S., Kumar, G.S., Ravindhranath, K. & Krishna Mohan, G.V. 2018. Removal of lead and fluoride from contaminated water using exhausted coffee grounds based bio-sorbent. *Journal of Environmental Management*, 218: 602–612. https://linkinghub.elsevier.com/retrieve/pii/S0301479718304791.

Oestreich-Janzen, S. 2010. Chemistry of Coffee. In *Comprehensive Natural Products II*. Elsevier: 1085–1117. https://linkinghub.elsevier.com/retrieve/pii/B9780080453828007085.

Ofomaja, A.E. & Naidoo, E.B. 2011. Biosorption of copper from aqueous solution by chemically activated pine cone: A kinetic study. *Chemical Engineering Journal*, 175(1): 260–270. http://dx.doi.org/10.1016/j.cej.2011.09.103.

Park, D., Yun, Y.-S. & Park, J.M. 2010. The past, present, and future trends of biosorption. *Biotechnology and Bioprocess Engineering*, 15(1): 86–102. http://link.springer.com/10.1007/s12257-009-0199-4.

Patterer, M.S., Bavasso, I., Sambeth, J.E. & Medici, F. 2017. Cadmium removal from acqueous solution by adsorption on spent coffee grounds. *Chemical Engineering Transactions*, 60: 157–162.

Perdana, B.M., Manihuruk, R., Ashyar, R., Heriyanti & Sutrisno. 2018. Evaluation of the effect of roasting process on the energy transition and the crystalline structures of Arabica, Robusta , and Liberica coffee from Jambi Indonesia. *IOP Conference Series: Materials Science and Engineering*, 345(1): 012021. https://iopscience.iop.org/article/10.1088/1757-899X/345/1/012021.

Prabhakaran, S.K., Vijayaraghavan, K. & Balasubramanian, R. 2009. Removal of Cr(VI) Ions by Spent Tea and Coffee Dusts: Reduction to Cr(III) and Biosorption. *Industrial & Engineering Chemistry Research*, 48(4): 2113–2117. https://pubs.acs.org/doi/10.1021/ie801380h.

Qaiser, S., Saleemi, A.R. & Ahmad, M.M. 2007. Heavy metal uptake by agro based waste materials. *Electronic Journal of Biotechnology*, 10(3): 409–416.

Rahimzadeh, Mehrdad Rafati, Rahimzadeh, Mehravar Rafati, Kazemi, S. & Moghadamnia, A.A. 2017. Cadmium toxicity and treatment: An update. *Caspian Journal of Internal Medicine*, 8(3): 135–145.

Rao, H.J., Kalyani, G., Rao, K.V., Anup Kumar, T., Mariadas, K., Prasanna Kumar, Y., Vijetha, P., Pallavi, P., Sumalatha, B. & Kumaraswamy, K. 2010. *Kinetic Studies on Biosorption of Lead from Aqueous Solutions using Egg Shell Powder*.

Sameera, V., Naga Deepthi, C., Srinu Babu, G. & Ravi Teja, Y. 2011. Role of Biosorption in Environmental Cleanup. *Journal of Microbial & Biochemical Technology*, 03(03): 1–8. https://www.omicsonline.org/role-of-biosorption-in-environmental-cleanup-1948-5948.R1-001.php?aid=2050.

Savolainen, H. 1992. Tannin content of tea and coffee. *Journal of Applied Toxicology*, 12(3): 191–192. http://doi.wiley.com/10.1002/jat.2550120307.

Simões, J., Madureira, P., Nunes, F.M., do Rosário Domingues, M., Vilanova, M. & Coimbra, M.A. 2009. Immunostimulatory properties of coffee mannans. *Molecular Nutrition & Food Research*, 53(8): 1036–1043. http://doi.wiley.com/10.1002/mnfr.200800385.

Somnuk, K., Eawlex, P. & Prateepchaikul, G. 2017. Optimization of coffee oil extraction from spent coffee grounds using four solvents and prototype-scale extraction using circulation process. *Agriculture and Natural Resources*, 51(3): 181–189. https://linkinghub.elsevier.com/retrieve/pii/S2452316X17303393.

Spies, A.R.L. & Wewers, F. 2020. Equilibrium, kinetics and thermodynamics studies of Cd sorption onto a dithizone-impregnated Amberchrom CG-300m polymer resin. *Arabian Journal of Chemistry*, 13(4): 5050–5059.

Tokimoto, T., Kawasaki, N., Nakamura, T., Akutagawa, J. & Tanada, S. 2005. Removal of lead ions in drinking water by coffee grounds as vegeTable biomass. *Journal of Colloid and Interface Science*, 281(1): 56–61.

Utomo, H.D. & Hunter, K.A. 2006. Adsorption of heavy metals by exhausted coffee grounds as a potential treatment method for waste waters. *e-Journal of Surface Science and Nanotechnology*, 4: 504–506. http://joi.jlc.jst.go.jp/JST.JSTAGE/ejssnt/2006.504?from=CrossRef.

Volesky, B. 2007. Biosorption and me. *Water Research*, 41(18): 4017–4029. https://linkinghub.elsevier.com/retrieve/pii/S0043135407004344.

Yen, H.Y. & Lin, C.P. 2016. Adsorption of Cd(II) from wastewater using spent coffee grounds by Taguchi optimization. *Desalination and Water Treatment*, 57(24): 11154–11161.

APPENDICES

APPENDIX A: SEM images of the sorbent (SCG) before sorption experiments

SCG before SFE

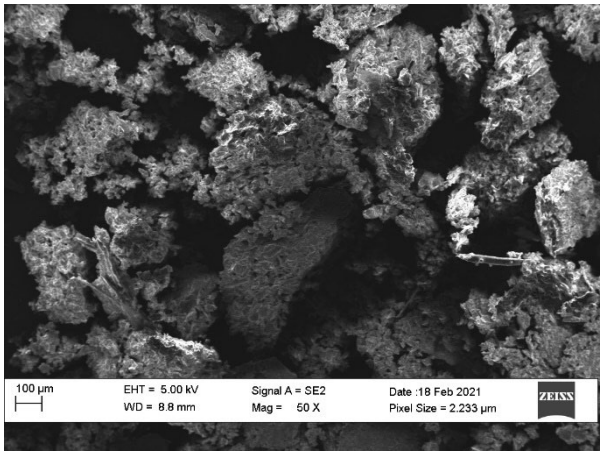

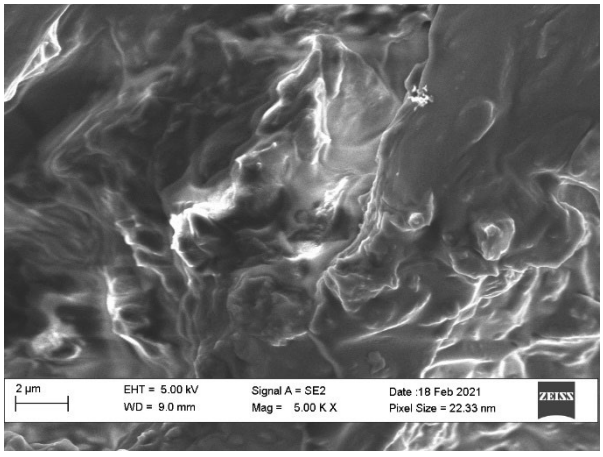

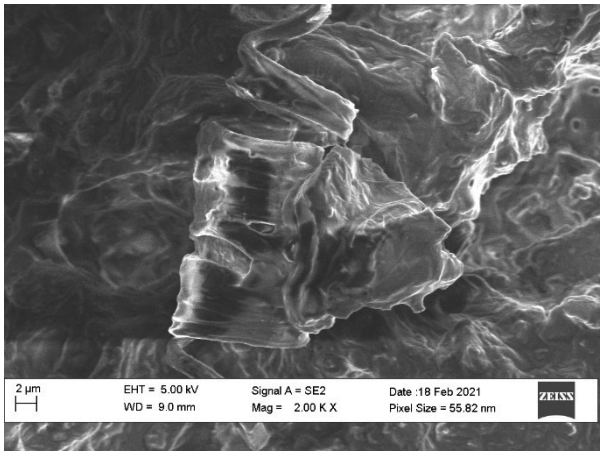

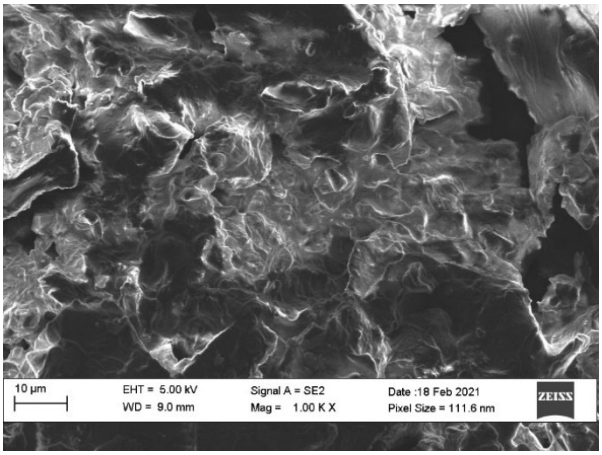

SCG after SFE

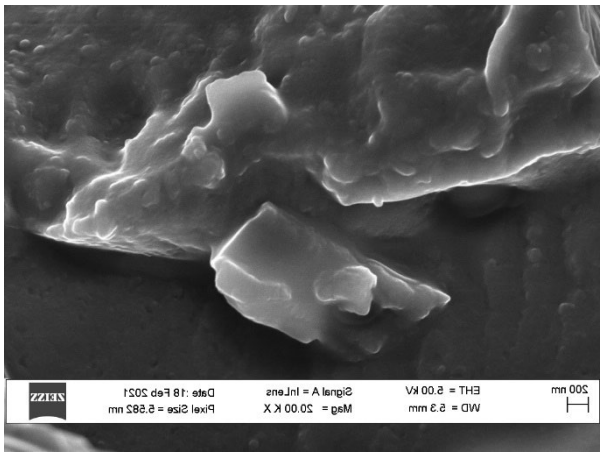

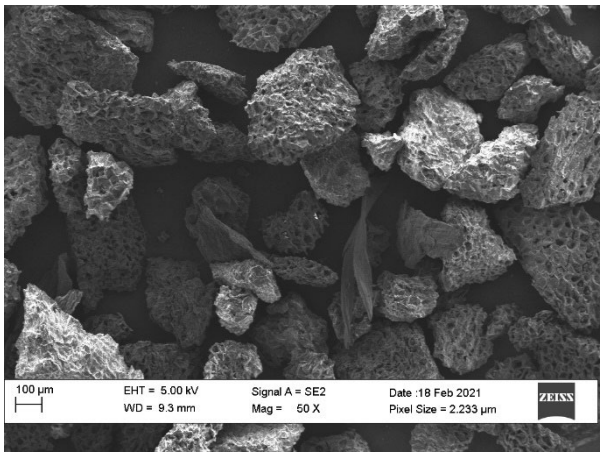

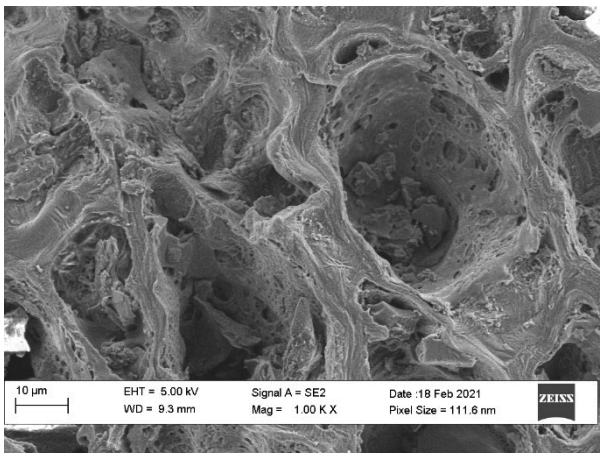

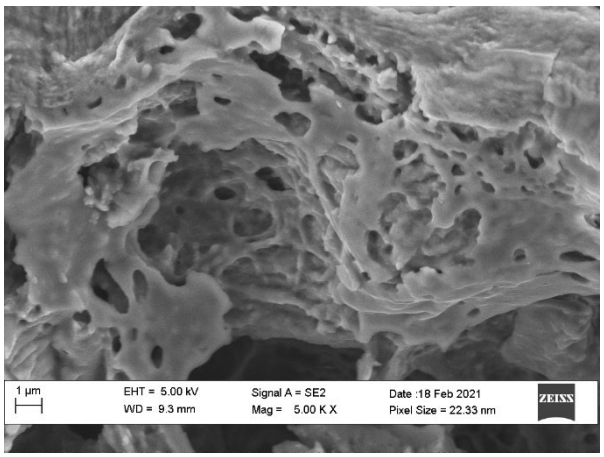

APPENDIX B: SEM images of the sorbent after Cd sorption batch experiments

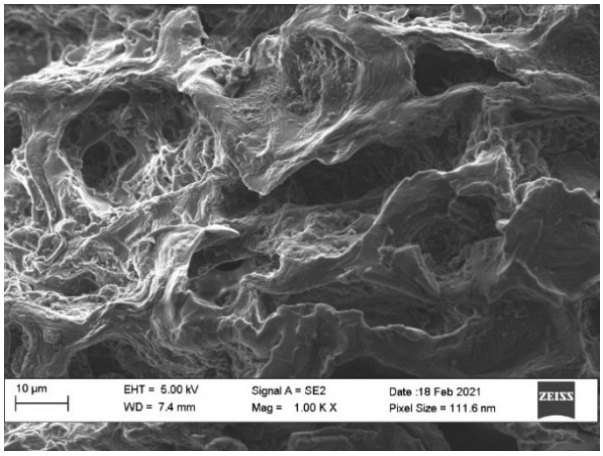

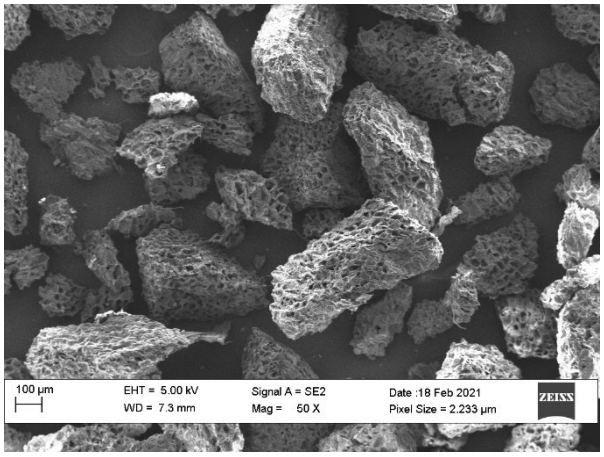

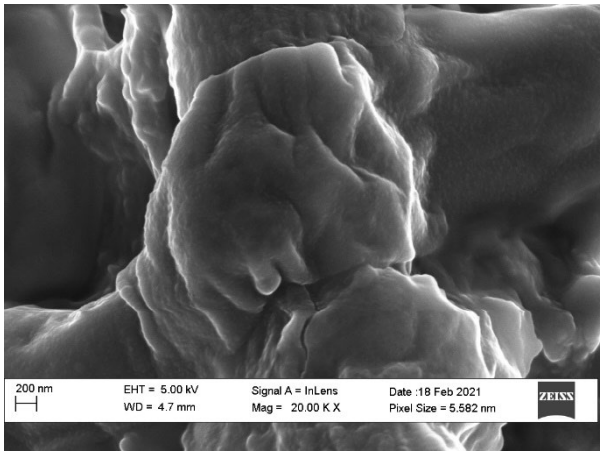

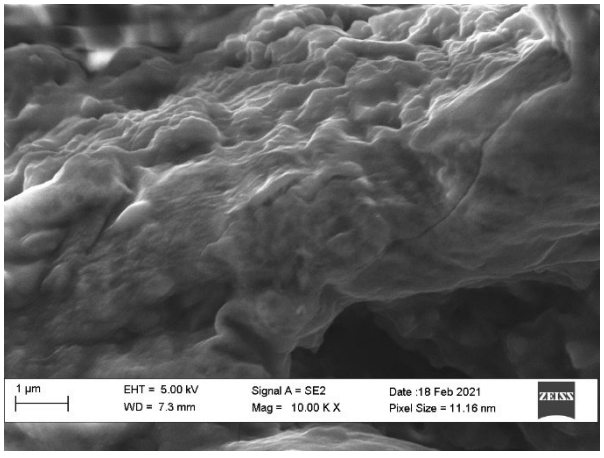

APPENDIX C: SEM images of the sorbent after Ni sorption experiments

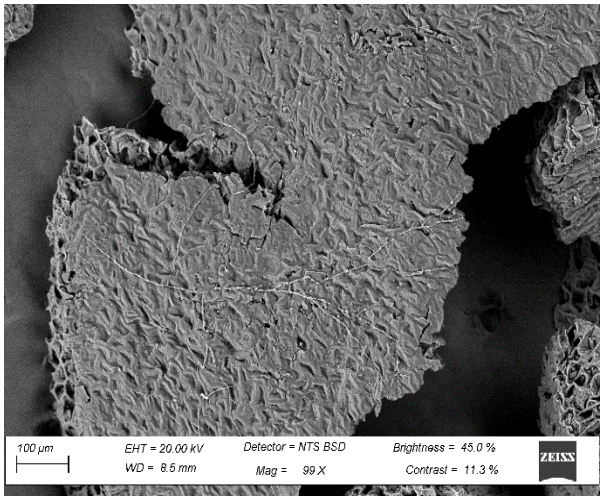

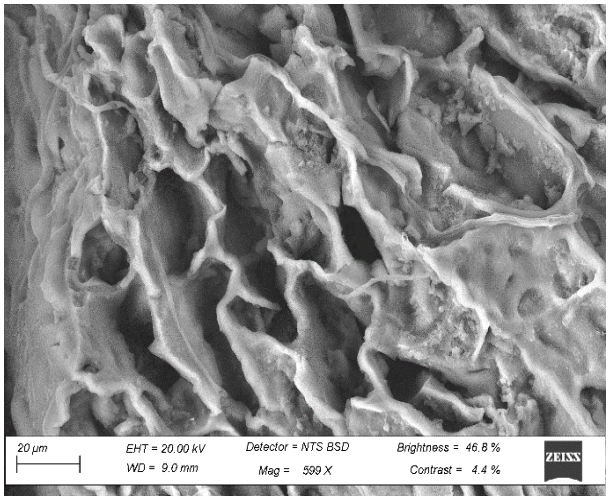

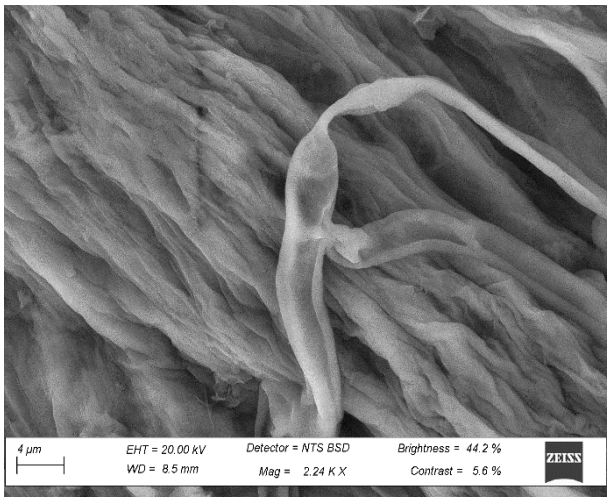

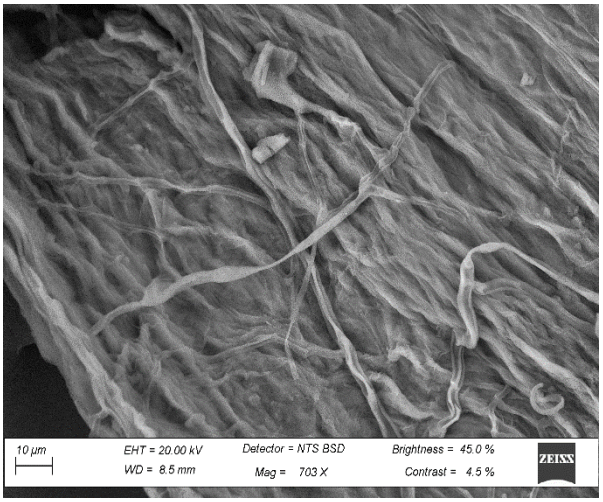

APPENDIX D: Sorbent dosage of Cd using batch reactions; $[Cd]_0$ = 10.764 mg/L; ph = 6

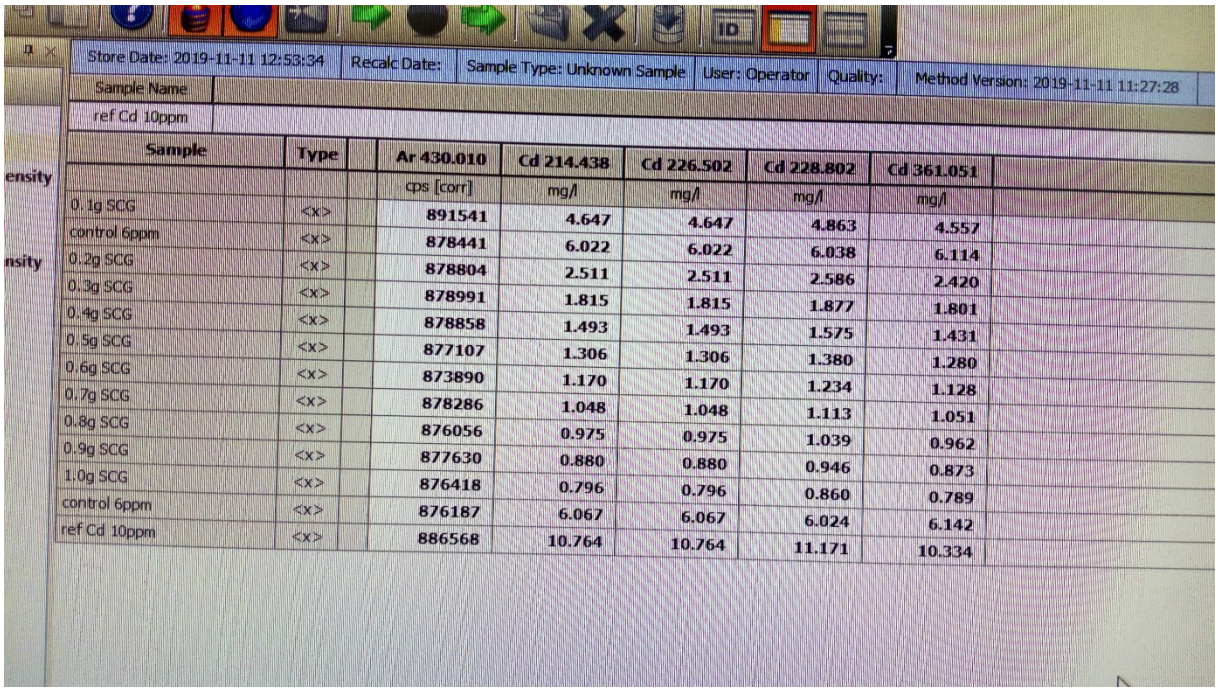

Store Date: 2019-11-11 12:53:34 | Recalc Date: | Sample Type: Unknown Sample | User: Operator | Quality: | Method Version: 2019-11-11 11:27:28

Sample Name: ref Cd 10ppm

Sample	Type	Ar 430.010	Cd 214.438	Cd 226.502	Cd 228.802	Cd 361.051
		cps [corr]	mg/l	mg/l	mg/l	mg/l
0.1g SCG	<x>	891541	4.647	4.647	4.863	4.557
control 6ppm	<x>	878441	6.022	6.022	6.038	6.114
0.2g SCG	<x>	878804	2.511	2.511	2.586	2.420
0.3g SCG	<x>	878991	1.815	1.815	1.877	1.801
0.4g SCG	<x>	878858	1.493	1.493	1.575	1.431
0.5g SCG	<x>	877107	1.306	1.306	1.380	1.280
0.6g SCG	<x>	873890	1.170	1.170	1.234	1.128
0.7g SCG	<x>	878286	1.048	1.048	1.113	1.051
0.8g SCG	<x>	876056	0.975	0.975	1.039	0.962
0.9g SCG	<x>	877630	0.880	0.880	0.946	0.873
1.0g SCG	<x>	876418	0.796	0.796	0.860	0.789
control 6ppm	<x>	876187	6.067	6.067	6.024	6.142
ref Cd 10ppm	<x>	886568	10.764	10.764	11.171	10.334

APPENDIX E: Picture of sorbent before furnace exposure for ash content determination

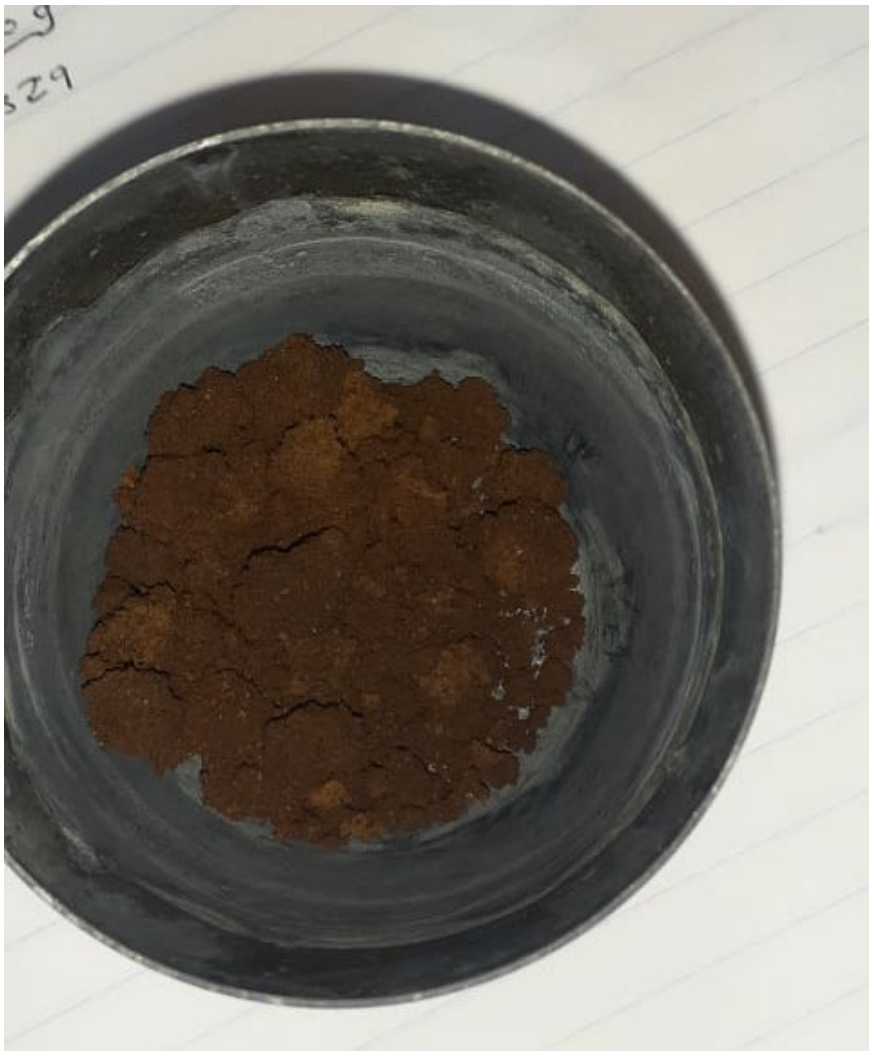

APPENDIX F: Sorbent after ash content determination

APPENDIX G: ICP contact time data for Ni

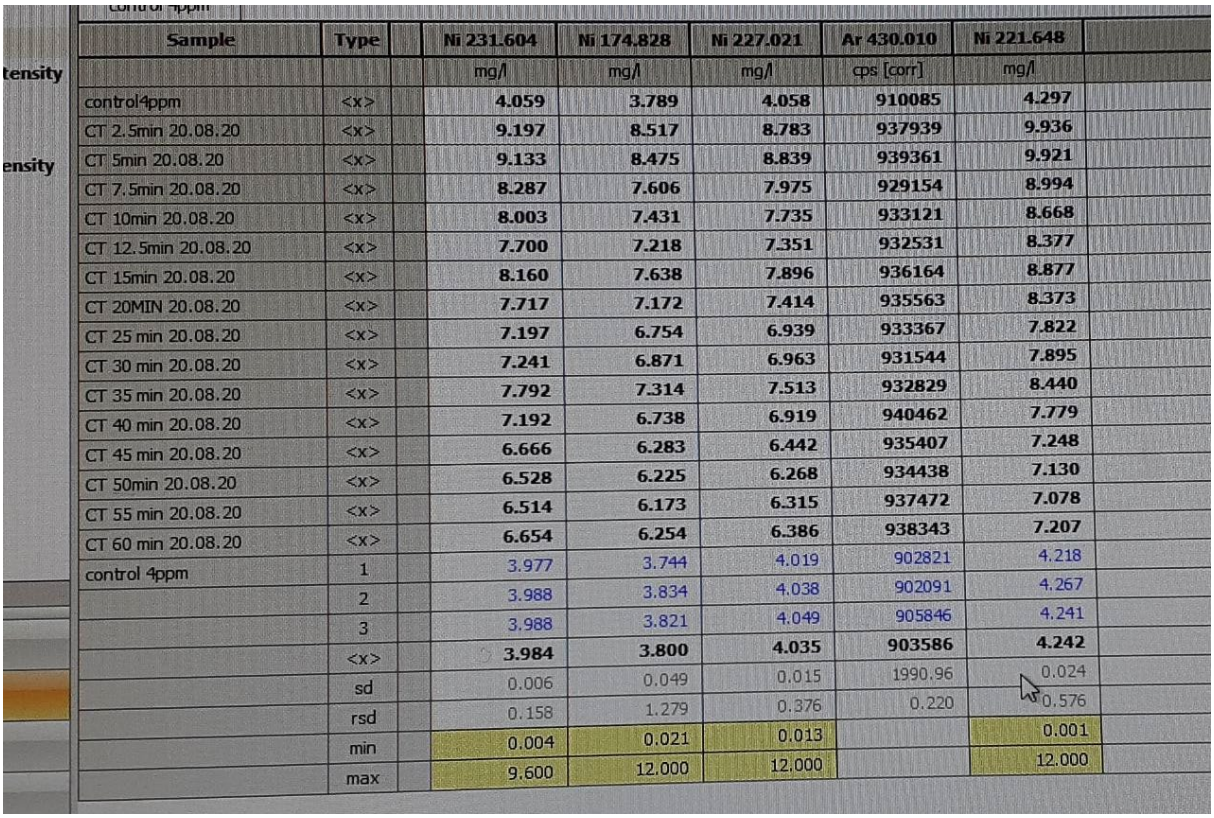

Sample	Type	Ni 231.604	Ni 174.828	Ni 227.021	Ar 430.010	Ni 221.648
		mg/l	mg/l	mg/l	cps [corr]	mg/l
control4ppm	<x>	4.059	3.789	4.058	910085	4.297
CT 2.5min 20.08.20	<x>	9.197	8.517	8.783	937939	9.936
CT 5min 20.08.20	<x>	9.133	8.475	8.839	939361	9.921
CT 7.5min 20.08.20	<x>	8.287	7.606	7.975	929154	8.994
CT 10min 20.08.20	<x>	8.003	7.431	7.735	933121	8.668
CT 12.5min 20.08.20	<x>	7.700	7.218	7.351	932531	8.377
CT 15min 20.08.20	<x>	8.160	7.638	7.896	936164	8.877
CT 20MIN 20.08.20	<x>	7.717	7.172	7.414	935563	8.373
CT 25 min 20.08.20	<x>	7.197	6.754	6.939	933367	7.822
CT 30 min 20.08.20	<x>	7.241	6.871	6.963	931544	7.895
CT 35 min 20.08.20	<x>	7.792	7.314	7.513	932829	8.440
CT 40 min 20.08.20	<x>	7.192	6.738	6.919	940462	7.779
CT 45 min 20.08.20	<x>	6.666	6.283	6.442	935407	7.248
CT 50min 20.08.20	<x>	6.528	6.225	6.268	934438	7.130
CT 55 min 20.08.20	<x>	6.514	6.173	6.315	937472	7.078
CT 60 min 20.08.20	<x>	6.654	6.254	6.386	938343	7.207
control 4ppm	1	3.977	3.744	4.019	902821	4.218
	2	3.988	3.834	4.038	902091	4.267
	3	3.988	3.821	4.049	905846	4.241
	<x>	3.984	3.800	4.035	903586	4.242
	sd	0.006	0.049	0.015	1990.96	0.024
	rsd	0.158	1.279	0.376	0.220	0.576
	min	0.004	0.021	0.013		0.001
	max	9.600	12.000	12.000		12.000

APPENDIX H: Thermodynamic ICP data of Cd batch experiments

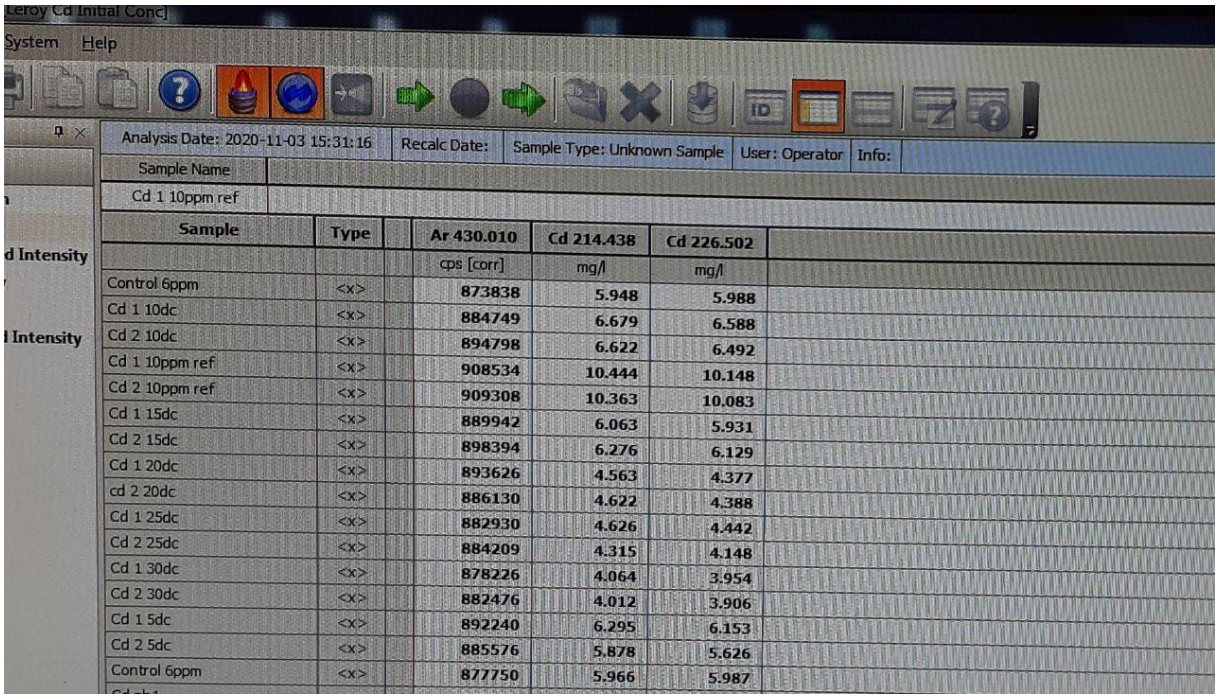

Leroy Cd Initial Conc]

System Help

Analysis Date: 2020-11-03 15:31:16 | Recalc Date: | Sample Type: Unknown Sample | User: Operator | Info:

Sample Name: Cd 1 10ppm ref

Sample	Type	Ar 430.010	Cd 214.438	Cd 226.502
		cps [corr]	mg/l	mg/l
Control 6ppm	<x>	873838	5.948	5.988
Cd 1 10dc	<x>	884749	6.679	6.588
Cd 2 10dc	<x>	894798	6.622	6.492
Cd 1 10ppm ref	<x>	908534	10.444	10.148
Cd 2 10ppm ref	<x>	909308	10.363	10.083
Cd 1 15dc	<x>	889942	6.063	5.931
Cd 2 15dc	<x>	898394	6.276	6.129
Cd 1 20dc	<x>	893626	4.563	4.377
cd 2 20dc	<x>	886130	4.622	4.388
Cd 1 25dc	<x>	882930	4.626	4.442
Cd 2 25dc	<x>	884209	4.315	4.148
Cd 1 30dc	<x>	878226	4.064	3.954
Cd 2 30dc	<x>	882476	4.012	3.906
Cd 1 5dc	<x>	892240	6.295	6.153
Cd 2 5dc	<x>	885576	5.878	5.626
Control 6ppm	<x>	877750	5.966	5.987

APPENDIX I: Thermodynamic ICP data of Ni batch experiments

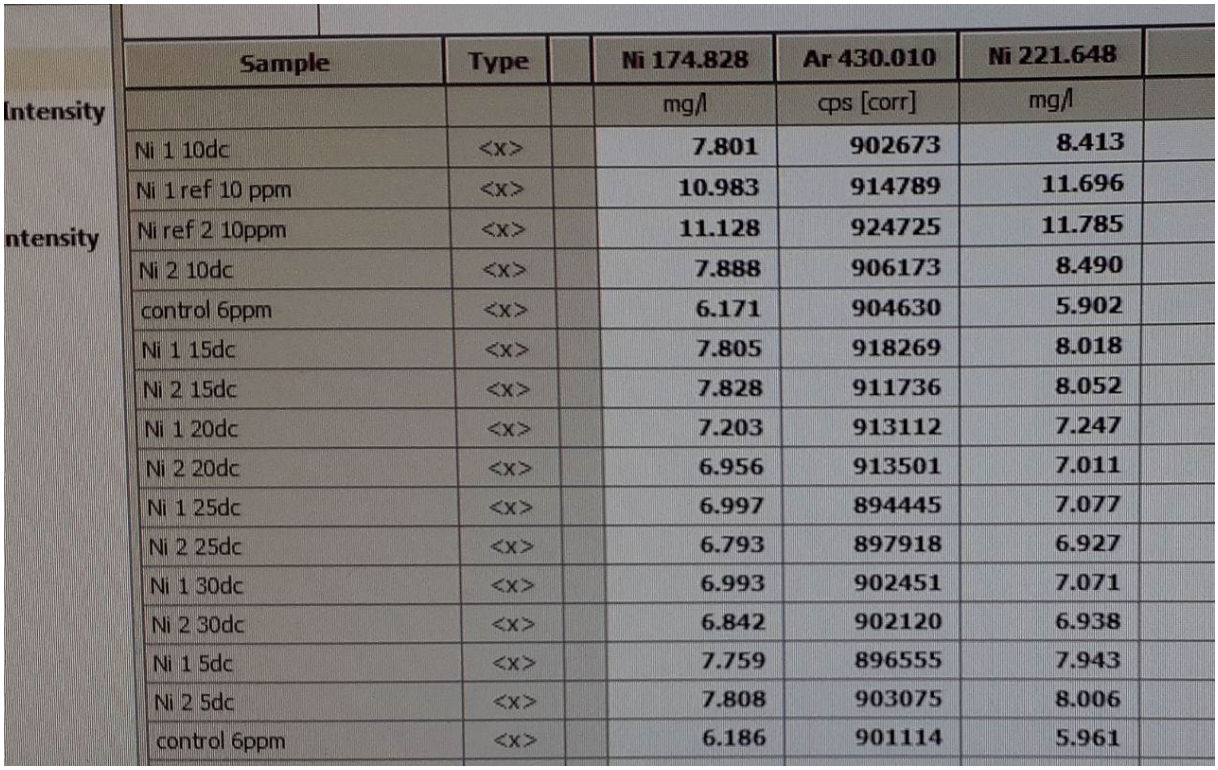

Sample	Type	Ni 174.828	Ar 430.010	Ni 221.648
		mg/l	cps [corr]	mg/l
Ni 1 10dc	<x>	7.801	902673	8.413
Ni 1 ref 10 ppm	<x>	10.983	914789	11.696
Ni ref 2 10ppm	<x>	11.128	924725	11.785
Ni 2 10dc	<x>	7.888	906173	8.490
control 6ppm	<x>	6.171	904630	5.902
Ni 1 15dc	<x>	7.805	918269	8.018
Ni 2 15dc	<x>	7.828	911736	8.052
Ni 1 20dc	<x>	7.203	913112	7.247
Ni 2 20dc	<x>	6.956	913501	7.011
Ni 1 25dc	<x>	6.997	894445	7.077
Ni 2 25dc	<x>	6.793	897918	6.927
Ni 1 30dc	<x>	6.993	902451	7.071
Ni 2 30dc	<x>	6.842	902120	6.938
Ni 1 5dc	<x>	7.759	896555	7.943
Ni 2 5dc	<x>	7.808	903075	8.006
control 6ppm	<x>	6.186	901114	5.961

APPENDIX J: working solutions as used in batch experiments

APPENDIX K. Cadmium icp-oes calibration curve

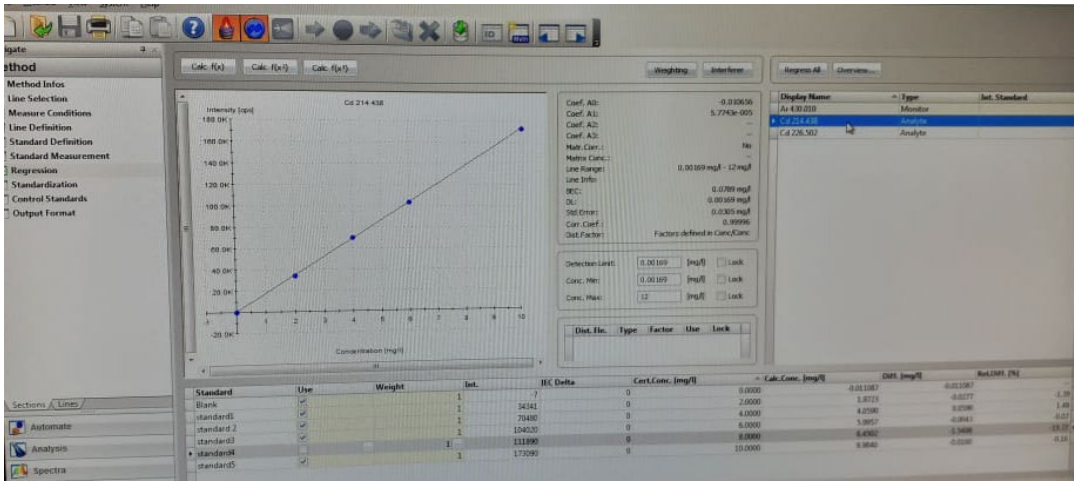

APPENDIX L. Additional pH dependence graph

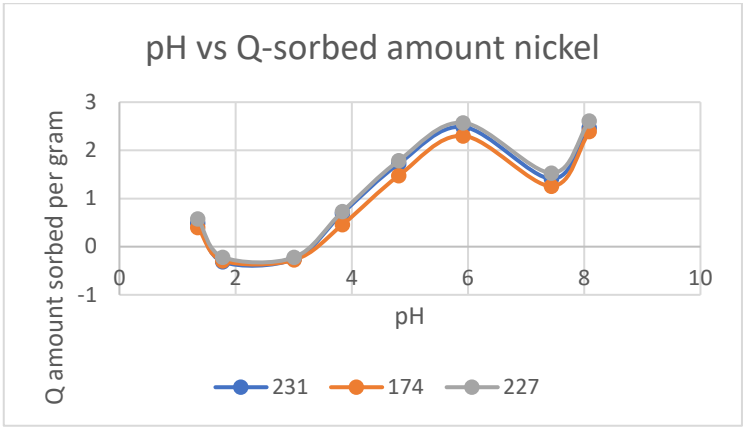
pH vs Q-sorbed amount nickel
Q amount sorbed per gram
3
2
1
0
-1
0
2
4
6
8
10
pH
231
174
227